UNIVERSITY OF BIRMINGHAM

Comparison of radio frequency path loss models in soil for wireless underground sensor networks

By

Danial Abdorahimi

A thesis submitted to

The University of Birmingham

For the degree of

Master of Philosophy

School of Mechanical Engineering

The University of Birmingham

October 2014

Abstract

Recent developments in electronics and wireless communication systems have enabled the expansion of low cost and low power Wireless Underground Sensor Networks. WUSNs consist of groups of nodes which are buried or partially buried underground and are responsible for data collection, transmission and reception in an underground environment. They can be considered as having the potential to provide localised and real time data about a specific medium, for example in precision agriculture, subsurface environmental monitoring, geotechnical and buried infrastructure.

WUSNs, which are buried, have two major limitations when compared to above ground WSNs, namely: Radio Frequency (RF) signal transmission through the soil and lack of access to an energy supply. RF transmission is the most challenging aspect of WUSNs due to the high attenuation of electromagnetic (EM) signals in soil. In these systems, signals are sometimes required to travel inhomogeneous soils with a high density and or water content that can significantly attenuate the signal. The attenuation of the signal through the ground depends on several factors, such as the soil type, including its variability, water content, density, dielectric properties, as well as the frequency of the signal.

In this research existing models such as the Modified-Friis and Crim-Fresnel for RF transmission were critically reviewed and the results from these models compared with measurements obtained from laboratory and field trials. This provides a further understanding of the dielectric properties of soil affecting the attenuation of EM signals and their relationship with soil type and condition (i.e. water content, clay content and density). A new methodology has been developed to accurately measure the EM signal attenuation for a range of soil compositions (using mixtures of Leighton Buzzard sand and English China clay) with a range of water contents of 10%, 20% and 30%.

Both Modified-Friis and Crim-Fresnel models require the real and imaginary parts of the permittivity to be determined. Permittivity can be measured using either a Time Domain Reflectometry (TDR) probe or a Vector Network Analyser (VNA) probe. In this research, it is proposed to use the extracted complex permittivity values from the TDR as the input to the Modified-Friis estimation model. This is tested and compared with the conventional methods. Results from this research showed that neither of the two existing models (Modified-Friis and CRIM Fresnel) failed to predicted the signal attenuation accurately over the full range of tested soil mixtures and water contents. From the results, it was concluded that the Modified-Friis provided a better prediction for soils with clay content over 50% and also soils with water contents less than 20%. In contrast, the Crim-Fresnel model provided a more accurate estimation of the signal attenuation in soils with clay contents less than 50% and water contents over 20%. Based on the findings from this research a suitability matrix is developed to identify the range in which each of the analysed models provide more accurate estimation of signal attenuation in soil. This can provide valuable information to researchers and designers of underground wireless sensor networks.

In addition, the results of this research showed that at medium to long internode distances (>30cm) the CRIM Fresnel largely overestimate the attenuation and Modified-Friis model is a more suitable model for estimation of the signal attenuation.

From a comparison of the results obtained during this research, it is concluded that the permittivity values extracted from the TDR can be used as an input parameter to the Modified-Friis model. In addition, results from this study showed that the Modified-Friis model based on TDR values provided a better estimation of RF attenuation compared to the conventional Modified-Friis model. This can greatly simplify the process of estimation of RF attenuation in soil by removing the sampling and laboratory analysis (i.e. particle size distribution tests) steps which are required for the conventional mixing models.

Acknowledgements

This research and thesis was made possible with the fantastic support and help that I have received from a number of people and I would like to express my gratitude towards them.

Firstly, I would like to especially thank my supervisory group: Dr. Nicole Metje, Prof. David Chapman Dr. Carl Anthony for their invaluable help, guidance and support through the course of my studies.

I would also like to thank all of my present and former colleagues and friends. A special thank you also goes to Dr. Ali Sadeghioon who helped me all the time during my study.

A very special thanks to my father that support me at different stages of my life especially when I started to study abroad. Thanks to my mom and my sisters by giving love and passionate to me. A very huge thank to my lovely wife Gilda for supporting me at the all times with love it was not possible to complete my study without her.

Danial Abdorahimi

Birmingham

June 2018

Table of Contents

List of Figures

List of Tables

Chapter 1 INTRODUCTION

1.1 Introduction

Wireless Underground Sensor Networks (WUSNs) consist of groups of nodes which are buried or partially buried underground and which are responsible for data collection, transmission and reception in an underground environment (Li et al., 2007; Chaamwe et al., 2010; Stoianov et al., 2007). Recent developments in electronics and wireless communication systems have enabled the expansion of low cost and low power WUSNs (Vuran and Akyildiz, 2010; Sadeghioon et al., 2014). WUSNs can be considered as a potential area that enables various applications, which have not existed previously, compared to the recent development in this field. The applications, such as precision agriculture, environmental monitoring, underground monitoring (i.e. pipe monitoring and mine monitoring) are all possible because the WUSNs can provide localised and real time data about the specific medium (Silva and Vuran, 2010).

WUSNs have two major limitations as compared to Wireless Sensor Networks (WSN) over-ground, namely: Radio Frequency (RF) signal transmissions in soil and lack of access to an energy supply for long term perform i.e. use of battery underground would last up to the 5 years (Stuntebeck and Akyildiz, 2006). RF transmission is the most challenging aspect of WUSNs due to the high attenuation of electromagnetic (EM) signals in soil mediums (Li et al., 2007). In these systems, signals are sometimes required to travel through homogenous soils that can rapidly attenuate the signal over short distances compared to the attenuation of the signal in the air. For example, a RF signal of 434Mhz would reduce in strength by 80 dBm

after 1 metre with the attenuation of the signal depending on the medium mixture (Chaamwe, 2010; Peplinski et al., 1995b; Stoianov et al., 2007), and factors such as soil types, condition, dielectric properties and the frequency of the signal.

Underground sensor network communication can be classified into two categories (Silva, 2010):

- Wireless communication networks for mines and tunnels
- Wireless underground sensor networks (WUSNs)

There have been several studies which focused on the WUSNs for mines and tunnels (Kennedy, 2006; Chehri, 2006). Although the networks are placed underground the communication transmits through in the air. Therefore, this network communication is considered as terrestrial communication. **Error! Reference source not found.** presents the classification of the WUSNs types (Silva, 2010):

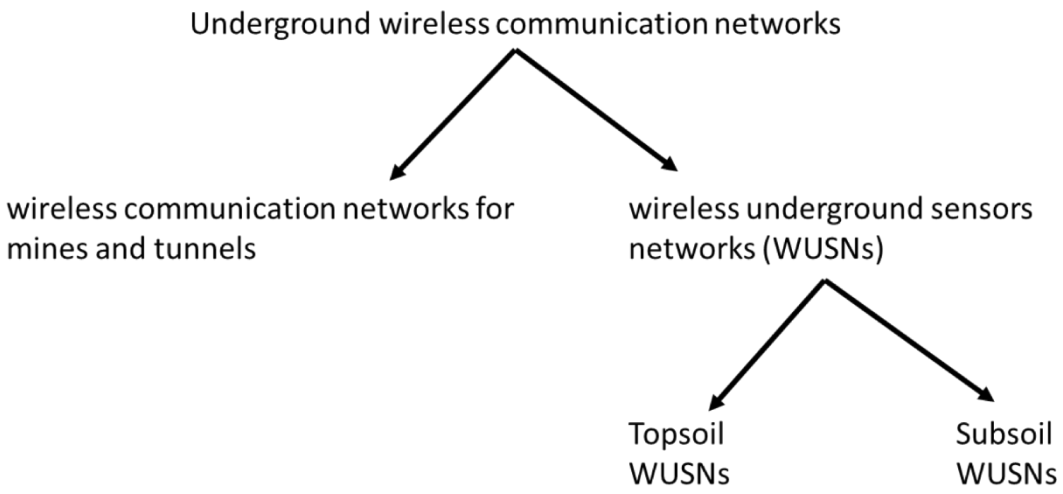

Figure 1-1 Classification of the underground communication networks (Silva, 2010)

The topsoil region of wireless underground sensor networks refers to the top 30cm of soil down from the ground surface, the subsoil refers to 30-100cm below the ground surface (Silva, 2010).

The soil layers are distinct in terms of the soil texture which has a major impact on the signal transmission. In addition, the topsoil's underground signal channelling may be affected by the reflection signal from the surface of the soil's interface.

Overall, communication in WUSNs is classified as underground to underground communication (UTUC) and underground to aboveground communication (UTAC); and these types of communication are dependent on the desired application. The UTAC is less challenging than the UTUC because a certain portion of the communication takes place over the ground's surface (Silva, 2010). The underground to underground communication is the focus of this study and the underground channel for the underground sensor network communication is discussed in the following section.

The signal can undertake multiple paths in the soil and the study of the paths is essential for propagation of the signal in the soil. Generally, a signal can be refracted and reflected due to the properties of the soil and this affects the signal's intensity (Akyildiz et al., 2005). The overall path of the underground signal propagation can be classified as single path (direct) or multipath (reflected) (Akyildiz et al., 2009). The schematic of the general paths of signal propagation underground is illustrated by**Error! Reference source not found.**.

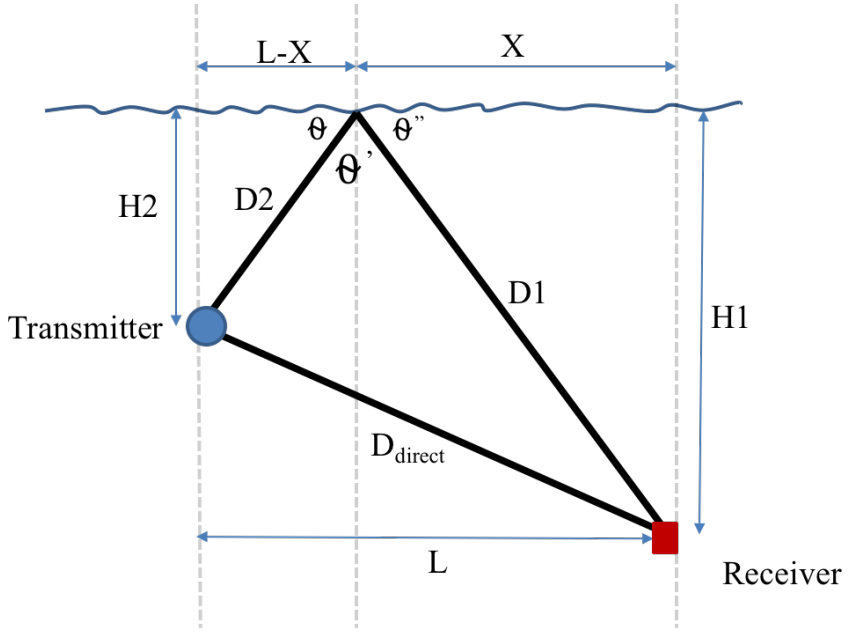

Figure 1-2 Schematic of different paths for underground communication network systems. The transmitter and receiver are buried underground.

As shown in**Error! Reference source not found.**, the signal transmitted from the transmitter travels in two propagation forms. The single path (D_{direct}) is the spherical wave which travels towards the receiver antenna in a line of sight (Akyildiz et al., 2009). RF transmissions can be assumed as the single path when there are no reflecting boundaries or where the boundaries are far from the sensor. In the case of RF transmission in the soil, a single path model can be used where wireless transmitters are buried deep in the soil (Akyildiz et al., 2009). From **Error! Reference source not found.** the single path is calculated by Equation (2-22) as follows:

$$D_{direct} = \sqrt{(H1 - H2)^2 + L^2} \tag{1-1}$$

The multipath model takes into account the effect of the reflected signal on the soil's surface. This effect is highly dependent upon the length of the reflected path which, in turn, is dependent on the depth of the transmitter. The lengths $D1$ and $D2$ and The assumptions identified to calculate the reflected wave which are given by Equations (2-23) - (2-29)

$$\theta = \theta" \tag{1-2}$$

$$tan\theta = tan\theta" \tag{1-3}$$

$$tan\theta" = \frac{H1}{X} \tag{1-4}$$

$$tan\theta = \frac{H2}{L - X} \tag{1-5}$$

$$\frac{H1}{X} = \frac{H2}{L - X} \quad \therefore \quad X = \frac{H1L}{(H1 + H2)} \tag{1-6}$$

Then $D1\ and\ D2$ are calculated by:

$$D1 = \sqrt{H1^2 + \mathrm{X}^2} \tag{1-7}$$

$$D2 = \sqrt{H2^2 + (L - X)^2} \tag{1-8}$$

The reflected wave is calculated by adding the two paths $D1\ and\ D2$ and also the signal losses part of the energy by interfacing the soil surface (Ds) with so the final reflected equation are given by equation (2-30):

$$D_{reflect} = D1 + D\mathrm{s} + D2 \tag{1-9}$$

The environment has a significant influence on the WUSNs and has a direct impact on the communication performance between the nodes as it affects RF transmission. The main parameters affecting the overall attenuation of EM signals in the soil are listed as:

- Complex dielectric permittivity of the soil (ε^*)
- Electrical conductivity of the soil (σ_{dc})

- Magnetic permeability of the soil (μ)
- Soil water content (bound and free water content)
- Bulk density (ρ_b) and temperature of the soil (T)
- Mineralogy of the soil
- Frequency of the transmitted EM signal.

The variability of the soil and other conditions and complexity of the behaviour of signal attenuation, with respect to these parameters, makes an accurate estimation of EM signal attenuation in soil challenging. Several EM propagation models exist alongside measuring and analysing techniques for extracting data from the soil; all of which aims to estimate the effect of these parameters on the attenuation of a signal in the soil (Xiaoqing Yu, 2013; Dam et al., 2005). There is some question on the validity of these models in different soil types. Hence this thesis sets out to experimentally investigate the validity of these models at different soil types.

1.2 Aim and objectives

The aim of this research is to validate usage of the complex permittivity values extracted from Time Domain Reflectometry (TDR) in RF estimation model and also to identify the suitability of each of the existing RF estimation models in different soil types and conditions. In order to accomplish this aim, the following objectives were set:

- To critically review the existing literature regarding the estimation of electromagnetic signal attenuation in the soil, specifically identifying current RF models used for estimation of the attenuation of the signal in the soil.

- To identify the dielectric properties of soil affecting the attenuation of EM signals and their relationship with soil types and conditions (i.e. water content, clay content and density).
- To define a methodology for EM signal attenuation measurements in laboratory tests and to conduct laboratory experiments in order to measure the attenuation of EM signals in various soil compositions and conditions.
- To compare the accuracy of RF estimation models based on the usage of complex permittivity values obtained from Time Domain Reflectometry (TDR) measurements with attenuation estimation models which use conventional mixing models (i.e. Peplinski).
- To compare the accuracy of existing RF models for the estimation of electromagnetic attenuation in soil with the results from the laboratory experiments.
- To identify the range of soil types and conditions and transmission distance in which each of the attenuation models are more suitable (i.e. provide a better estimation).

1.3 Thesis layout

This thesis comprises five chapters, detailing the research.

A critical review of the RF models used for estimation of the signal attenuation and also the factors which affect the signal is presented in Chapter 2. Chapter 3 illustrates the design of the methodology regarding the measurement of the signal propagation through soil in the laboratory. This chapter also describes the methodology that is used for signal propagation measurements in the field trials. Chapter 4 reports the effect of the soil composition on the dielectric properties of the soil and on the signal and also describes the comparison of the existing RF models. This chapter presents the result and discussion of the signal propagation

from the field trials. Finally, the thesis is concluded in Chapter 5. This includes recommendations for the future work.

Chapter 2 LITERATURE REVIEW

2.1 Introduction

This chapter provides an introduction to signal propagation through the soil, followed by a description of the existing radio frequency (RF) models which predict the attenuation and intensity of a signal and then continues with a review of the general underground channels for wireless underground sensor networks. This chapter also reviews the interaction of the soil with electromagnetic (EM) signals and the important parameters of soil that affect the propagation of a signal through it. This is followed by a comparison of the existing RF methodology for estimations the real and imaginary part of the dielectric permittivity of soil.

Finally, this chapter identifies the key gaps in the literature concerning wireless underground sensors networks and EM signal propagation through the soil.

Wireless sensors networks (WSNs) are mainly used for communication between two points. However, these points can be partly or completely underground and for systems completely underground the network is assumed as wireless underground sensors network (WUSN). Attenuation of a signal is caused by reflection, refraction, absorption and scattering of the signal with its interaction with different mediums i.e. soil (Sun and Akyildiz, 2010). This affects the electromagnetic signal travelling through free space or through different media (Li et al., 2007) and ultimately limits the distance over which the signal can be detected. The EM signal includes electric and magnetic fields that oscillate at right angles to each other, as can be seen from Figure 2-1 where both the fields oscillate and move along the axis of travel.

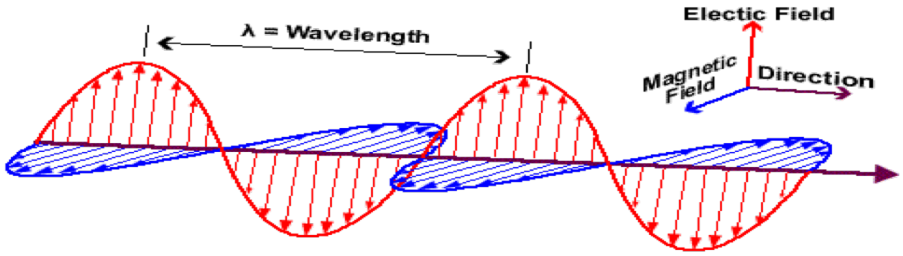

Figure 2-1 Schematic of electromagnetic wave oscillation (Lucas, 2015)

Maxwell (Zhang and Satpathy, 1990) proposed the equations for understanding the movement of the electromagnetic (EM) signals in free space. Equations (2-1), (2-2), (2-3) and (2-4) describe the signal propagation as defined by Maxwell in free space:

$$\nabla . E = \frac{1}{\varepsilon} \rho v \tag{2-1}$$

$$\nabla . H = 0 \tag{2-2}$$

$$\nabla \times E = -\mu \frac{dh}{dt} \tag{2-3}$$

$$\nabla \times H = \sigma E + \varepsilon \frac{dE}{dt} \tag{2-4}$$

$$D = \varepsilon E \tag{2-5}$$

$$B = \mu H \tag{2-6}$$

$$J = \sigma E \tag{2-7}$$

Where E $(V\ m^{-1})$ is the electrical field; D $(C\ m^{-2})$ is the electric flux density; H $(A\ m^{-1})$ is the magnetic field; J is the external current density; B (Wb) is the magnetic flux; ρv is the volumetric free charge density, σ (S) is the permittivity and $\mu(Hm^{-1})$ is the vacuum permeability $\left(4\pi \times 10^{-7}\ {}^{N}/_{A^2}\right)$. For non-magnetic substances the relative permeability is equal to 1 (Cross, 2014) and ε is the permittivity ($F\ m^{-1}$).

2.2 Free-space signal propagation

As Electromagnetic signals travel through space their power density reduces. This attenuation is usually described as the Free Space Path Loss (FSPL). A FSPL model is used for the calculation of the attenuation between two points (transmitter and receiver) based on a clear line of sight (no obstacles at either of the nodes). The main attenuation formula for electromagnetic signals in free space is given by Equation (2-8) (Friis, 1946):

$$P_r(d) = \frac{P_t G_t G_r \lambda^2}{(4\pi)^2 d^2} \tag{2-8}$$

Where $P_r(d)$ is the received transmission power as a function of distance; P_t is the transmission power; G_t, G_r are the gain of transmitter and receiver; d is the distance between the transmitter and receiver and λ is the wavelength of frequency that describes $^{c}/_{f}$; c is the speed of light and f is the operation frequency. From Equation (2-8) the FSPL, $\frac{P_t}{P_r}$ can be derived from Friis, transmission equation by the condition of $G_t = G_r = 1$ (Yoon et al., 2011).

$$\frac{P_t}{P_{r(d)}} = \left(\frac{4\pi d}{\lambda}\right)^2 \tag{2-9}$$

The FSPL equation (2-9) can be reformed into a logarithmic format leading from equation (2-10) to equation (2-12).

$$FSPL = 10log_{10}\, d + 10log_{10}\, \mathrm{f} + 10log_{10}\left(\frac{4\pi}{c}\right)^2 \tag{2-10}$$

$$FSPL = 10log_{10}\, d\,(m)^2 + 10log_{10}\, \mathrm{f}\,(H)^2 - 147.55 \tag{2-11}$$

$$FSPL = 20log_{10}\, d\,(m) + 20log_{10}\, \mathrm{f}\,(H) - 147.55 \tag{2-12}$$

Where the FSPL is the total path loss in dB; d is the distance (m), between sensors and *f* (MHz), is the frequency. From equation (2-12) it is shown that the FSPL depends on the distance between the two nodes and the frequency of the signal to show effect of frequency on the path loss the path loss for different frequencies (434 MHz, 868 MHz, 2.4 MHz and 5GHz which are common Industrial, scientific and medical (ISM) radio bands) in free space calculated and is shown in Figure 2-2.

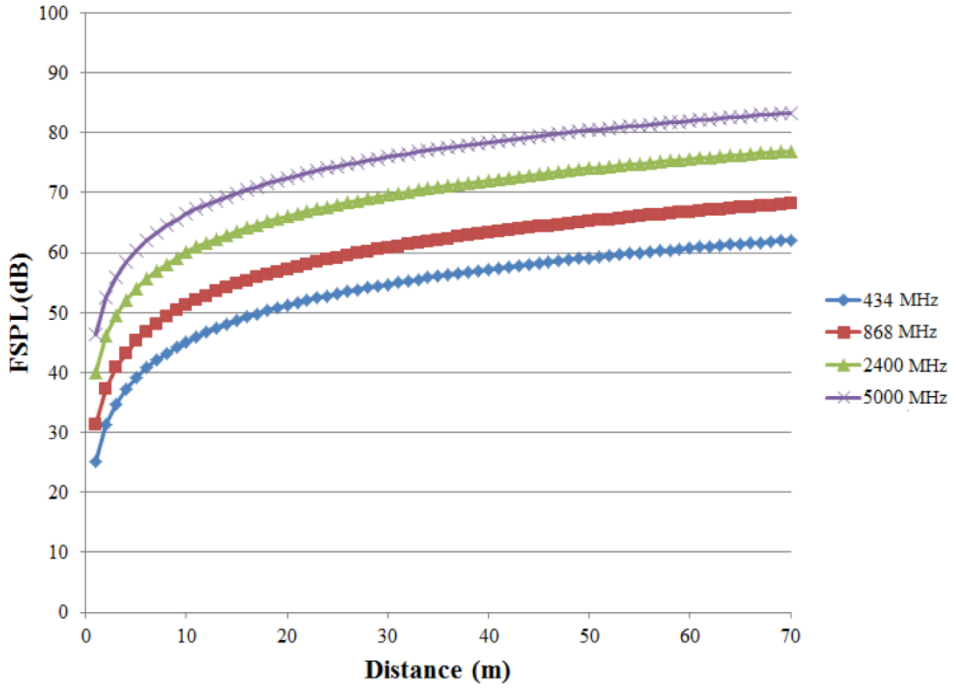

Figure 2-2 Comparison of attenuation of different frequencies by distance in free space based on a free space path loss (FSPL) model

Figure 2-2 clearly shows that the attenuation of a signal increases in free space with the increase in the signal frequency. Therefore, lower frequencies would be able to travel further in space compared to higher frequencies (given equal transmission power). The Modified-Friis model and Crim-Fresnel model are the well-known electromagnetic models which are used for signal attenuation estimation in mediums.

2.2.1 Modified-Friis model

There are a number of different models which predict the signal attenuation. The Modified-Friis model is based on the transmission link budget which is derived from the transmission equation in free space (Akyildiz et al., 2009; Li et al., 2007; Sun and Akyildiz, 2010). The link budget given by Equation (2-13) describes the general relation between the transmitted and

received power considering the loss in free space, gains at the receiver and transmitter and the loss caused by the medium; where P_t is the transmitter power; $G_r\ and\ G_t$ are the gain of the receiver and transmitter nodes respectively; d is the distance between the transmitter and receiver; L_0 is the path loss in free space and L_m is the attenuation caused by the medium.

$$P_r = P_t + G_r + G_t - (L_0 - L_m) \tag{2-13}$$

Equation (2-13) is widely used as the basis for existing models for the estimation of EM signal attenuation in soil (Chaamwe, 2010; Sun and Akyildiz, 2010). The Modified-Friis model is based on the transmission equation in free space proposed by Friis et al., (1946). This is determined based on the differences of the EM signal propagation in soil compared to air, (Akyildiz et al. 2009), These differences are 1) the wave velocity and the different frequency wavelength in soil and air; 2) the amplitude of the signal which is attenuated according to the frequency and 3) the phase velocity which is correlated with frequency causing scattering delay distortion of the signal. L_m is given by Equation (2-14).

$$L_m(dB) = L_\beta(dB) + L_\alpha(dB) \tag{2-14}$$

Where L_β is the attenuation due to the wavelength differences in soil $\left(\lambda = \frac{2\pi}{\beta}\right)$ compared to air $\left(\lambda_0 = \frac{c}{f}\right)$ and $L_\alpha = 8.69\alpha d$ is the loss due to attenuation and α is the attenuation constant which is given in Equations (2-16).

The equation for the total path loss $P_L = L_0 - L_m$ based on the Modified-Friis model (Li et al., 2007) is given by Equation (2-15):

$$P_L = 6.45 + 20\log(\mathrm{d}) + 20\log(\beta) + 8.69\alpha\mathrm{d} \quad (2\text{-}15)$$

Where α $\left({}^{1}/_{m}\right)$ is the signal attenuation coefficient and β $({}^{radian}/_{m})$ is the phase shifting coefficient of the material which depend on the dielectric and magnetic properties of the material, Equations (2-16) and (2-17) gives the definition for α and β respectively.

$$\alpha = \omega \sqrt{\frac{\mu\varepsilon'}{2}\left(\sqrt{1+\left(\frac{\varepsilon''}{\varepsilon'}\right)^2}-1\right)} \quad (2\text{-}16)$$

$$\beta = \omega \sqrt{\frac{\mu\varepsilon'}{2}\left(\sqrt{1+\left(\frac{\varepsilon''}{\varepsilon'}\right)^2}+1\right)} \quad (2\text{-}17)$$

Where $\omega = 2\pi f$; μ is the magnetic permeability of soil and ε' is the real part of the complex dielectric permittivity $\varepsilon^* = \varepsilon' + j\varepsilon''$ and ε" is the imaginary part of the complex dielectric permittivity. As shown in Equations (2-16) and (2-17), the values of α and β are directly related to the dielectric properties of the soil and therefore the path loss in soil is also directly related to the properties of the soil. Li et al., (2007) used the Peplinski mixing model. (Peplinski et al. 1995b) to calculate the real and imaginary parts of the complex dielectric permittivity of the soil based on the composition and volumetric water content. The mixing model is described in detail in Section 2.5.1.

2.2.2 Crim-Fresnel model

Crim-Fresnel model is another EM model for measuring the signal attenuation in the soil. The Crim-Fresnel model of estimating the attenuation of a signal in soil was initially presented by Bogena et al. (2009) to estimate the signal attenuation through a sandy soil in laboratory

experiments. The test was repeated three times. The Figure 2-3 shows the measured data compared with the estimated values calculated from CRIM Fresnel model at varying soil water contents.

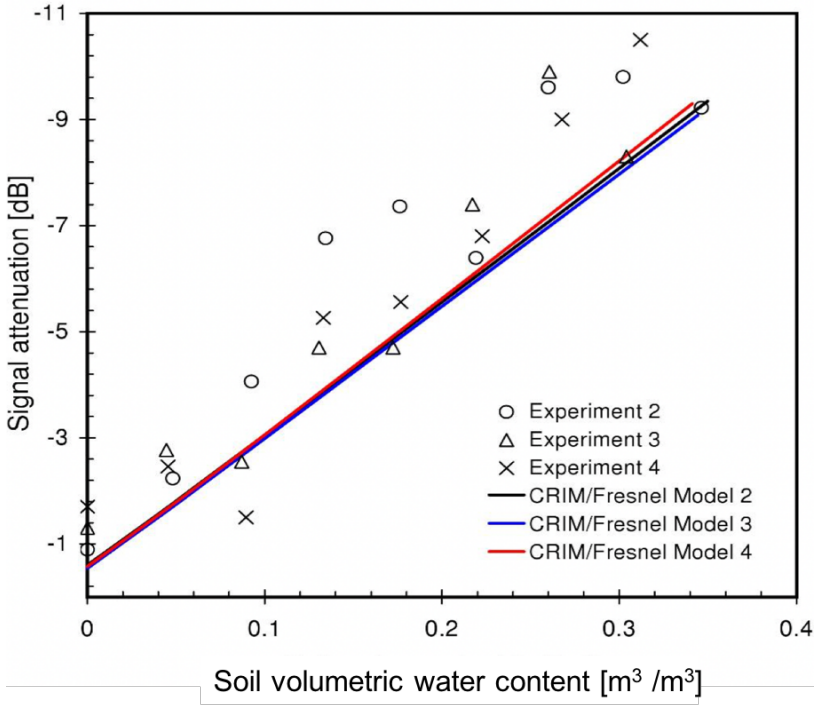

Figure 2-3 The signal attenuation based on the Crim-Fresnel model (Bogena, 2009)

Crim-Fresnel model is also based on the link budget model given by Equation (2-13). The Crim-Fresnel model takes the attenuation of the signal due to reflection into account. The total attenuation of a signal is introduced (Bogena, 2009) as the sum of the soil attenuation as well as signal reflection. The total attenuation of the EM signal (A_{tot}) based on this model is given by Equation (2-18), where α_{CRIM} is the attenuation coefficient of the signal and d is the distance between two sensor nodes; R_c is the attenuation due to reflection (Chaamwe, 2010).

$$A_{tot} = \alpha_{CRIM} \times d + R_c \tag{2-18}$$

The attenuation coefficient α_{CRIM} $\left(\frac{dB}{m}\right)$ is calculated by Equation (2-19) and attenuation due to reflection R_c is given by Equation (2-20), where symbols have the same meaning as ones mentioned in equations 2-8 – 2-17.

$$\alpha_{CRIM} = 8.68 \frac{60\pi(2\pi f \varepsilon_0 \varepsilon'' + \sigma_{dc})}{\sqrt{\frac{\varepsilon'}{2}\left(1 + \sqrt{1 + \left(\frac{\varepsilon'' + \frac{\sigma_{dc}}{2\pi f \varepsilon_0}}{\varepsilon'}\right)^2}\right)}} \tag{2-19}$$

$$R_c = 10log_{10}\left(\frac{2R}{1+R}\right) \tag{2-20}$$

Where R is the reflection coefficient and is given by Equation (2-21).

$$R = \left(\frac{1-\sqrt{\varepsilon'}}{1+\sqrt{\varepsilon'}}\right)^2 \tag{2-21}$$

Unlike the Modified-Friis model, the permittivity of the soil in the Crim-Fresnel model is calculated based on the Complex Refractive Index Model (CRIM). The CRIM model calculates the soil's dielectric permittivity by using the permittivity of solids (ε_s), water (ε_w) and air (ε_a) at a specific frequency, based on the fact that the only loss source is water (Bogena et al., 2009). The Crim-Fresnel model is claimed by Bogena et al., (2009) to be a better estimation for the signal propagation in soil compared to the Modified-Friis model. This is due to the fact that the proposed mixing model, in regards to identifying the real and imaginary parts of dielectric permittivity used in Modified-Friis, is not developed, based on the various soil types and compositions. Chaamwe et al., (2010) compared these two models and measured the signal attenuation in soild with three different densities and claim that the signal reflections also affect signal attenuation. In addition, the Crim-Fresnel model is not validated by field test trials. By

considering the effect of reflection on signal attenuation the signal propagation classifies in different categories.

2.2.3 Comparison of Modified-Friis and CRIM-Fresnel models

Two common RF signal attenuation models (Modified-Friis and Crim-Fresnel) were presented in sections 2.2.1 and 2.2.2. The Modified-Friis model estimates the attenuation of EM signals mainly based on the effect of phase shifting on the signal, while the Crim-Fresnel considers the effect of the material absorption and signal reflection. Estimation of signal attenuation for typical soil ($\varepsilon' = 13.25\ and\ \varepsilon'' = 2.18$ of the soil at 434MHz) is shown in **Error! Reference source not found.** (Sadeghioon, 2014).

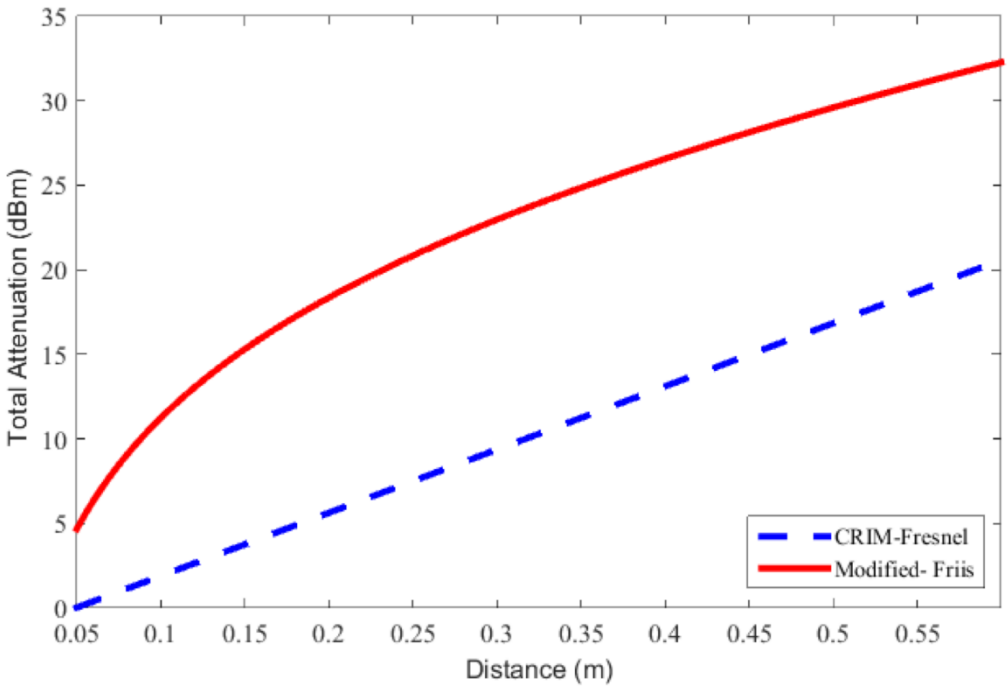

Figure 2-4 Comparison of Modified-Friis and Crim-Fresnel models, (Sadeghioon, 2014)

The comparison of the RF propagation models**Error! Reference source not found.** shows that the estimated values for attenuation of a signal by the Modified-Friis and Crim-Fresnel models

are broadly different from each other. The modified-Friis is estimating the signal attenuation in dBm as a non-linear function, while the Crim-Fresnel model estimates the attenuation of the EM signals as a linear function in dBm. These differences suggest a need for further investigation into the accuracy of these models by comparing the predicted values from the models with measured values from laboratory or field trials.

Soil characteristics have a significant effect on the signal attenuation in the soil. These characteristics will change with soil composition and conditions (i.e. water contents and density). The next section (2.3) describes the interaction of soil with an electromagnetic signal.

2.3 Soil and interaction with electromagnetic signals

This section presents a definition of soil and this is followed by the important soil parameters which can affect the propagation of a signal. The dielectric properties of soil and the existing method used to extract the dielectric properties from the soil mixture and the signal attenuation estimation by the models such as Crim-Fresnel and Modified-Friis are also described.

Generally, soil is presented as a "natural body" which is differentiated into horizons of mineral and organic constituents (Jenny and Amundson, 1941). Soil can be defined 'as any uncemented or weakly cemented accumulation of mineral particles formed by the weathering of rocks, the void space between the particles containing water and/or air' (Craig, 2004). Jenny and Amundson. (1941) introduced soil as a function of different factors as given by equation (2-31):

$$S = f(cl, o, p, r, t) \tag{2-22}$$

Where S shows soil as a function of five parameters: cl climate, o living organic, p parent material, r relief and t time (Curioni, 2013).

Soil can be classified by the relative proportion of the sand (with particles diameter range of 0.6 up to 2mm), clay (with particles diameter less than 2μm) and silt (with particle range of 0.02 - 0.06mm) of the soil attained by the laboratory. Particle-size distribution test separates the particles into different size ranges (BSI 1377, 1990).

Soils with different water contents, composition and condition (different temperature) perform differently in the interaction with an electromagnetic signal. In particular, the water content of the soil is the main parameter that affects the propagation of the signal through the soil (Chaamwe, 2010). Water content is defined as the fraction of the amount of water in the soil, which can be classified into bound water and free water (Chaamwe, 2010). Bound water corresponds to the water molecules that are held by the soil particle surfaces; while the free water is free of the action of the soil particles and move freely by the gravitational force (Silva, 2010). The clay content of the soil determines the amount of bound water in the sample (Sabey, 1966; Bradford, 1976). Bound water increases with increase in clay content as a larger portion of water content are bound to the clay particles. Water content can be described in two ways: gravimetric water content (GWC) and volumetric water content (VWC). GWC is determined as the ratio of the mass of water $\left(M_w\ (g)\right)$ and the mass of the dry soil $(M_s\ (g))$; and VWC is expressed as the ratio of the mass of water (M_w) and the volume of the soil $(V_s\ (cm^3)$. Equations (2-32) and (2-33) show the GWC and VWC relations:

$$GWC = \frac{M_w}{M_s} \qquad g \tag{2-23}$$

$$VWC = \frac{M_w}{V_s} \quad {}^{g}/_{cm^3} \tag{2-24}$$

VWC is important with the present to the geophysics properties of the soil. Therefore the concept of the dry density $\left(\rho_{dry}, {}^{g}/_{cm^3}\right)$ becomes more important for VWC measurement from the known GWC as in Equation (2-34) (Thomas, 2010):

$$VWC = \rho_{dry}\, GWC \tag{2-25}$$

The VWC is related to the GWC by dry density of the soil as shown by Equation (2-34). Topp et al., (2000) showed that the attenuation of the signal increases due to a rise of the free water content of the soil. A rise in the free water content of the soil increases the dielectric constant of the soil which affects the signal propagation through the soil (Topp et al., 2000).

Soil composition greatly affects the signal propagation based upon the soil particulate content. An increase in clay content increases the attenuation of the signal and a soil with more sand particles has less of an effect on the signal attenuation (Yu, 2013a). A different fraction of sand and clay will change the percentages of bound and free water in the soil, which will in turn act on the EM signal attenuation. The physical properties of soil, such as particle density, the size of the particles and the porosity, may also affect the bulk density of the sample, which directly affects the dielectric properties of the soil (Gupta, 2011). As can be seen from Figure 2-5., as the bulk density increases the dielectric properties of the soil, such as the real and imaginary dielectric values of material also increase. The dielectric values were calculated for this study based on the Peplinski et al., (1995b) model and the laboratory measurements. As shown from Figure 2-5., the value from experiment for $\varepsilon'$is lower than the predicted value by Peplinski; This is caused by the effect of free water in the soil (Topp et al., 2000). As free water of the soil mixture increases the apparent dielectric permittivity of the soil decreases too and it is due

to the more energy loss of the travelled signal in the soil. Furthermore, the experimentally based ε'' is moves closer to the predicted value as the bulk density increases.

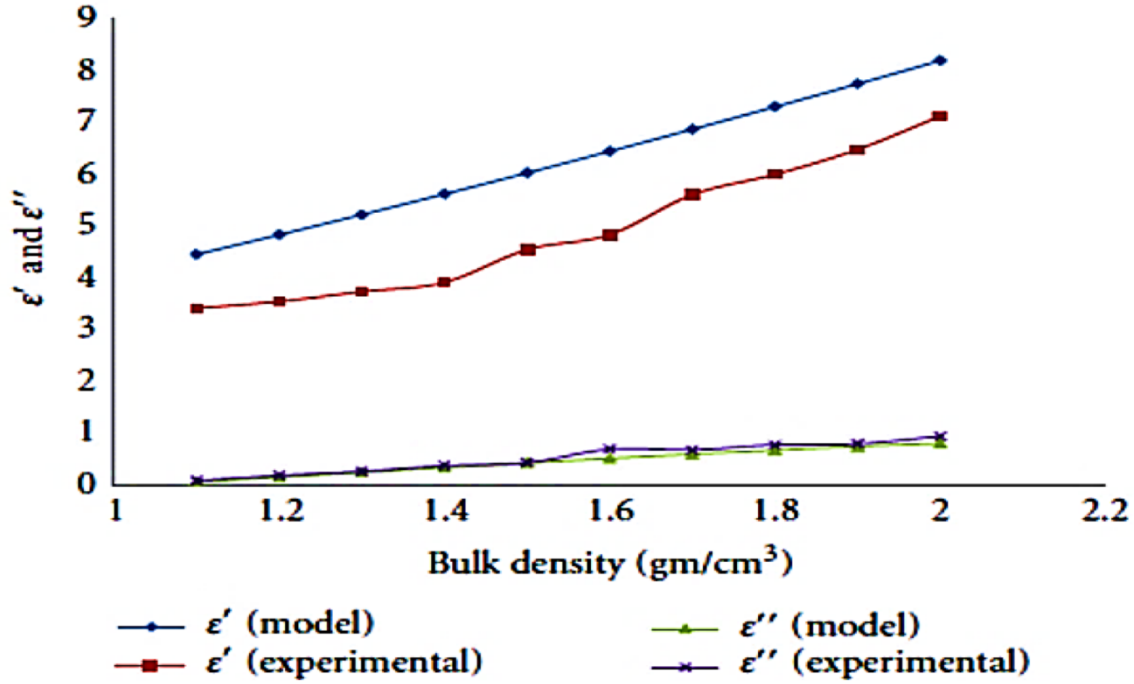

Figure 2-5 Effect of bulk density on the real ε' and imaginary ε'' constants of the electromagnetic signal dielectric constant (Gupta, 2011)

where ε' is real part of the dielectric permittivity and ε'' is imaginary part of the dielectric permittivity. Gupta (2011) used soil samples from the north India, the soil particle size distribution includes of clay 7.20%, silt 21.50% and sand 71.20% respectively and different bulk densities of the same soil samples prepared with a variation of 1.3 to 2.0 g/cm^3. The result from the figure shows that an increase in the bulk density increases the real and imaginary constant parts of permittivity in both model and experimental data.

2.4 Electromagnetic properties of soil

The main criteria for the attenuation of electromagnetic signals in soil is energy loss of the signal through the soil. Therefore, the signal propagation characteristics are defined by the soil properties (Yu, 2013b). Despite the massive effect the geotechnical properties of the soil, such as density and water content on the signal propagation, the dielectric properties of the soil also have an effect on the signal propagation (Stuntebeck and Akyildiz, 2006). The dielectric properties of soil described by the following sections from 2.4.1 to 2.4.3.

2.4.1 Dielectric permittivity (ε)

Dielectric permittivity is the ability of a material to transmit an electric field. It is the energy of a signal that can be stored in the medium as the effect of a separation of charge (Curioni, 2013). Initially from the Maxwell equation, the permittivity of a material defines the electric field, which results from the charge density or electric flux (Cross, 2014). Dielectric permittivity is defined by a complex number (ε^*) with both real and imaginary parts (Curioni, 2013). The real part (ε') of the dielectric permittivity represents the storage of the energy that is created by the electric field, while the imaginary part shows the degradation of the stored energy (Curioni, 2013; Dam et al., 2005). In general, the dielectric permittivity is to be defined as the ratio of absolute permittivity to the permittivity of free space ($\varepsilon_0 = 8.854\times 10^{-12}\, F/m$), and thus referred to Relative Dielectric Permittivity(ε_r). In addition, the frequency dependency of the permittivity can be considered by the function given by Equation (2-35) (Curioni, 2013).

$$\varepsilon^*(f) = \varepsilon'(f) - j\left(\varepsilon''(f) + \frac{\sigma_{dc}}{2\pi f \varepsilon_0}\right) \tag{2-26}$$

Where $\varepsilon'(f)$ is the real part of the complex function of dielectric permittivity; $\varepsilon''(f)$ is the dipolar phenomenon (separation of charges) due to relaxation or the imaginary parts of dielectric permittivity; σ_{dc} is the electric conductivity $\left(\frac{S}{m}\right)$; f is the frequency applied by the electric field (Hz) and j is the imaginary part of complex number which is $\sqrt{-1}$ (Robinson, 2002; Curioni, 2013).

The imaginary part of the complex permittivity is obtained by Equation (2-36) (Robinson, 2002; Curioni, 2013):

$$\varepsilon'(f) = \varepsilon''(f) + \frac{\sigma_{dc}}{2\pi f \varepsilon_0} \tag{2-27}$$

Therefore, the degree of loss tangents is defined by the ratio of the imaginary and real part of the complex permittivity can be obtained by Equation (2-37).

$$tan\,\delta = \frac{\varepsilon''(f) + \frac{\sigma_{dc}}{2\pi f \varepsilon_0}}{\varepsilon'(f)} \tag{2-28}$$

2.4.2 Electrical conductivity (σ, EC)

Electrical conductivity can be thought of as the ability of a material to conduct electric current $\left(\frac{S}{m}\right)$. Ionic substances contained in soils have the most effect on the EC, meaning that conductivity depends on the concentration of salts in water (Curioni, 2013). One of the imaginary parts of the dielectric permittivity function in Equation (2-36), σ_{dc} (DC conductivity), is the factor that has the most effect on the signal attenuation due to the presence

of the ionic matter in the soil. The DC conductivity is most notable in the low frequency KHz range rather than high frequency MHz range (10 MHz - 1 GHz) (Campbell, 1990).

2.4.3 Magnetic permeability (μ)

Magnetic permeability is the material's ability to be magnetized when exposed to a magnetic field (Curioni, 2013). Magnetic permeability is included the real and imaginary number parts (Curioni, 2013). The real part (μ') is the storage of energy due to the lining of the domain in the atomic and subatomic spine direction, while the imaginary part (μ'') describes the loss of energy (Curioni, 2013). Magnetic permeability is described by the ratio of the absolute permeability of matter to the permeability of the free space ($\mu = 1.2564\times10^{-6}\, H/m$). The magnetic permeability is usually assumed to be one (Martinez and Byrnes, 2001).

2.5 Determining the EM properties of soil

To determine the dielectric properties of the soil, there are various prediction methods available and they are described in this section. The methods range from the phenomenological method, volumetric mixing models and semi-empirical functions. Methods such as the phenomenological method, such as the Cole-Cole and Debye models, connect the characteristic relaxation time to the frequency dependent material (Dam et al., 2005). These models predict the electromagnetic properties of soil for specific frequencies. For example, the Cole-Cole model investigates the polarization effect as a function of frequency that is given by Equation (2-38) (Dam et al., 2005).

$$\varepsilon^*(f) = \left[\varepsilon_\infty + \frac{\varepsilon_s - \varepsilon_\infty}{1 + \left({}^{jf}/_{f_{rel}}\right)^{1-\beta}}\right] - \frac{j\sigma_{dc}}{2\pi f \varepsilon_0} \tag{2-29}$$

Where $\varepsilon_s, \varepsilon_\infty$ are the static permittivity constant and the high-frequency limits of the real dielectric permittivity and f_{rel} is the dielectric relaxation frequency which is the frequency at ε'' reaches its maximum.

Another method introduces the use of volumetric mixing model attempt to characterise the dielectric permittivity of the material based on the relative amount of different soils and their individual dielectric permittivity (Curioni, 2013). The input parameters to the volumetric mixing models include the solid matter, water content and pore space which are dependent on the models used (Dam et al., 2005; Menziani and Rivasi, 1996).

The most recent models, which are semi-empirical, have tried to describe the relation between the dielectric properties, of the soil by considering the effects of the water content and soil composition (Topp et al., 1980). The models are valid only for the data developed in the models and do not necessarily offer a physical basis. Different semi-empirical models are proposed based on the measured data from the Time Domain Reflectometry technique such as Topp et al., (1980). Due to the direct measurement of soil moisture from the soil mixture these models are more accurate.

Information derived from the soil mixture will provide a good prediction of the soil characteristics; such as dielectric properties.

Overall, soil can be considered as a dielectric material and it is characterised by the dielectric properties, which are dependent on the temperature and soil composition (Dam et al., 2005). As described in section 2.4.1, the complex dielectric permittivity is defined by the real (ε') part and the imaginary part (ε''). The real part is the storage energy of the medium when it is impacted by an electric field and the imaginary part is the loss energy occurring during the relaxation of the medium. The real parts of the complex dielectric permittivity constitute the main parameter that affect the propagation of the signal through the soil. Thus, any increase in the smaller dielectric real part implies better conditions for the propagation of the EM signals (Vuran and Akyildiz, 2010). The imaginary part of the dielectric permittivity is caused by the rotation of the water molecules that are estimated to be in the range of 1MHz-10 GHz (Chudinova, 2009), and it is also caused by the electric conductivity during relaxation of the water molecules in the soil. Unfortunately, no reliable methodology exists to estimate the exact imaginary part of the dielectric permittivity from the soil directly. The dielectric losses can be eliminated in a material with a low conductivity of less than 10 $\frac{mls}{m}$ (Martinez and Byrnes, 2001). The recent common models that consider the real and imaginary parts of the dielectric permittivity of the soil used the soil mixtures and the Time Domain Reflectometry (TDR) (Peplinski et al., (1995); Topp et al., (2000)) mixing models described in section 2.5.1, which calculate the real and imaginary part of the relative dielectric permittivity in different frequency ranges (0.3-1.3GHz) and different soil mixtures.

From the review of the literature, it can be concluded that the behaviour of the electromagnetic signals in soil is mostly dependent on the soil properties and in particular the percentage of clay content, volumetric water content, porosity and the bulk density in the soil sample. A soil composition with a high parentage of clay content will tend towards more bound water and high bulk density, which directly affects the propagation of the signal. Water content is

assumed to be the main factor affecting the EM signals (Curioni, 2013). The soil mineralogy and dielectric properties of soil are described in section 2.4.

2.5.1 Prediction of the dielectric permittivity based on soil composition (mixing models).

Mixing models such as those of Peplinski et al., (1995) and Mironov et al., (2009) are used to characterise the real and imaginary parts of the relative dielectric permittivity of the soil based on the composition of the soil, specifically the proportion of the sand and clay of 19 set of distinctive soil condition, divided into four soil types and several moisture conditions. Initially, the models used different proportions of water content and composition, and measured the real and the imaginary parts of each soil at 399 data point by method of inserting coaxial probe directed into the soil while the second step is the comparison of the taken data with the existing dielectric mixing models such as that of Wang & Schmugge (1980). The final stage is to choose the best fitting curve data in the range of 0.3 to 1.3Ghz.

Peplinski et al., (1995) proposed dielectric permittivity measurements at different spaced frequency points in the range of 0.3 to 1.3 GHz. The dielectric permittivity of the soil is considered as a complex dielectric permittivity in this model given by Equation (2-39) (Peplinski et al., 1995b):

$$\varepsilon_m = \varepsilon'_m - j\varepsilon''_m \tag{2-30}$$

Where ε_m is the complex dielectric constant of the soil; $\varepsilon'_m and\ \varepsilon''_m$ are the real and imaginary components of the dielectric permittivity of the soil respectively.

Peplinski et al., (1995) the real and imaginary parts of the dielectric permittivity, given by Equations (2-40) and (2-41) consider the effects of the volumetric water content (m_v); bulk density (ρ_b); specific particle size density of the soil (ρ_s), that is $2.65\,{}^{g}/_{cm^3}$ (average value for sand); the empirically constant factor ($\alpha = 0.65$) and the relative dielectric constant of the free water ($\varepsilon_{fw}'^{\alpha}\ and\ \varepsilon_{fw}''^{\alpha}$) (Heimovaara et al., 1996).

$$\varepsilon_m' = \left[1 + \frac{\rho_b}{\rho_s}(\varepsilon_s^{\alpha} - 1) + m_v^{\beta'}\varepsilon_{fw}'^{\alpha} - m_v\right]^{1/\alpha} \quad (2\text{-}31)$$

$$\varepsilon_m'' = \left[m_v^{\beta''}\varepsilon_{fw}''^{\alpha}\right]^{1/\alpha} \quad (2\text{-}32)$$

The empirical proportion of the sand and clay constant $\beta' and\ \beta''$ are calculated using Equations (2-42) and (2-43) with the effects of the sand and clay mass fraction (S and C).

$$\beta' = 1.275 - 0.519\,S - 0.125\,C \quad (2\text{-}33)$$

$$\beta'' = 1.338 - 0.603\,S - 0.166\,C \quad (2\text{-}34)$$

According to Peplinski et al., (1995), the measured real dielectric and calculated dielectric values exhibit a high correlation of (r = 0.974) and finally the calculated dielectric value of the soil is linearly adjusted for higher moisture content (>15% VWC) soil by the equation shown as (2-44):

$$\varepsilon' = 1.15\varepsilon_m' - 0.68 \quad (2\text{-}35)$$

The dielectric permittivity based on the Peplinski model is calculated at 0.3 GHz frequency, illustrates the dielectric constant measured at five different water content contents (Peplinski et al., 1995b).

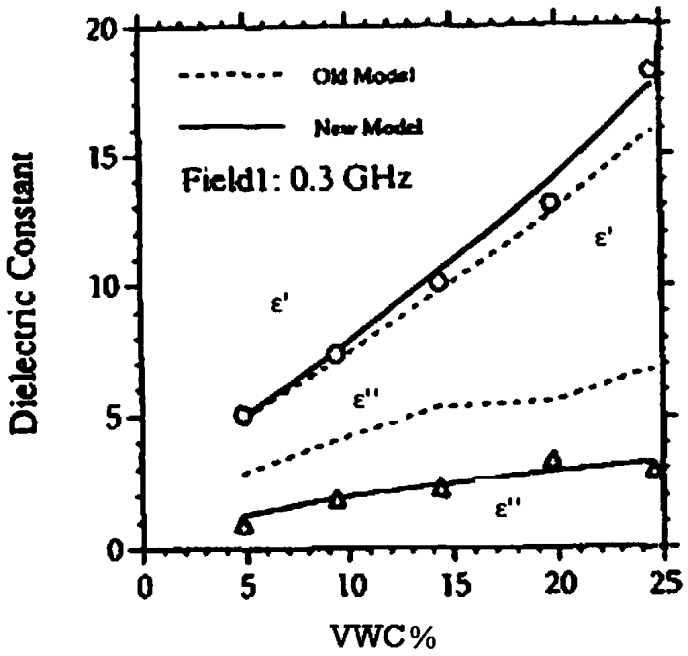

Figure 2-6 The effect of the volumetric water content on the real and imaginary parts of the dielectric constant of the soil, based on the Peplinski model (Peplinski et al., 1995b)

The old model indicated as mention equation as (2-39) and the new model refer to the equation (2-44). Mironov et al. (2004) proposed a model where the clay content is assumed to be a variable (0%-54%) input to the model and it investigates the effect of the dielectric properties of the soil by a combination of the mixing models to achieve a closer value for the real and imaginary parts of the complex dielectric permittivity.

Topp et al.,(1980) was developed as a model to predict the real and the imaginary parts of dielectric permittivity by the Time Domain Reflectometry (TDR) that described in details in Section 2.6.

2.6 Dielectric permittivity prediction model based on EM signals (Time Domain Reflectometry, TDR)

Time Domain Reflectometry is one of the most powerful techniques used for measuring the dielectric properties, such as apparent permittivity (ε_a) and bulk electrical conductivity (EC) of soil and also the volumetric water content (VWC) of the soil, based on the proposed models i.e. the Topp model (Topp and Davis, 1985). Basically, TDR is used to measure the changes of impedance of the EM signal along the transmission line. As long as a reflection is generated along the transmission line, the TDR source is responsible for measuring the voltage of the reflected signal. Therefore, it is possible to determine the location of the fault in the transmission line by measuring the return travelling time of the whole signal (Curioni, 2013). The Topp model used the parallel transmission line technique in soil science which can be considered as the turning point in the application of the TDR in geotechnical engineering aspects (Curioni, 2013).

2.6.1 TDR based on the Topp model

The Topp model (Topp et al.,1980) used the results from the TDR measurement for different varieties of soil (62 samples of mineral, organic, sea and river sand and etc) compositions and different soil particle size distributions in order to find the correlation with the TDR apparent permittivity(ε_a), using Equation (2-45) (Topp and Davis, 1985):

$$VWC = -5.3\times10^{-2} + 2.92\times10^{-2}\varepsilon_a - 5.5\times10^{-4}\varepsilon_a^2 + 4.3\times10^{-6}\varepsilon_a^3 \qquad (2\text{-}36)$$

Where VWC is the volumetric water content of the soil $\left({m^3}/{m^3}\right)$ and ε_a is the apparent permittivity of the soil measured by the TDR method (Curioni, 2013). The equation (2-45) developed based on four mineral soil material chosen to have different soil types (sandy loam to clay) and different organic matter. The particle size distribution applied to the soil samples to determine the soil particles (Topp et al., 1980). The model is considered to be suitable for soils with a water content of less than 50% (Curioni, 2013). Nowadays, TDR has become one of the most advanced technologies for achieving a good estimation of the VWC and bulk electrical conductivity of a soil sample, with an accuracy of $\pm 1-2\%$ (Jones et al., 2002; Robinson, 2002). The apparent dielectric permittivity of the soil is calculated based on the velocity of the signal propagation through the soil and the travelling time of the signal in the soil (Topp et al., 1980). Equation (2-46) shows the relationship between the velocity of a signal and the apparent permittivity.

$$v(f) = \frac{c}{\sqrt{\varepsilon_a}} \tag{2-37}$$

Where c is the speed of light in free space $3\times10^8\ {m}/{s}$. The apparent permittivity of the soil is calculated by the effects of the imaginary and magnetic permeability which is assumed to equal to one (Dam et al., 2013) and the operation frequency f.

$$\varepsilon_a = \frac{\varepsilon'(f)\mu_r}{2}\left(1+\sqrt{1+\left(\frac{\varepsilon_p''(f)+\frac{\sigma_{dc}}{2\pi f\varepsilon_0}}{\varepsilon'(f)}\right)^2}\right) \tag{2-38}$$

Topp et al., (2000) refined the equation by neglecting the effect of losses due to conductivity and dipolar losses by bound water and proposed a simpler relationship of apparent permittivity

equal to the real permittivity which is calculated. This was based on the TDR measurement waveform given by Equation (2-48). Figure 2-7 shows the apparent length of the soil from the head of the TDR probe where $L_{cal}\ (m)$ is the calibrated length of the probe which is obtained after the measurement reference materials with known permittivity and is very similar to the physical length of the rods, and $L_{app} = \left(\frac{ct_1}{2} - \frac{ct_2}{2}\right)\ (m)$ is the distance between two corresponding points (start and end point) of the probe (the ratio of the actual signal velocity and speed of light in free space is assumed as 1) for the convenience of analysis and this used to determine the apparent permittivity calculated in equation (2-49) by (Robinson et al., 2003).

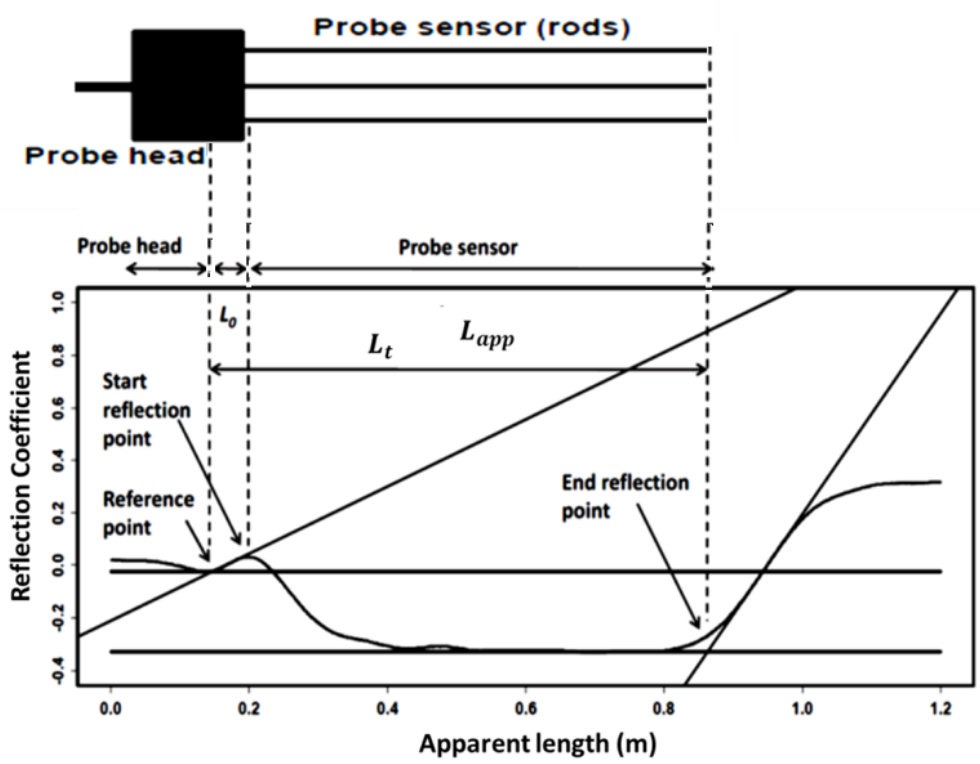

Figure 2-7 Schematic of the TDR waveform the soil (Curioni, 2013). L_0 is the distance along the TDR head probe. L_{app} is the distance between two corresponding points (start and end point) of the probe, L_t, is the total distance from the beginning of the probe head to the end of the TDR probe sensor.

Based on the TDR waveform, the velocity of the signal and the apparent permittivity are calculated Equations (2-48) and (2-49):

$$V(f) = \frac{2L_{cal}}{t} \tag{2-39}$$

$$\varepsilon_a = \left(\frac{ct}{2L_{cal}}\right)^2 = \left(\frac{L_{app}}{L_{cal}}\right)^2 \tag{2-40}$$

The Bulk Electrical Conductivity (EC) is calculated in the long apparent distance which measured by TDR, L_{app} from the Figure 2-7 because the last reflection of the EM signal may occurs at the longest apparent length. Giese and Tiemann, (1975) proposed a model in order to measure the bulk electrical conductivity. Different parameters are considered to calculate the EC to consider the effects of cable, multiplexor and connectors on the measured bulk electrical conductivity (Curioni, 2013). Finally, the EC equation (2-50), proposed by considering the TDR probe constant over the cable resistances is:

$$EC = \frac{K_p}{R_L - (DR_c + R_0)} \tag{2-41}$$

Where D is the cable length (m); $R_L and\ R_0$ are the resistance $\left(\Omega/m\right)$ due to cable and TDR device respectively; and $K_p = \frac{\varepsilon_0 c Z_0}{L}$ (Z_0 is the probe impedance and L is the physical probe length) is the probe constant that depends on the actual physical length of the probe which geometrically defined (Curioni, 2013).

2.6.1.1 Method of extracting complex dielectric permittivity values from TDR measurements based on the Topp model

Large scale studies have been performed on TDR measurements and it is important to understand the limitation of TDR accordingly in order to get an exact value of relative permittivity. Topp et al., (19 80) assumed $\varepsilon'' \ll \varepsilon''$ for the material with low conductivity and less than 50% clay content, because the soils with high EC and clay content will cause the imaginary part of the complex permittivity to increase and the Topp model will therefore be invalid (Topp et al., 2000). This becomes a serious issue with respect to the estimation of the water content of the soil by the Topp model. Different methodologies have been suggested by Topp, such as the separation of the real (ε') and imaginary (ε'') part of the complex permittivity and determination of the effective frequency, which has the greatest effect on the reflection of the signal and also includes effective conductivity losses (Bittelli et al., 2008; Topp et al., 2000).

From Figure 2-8., Topp et al., (2000) suggested a method in order to estimate the effective frequency as it carrying the majority of energy in along the TDR probe of the signal by considering the rise time (t_r) at the end of the probe reflection coefficient. It was recommended that the 10% to 90% of the end of the probe was the best approximation of the effective frequency $\left(f_{eff}\right)$ which is given by Equation (2-51) (Robinson et al., 2003).

$$f_{eff} = \frac{ln\left(\frac{0.9}{0.1}\right)}{2\pi t_r} \tag{2-42}$$

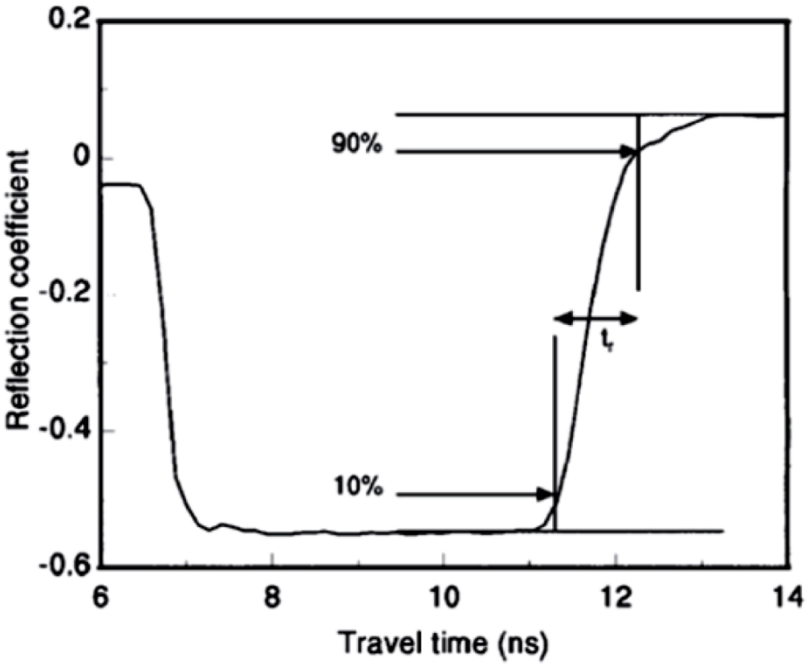

Figure 2-8 Measurement of the rise time, t_r from 90% to the 10% increase in the reflection coefficient of the TDR wave form based on the Topp model (Robinson, 2005)

In addition, Topp et al., (2000) initially assumed the apparent permittivity is the real part of the complex permittivity and through the determination of the effective frequency and conductivity estimated the corrected value for the real part of the complex permittivity, Topp et al., (2000). This process was repeated for the imaginary part, by initially assuming the imaginary part as zero and estimates the imaginary part by calculating the tangent loss of the TDR waveform (ratio of imaginary and real part of the complex permittivity). This way of soil complex permittivity was used in this experiment.

Overall, several definitions are available for describing the effective frequency, but the main definition is the frequency which included the highest energy from the TDR waveform (Robinson et al., 2003). However, different methods exist in the literature to estimate the effective frequency and the rise time from the TDR waveform such as Topp model. In fact, there is not enough explanation and evidence to show the existing models are suitable for

different soils as the models are limited to the laboratory experiments using the limited soil mixtures.

2.7 Key gaps in knowledge

The following are the main gaps identified based on the conducted review of the literature.

- The existing methods of estimating the EM signal attenuation in the soil are based on semi-empirical mixing models (i.e. Peplinski) which are not validated by a large range of soil and therefore, a more robust method for the extraction of the real and imaginary parts of the soil permittivity would be highly beneficial to the estimation models.
- Comparison of the Crim-Fresnel and the modified-Friis models of the estimation of the attenuation showed a large difference between these models which demonstrated that there is a need of further investigation into the accuracy of these models and comparison of their estimation accuracy in the same soil sample.
- Several methods exist for the estimation/calculation of the dielectric properties of soil, However, comparison of these models and their effect as input parameters for the existing attenuation estimation models. There is a need for an improved universal method for the estimation of the attenuation of the RF signals in soil based on the soil dielectric input parameters calculated by TDR as current estimation models cannot be universally applied for all types of soil and conditions.

Chapter 3 METHODOLOGY

3.1 Introduction

Based on the key findings from the review of the literature (see Chapter 2), it was evident that there was a gap in the previous research related to the uncertainty of the existing radio frequency (RF) models to accurately predict EM signal attenuation in different soil conditions. Therefore, this chapter describes the development of a laboratory based testing methodology to accurately measure EM signal attenuation for a range of soil compositions with a range of water contents that can then be used to more accurately validate existing models. Initially, it describes the preliminary experiment arrangement and the development of the final version.

There is a number of factors, such as shielding of the signal, which need to be considered as the EM signals are sensitive to environmental interference. Other factors discussed in this chapter are the material choice for the container construction, the soil to be used in the research and the measurements determined to be used to complete the laboratory experiments and a field test also conducted in parallel with the laboratory experiments in order to validate the measured results.

As a summary of the methodology, a container was developed to be filled with different soil compositions and to be able to insert the signal transmitter and signal receiver antennas to measure signal strength along certain distances. Two types of materials were tested for the container (plastic and aluminium) and after some initial trials, the aluminium container was chosen for the rest of the tests (the container design is described in detail in section 3.2.2). Two types of soil were tested for this research (Leighton Buzzard sand and English China clay) and the soil samples for this test were prepared in accordance with BSI (1990). To ensure maximum

control over the experiment against the effect of environment, a decision was made to initially carry out the RF signal measurement in the laboratory.

The soil samples were tested for RF measurement and the Time Domain Reflectometry (TDR) technique was used to characterise the soil type as well as dielectric properties of the soil. Finally, all the measurement results were gathered and compared with the existing RF models (i.e. the Modified-Friis). Two different set of tests were carried out during this project. 1) Laboratory tests of propagation of RF signals in various soil compositions and conditions and 2) Measurement of signal attenuation in a real environment (field trials).

As was mentioned in the section 2.1 signal propagation in a soil is a challenging issue for EM signal prediction, as the signal characteristic of the soil could change between soil types and soil conditions (Stuntebeck and Akyildiz, 2006).
This chapter provides the details of the development of the methodology used in this research.

3.2 Experimental design

In order to test the RF transmission, a laboratory set-up had to be developed. A container was required that would allow consistent soil composition and methods to insert antennas at different distances along the sample to measure signal intensities. The signal intensity measurements required a signal generator and a signal spectrum analyser for reading the received power of the signal at each hole placed on the container. Moreover, the signal propagation measurement was limited in the laboratory requiring controlling the effect of the environment on the signal. Based on these requirements the test apparent was developed, also taking practical consideration into account.

3.2.1 Limitations and factors affecting the laboratory trials

The aim of the experiment was to determine the attenuation of the radio frequency (RF) signal through different soil mixtures. As the propagation of the RF signal has a complex nature, it was important to consider any negative factors affecting the measurement results in order to minimise their effects (Silva and Vuran, 2010). The main factors that affect the signal propagation in a laboratory are:

- Environment interference (i.e. coupling) on the sensitivity of RF equipment
- RF antenna orientations
- Electromagnetic signal shielding which eliminates the effects of reflection and refraction of the signal
- Uniformity of the soil samples (water content, mixture and density)
- Compaction of prepared soil samples

Regarding the issues listed above, the design of the experiment arrangement was an important stage of the experiment. Therefore, several factors needed to be considered in the methodology of the experiment which is described in section 3.2.2 (below).

3.2.2 Soil container design

Based on the issues listed above in section 3.2.1 several factors needed to be considered in the design process of the test bed and are listed below:

- Soil container's shape, geometry and material
- Elimination of any environmental interferences (i.e. reflection of the signal)
- Soil composition and compaction methods
- Measurement techniques

- Equipment (measurement and mixing equipment)

The geometry and material of the soil container had to satisfy both practical (i.e. handling) and technical (i.e. RF signal transmission) aspects of the experiments. The main parameters used for the determination of the design of the soil container were:

- The frequency of the transmitted RF signal
- Compaction method for the soil inside the container
- Protection of the signal from environmental interference (reflections

In addition to the above mentioned factors, there are several practical issues such as the estimated weight of the container when full and the total volume of the container had to be taken into account in order to ensure that the soil preparation and material handling involved in the experiments was possible in the laboratory.

Frequency was an important issue with developing a container size. As RF propagation has two phases, first one is near-field transmission and the second one is far field transmission. These two phases related to the operating frequency wavelength and also the RF models that have been introduced in the literature review (Chapter 2, Section 2.2.1 and 2.2.2) are validated in the far field transmission. Moreover, the required frequency for this test initially calculated based on this field and the size of the container was also taken into the account.

In term of the frequency of the RF transmission signal, the signal generation and measurement were carried out by transmitting an electromagnetic signal through the soil using a signal generator from the frequency range of 434MHz – 2604MHz in multiple frequencies of 434MHz and measuring the signal strength at the required distances via an RF spectrum analyser. These frequencies were selected mainly due to their availability as commercially available bands (434 and 868MHz) and based on the multiple frequencies of 434MHz (to ensure a more uniform response from the antenna across the frequencies). Multiple holes were

required to be located along the container in order to place the transmitter and receiver into the soil for measuring the signal strength without removing the soil from the container and also to determine the effect of the distance on the signal intensity. The distance between the holes was calculated based on half the wavelength of the carrier frequency. The reason for this was that the minimum distance of the holes should be calculated in order to eliminate the influence of the near field and far field transmission on the signal measurement. The near field measurement was conducted very close to the non-radiative transmitter antenna, while the far field was at a further distance from the electromagnetic radiation transmitter antenna, the operational frequency of which the range of the near field and far field is related (Yaghjian et al., 1986). The near field is generated by the magnetic and electric dipole, which transfers power close to the source of the signal; but this power dies very rapidly as the distance increases. This field does not propagate freely with signal oscillation. Therefore, none of this behaviour is counted as the EM radiation.

Equation (3-1) gives the calculation of the wavelength of the operational frequencies relates the wavelength, λ, of the signal; the speed of light, $C\ is\ \left(3\times10^{8}\frac{m}{s}\right)$; the frequency of the signal, f:

$$\lambda = \frac{C}{f} \tag{3-1}$$

The diameter of near-field radiations, R is given by Equation (3-2)

$$R \geq \frac{2D^{2}}{\lambda} \tag{3-2}$$

Where D the largest length of antenna which is 0.328m, for a carrier frequency of 434MHz. Hence, the 434MHz signal has a largest half wavelength (0.34m) in the air. Based on equation

(3-2) the calculated near field for a frequency of 434MHz is ≤0.34m. Therefore, the distances between the holes were chosen to be half of the diameter of radiation. Table 3.1. illustrates the calculated wavelength and diameter of radiation for the operational frequencies used in the experiment.

Table 3-1 Calculated wavelength and the diameter of radiation for the operational frequencies

Frequency (MHz)	Wavelength in air (m)	Diameter of radiation near field (m)
434	0.691	0.340
868	0.345	0.167
1300	0.230	0.104
1736	0.172	0.085
2170	0.138	0.068
2604	0.115	0.056

Based on the calculated wavelengths Table 3-1 the minimum distance between the signal generator and the signal receiver was assumed to be bigger or equal to the half diameter of radiation for the 434MHz, in order to eliminate the effect of the near field transmission on the measurable signal intensity.

A container with holes was required for the soil samples in order to measure the signal strength along the desired holes. Initially, a cylindrical shape with the diameter of 10 cm was chosen to ensure maximum contact between the compaction rammer (4.5 kg rammer with the diameter of 10cm) to have maximum contact surface between soil and rammer and the soil surface at the edges of the container (is avoiding sharp corners which the rammer cannot get to). Also

the size of the antenna (length = 58mm and width = 10mm) used must be located in the centre of the container to ensure a direct transmission path. The length of the container was chosen based on the initial minimum distance for placing the signal generation antenna and the signal spectrum analyser antenna, although the longer container is not appropriate for the soil preparation for this test, as the compaction of the soil mixture will be more challengeable in the laboratory. In addition, for measuring the signal strength at different locations (at least four different distances) in the container, it was decided to have more holes 10cm apart from each other and investigate the effect of the distance on the transmitted signal from the signal generator. On the other hand, the length of the container was an important issue in order to ensure compaction of the soil and the correct amount of soil used for each soil composition type. Figure 3-1 shows the initial design of the container and also the location of the signal generation antenna in the container.

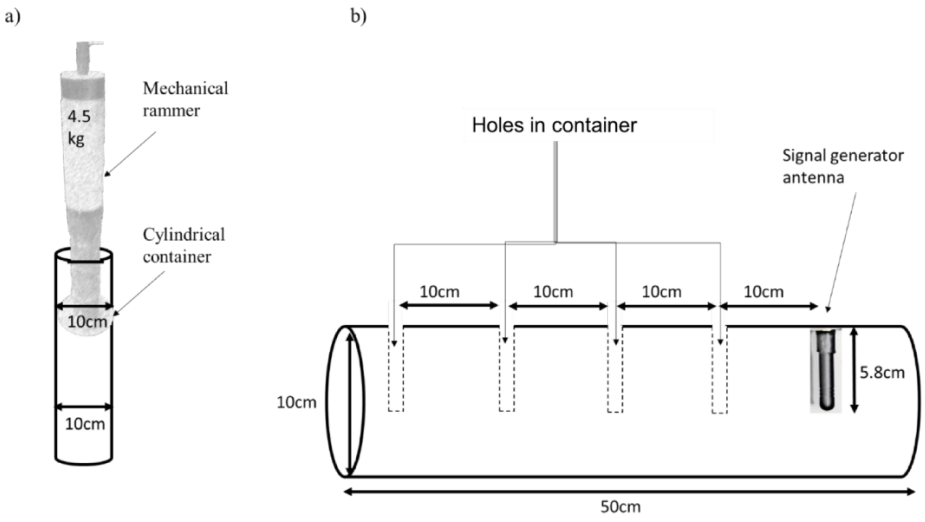

Figure 3-1 Schematic of the initial idea for the container b) the holes placed for measuring the signal strength along the container

The length of 50cm was selected for the container based on the initial minimum distance for placing the signal generator antenna and the signal spectrum analyser. Figure 3-2. illustrates

that the holes were placed 10cm apart. Despite the frequency of 434MHz needing more of an interval from the source of the EM signal i.e. 0.16 m, as discussed previously, the first hole was located for the multiple frequencies of 434MHz, as shown in Table 3-1, 10 cm bigger than the near-field transmission.

Based on the calculated sizes for the container, initially, a plastic container was chosen for the signal measurement test. Plastic as a material for the container was selected because of availability of plastic tubes in different sizes in the laboratory and also the weight of plastic was much less than other material such as Iron or aluminium and was easier to prepare the soil. The plastic container was made from separate smaller sections in order make the process of soil preparation easier in multiple stages repeatable and ensure uniformity and homogeneity in the soil sample. Figure 3-2. a) shows a photograph of the container assembled and in parts.

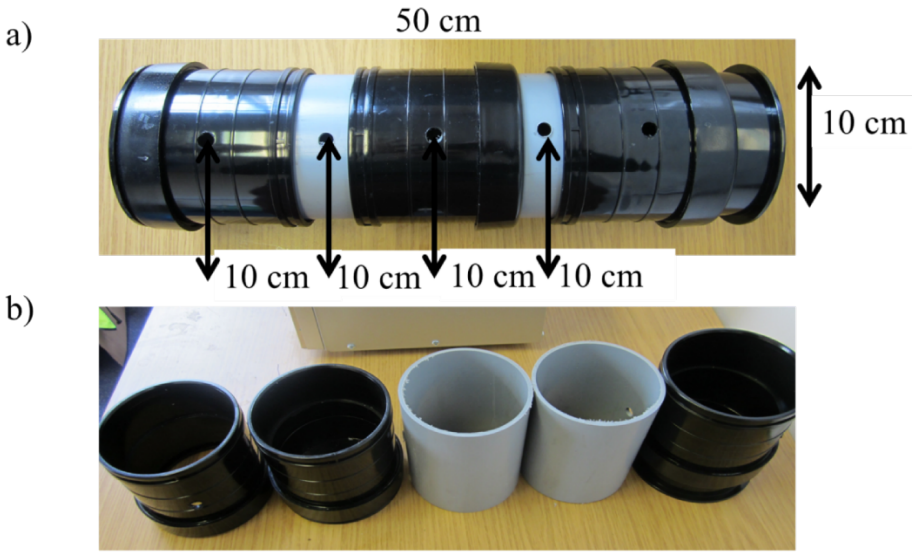

Figure 3-2 The plastic container assembled, b) the container in parts

The container was filled with a soil composition of 90% Leighton Buzzard sand, 10% English China clay and 10% GWC. This was the easiest composition to prepare and therefore was most

suitable for initial tests. A frequency of 434MHz was used for the signal transmission as this is one of the most commonly used frequency bands for wireless sensor networks. After the first signal transmitting tests through the soil, it was discovered that the difference between the permittivity of the soil (ε = 9.28) and the plastic (ε= 2.2 to 2.36) container caused reflection of signal at the container and soil boundary back into the container resulting in inconsistency of signal strength values along the container as the signal strength has to be decreed as travels in longer distances (Gershun, 1945). The test was repeated three times and the error bars represent the range of reading (min and max). The results show the importance of the material used for the container. Figure 3-3 shows the of the measured signal strength in the plastic container filled with soil compared to the empty container.

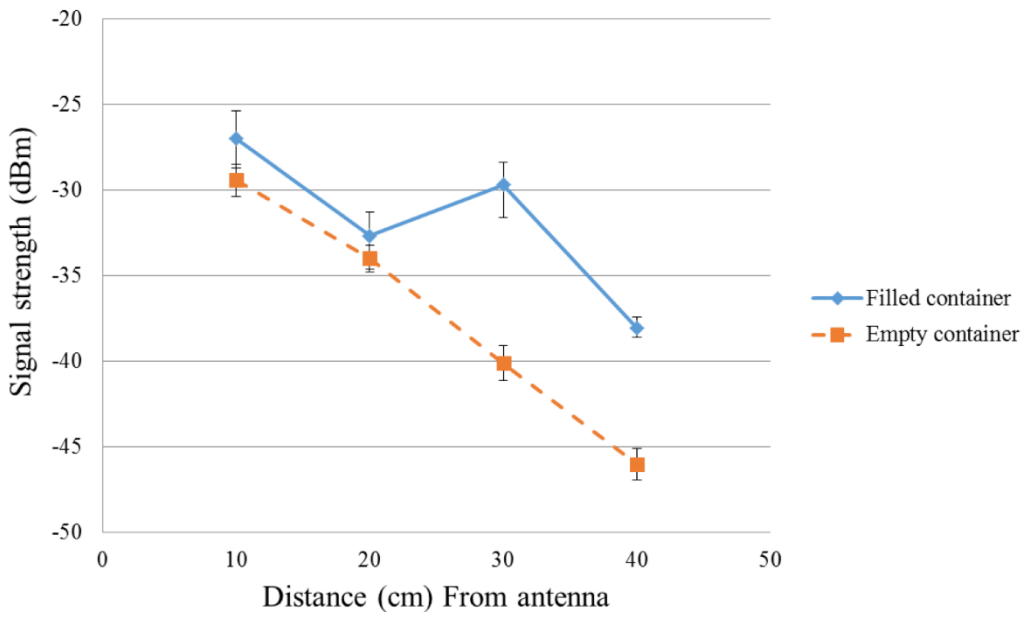

Figure 3-3 Signal strength with distance from an antenna measured through soil and air in the plastic container

As shown in Figure 3-3. the signal strength appeared to be bigger in the soil, despite the signal being expected to be lower in the soil and higher in the empty container. The data used for this figure can be found in Appendix B.1. The reason for this was due to the signal being reflected

back into the container as it reached the soil-container boundary due to the dielectric permittivity differences between container boundary and the soil, which made the container behave like to a waveguide. Figure 3-4 shows a schematic of the effect and how the signal is reflected back into the container when reaching the container wall and this continues all along the container. This results in a higher signal strength as it can carry higher energy along the container.

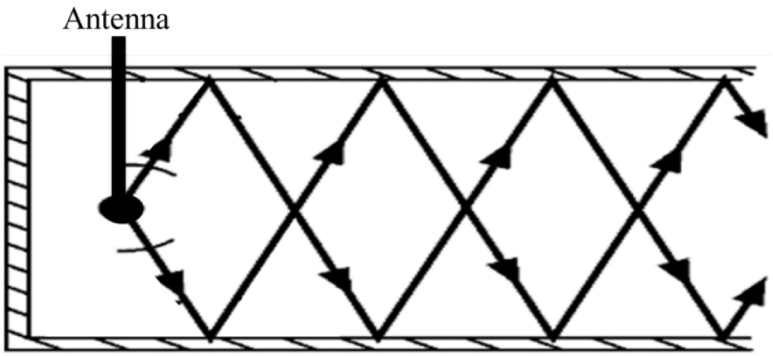

Figure 3-4 Effect of a waveguide along the container caused by the reflection of the signal at the soil container interface.

The test was continued with shielding the plastic container with aluminium foil in order to remove the waveguide effect in the container and repeated three times, however, it was not successful because the measured signal strength did not follow the expected trend of constant decline of signal strength as it was shown in Figure 3-3. As an example, the plastic container was surrounded with aluminium foil to eliminate the effect of environment signal interfacing container and also eliminate the signal crossing from inside the container, as can be seen from Figure 3-5, also the foil was earthed to the ground to cancel the generated current around the conducted material.

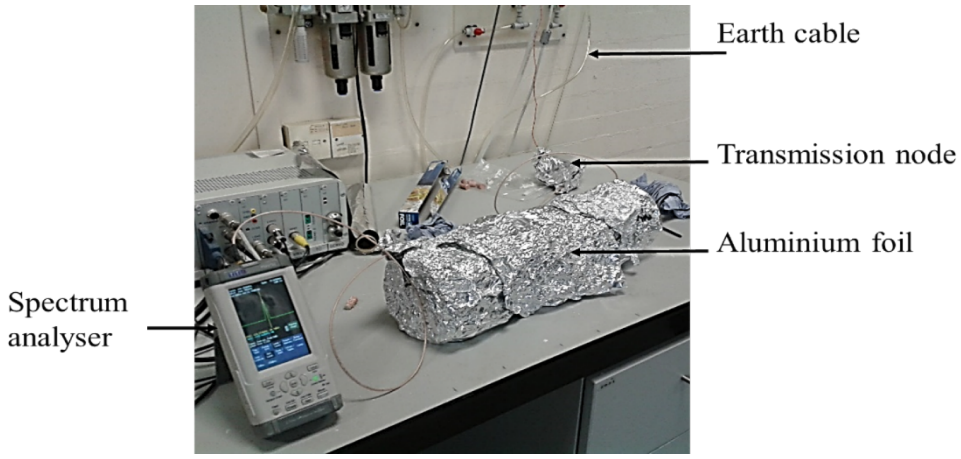

Figure 3-5 Signal measurement carried out using the plastic container which was wrapped in aluminium foil, the foiled container was earthed by the earth cable

Figure 3-6 shows that the measured data along the container is shifted by -10±3(dBm) to a lower signal strength when compared with Figure 3-3. Despite the cancellation of the waveguide effect, there was an inconsistent trend for the soil measurements compared to air measurements caused by an air gap between the container and the aluminium foil; where the signal was reflecting back into the container from the air gap resulting in inconsistency measurement values.

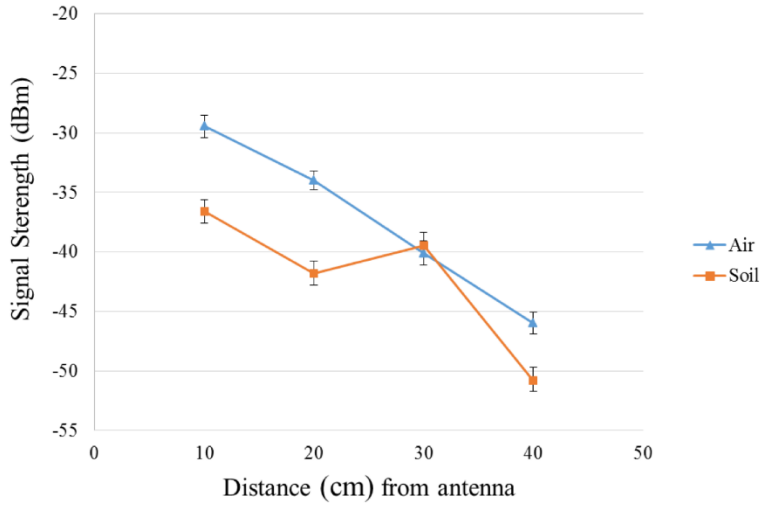

Figure 3-6 Signal strength with distance from an antenna for the plastic container soil and soil filled

The measurements were tested in the soil with similar composition as a previous test and the air. The error bars show the range of the three measured min value and max value and Appendix B.2 presents all the raw data used. It was noted that the plastic container acted like a traditional metallic container because of the aluminium foil reflecting the signal, due to its conductive nature which can be seen from the result of test in Figure 3-6 at distance of 30cm the signal strength became stronger compare to the signal strength at 20cm due to unwanted signal reflections. Therefore, a decision was made to use a metallic container for the rest of the tests. Figure 3-7 shows the aluminium container used in the tests.

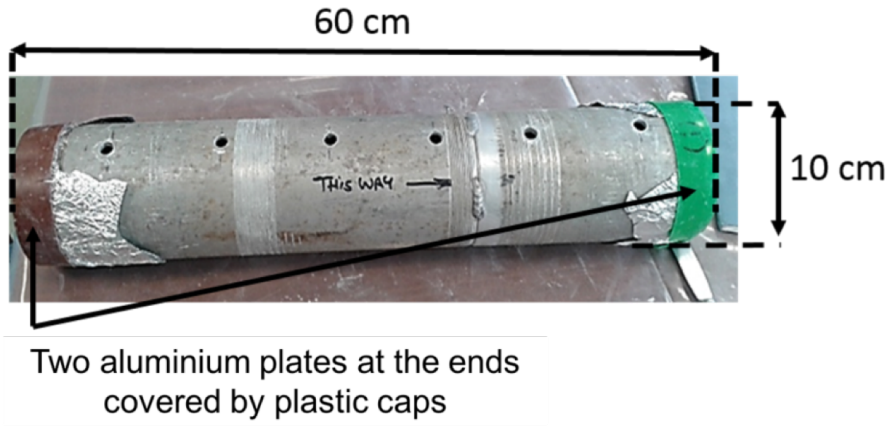

Figure 3-7 Aluminium container used to replace the plastic container.

The length of the container was increased in order to allow signal measurements at larger distances to observe and have a better understanding of a signal propagation at longer internode distance and also to able to have more points of measurement. Two aluminium plates were used as the caps of the container and as previously holes were placed at 10cm spacing. Figure 3-8 shows the signal strength measurement result from a soil with the composition of 50% clay, 50% sand and 10% GWC. The test repeated three and the error bars show the min and max measured value from the test.

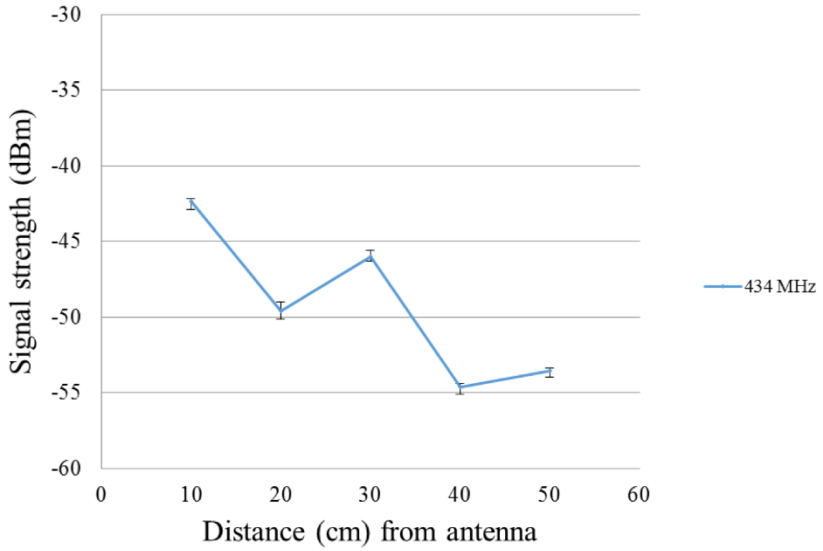

Figure 3-8 Result from signal measurement in an aluminium container with no earthing

Initially, the signal transmission was tested on an aluminium container which was not earthed and from Figure 3-8 can be concluded that another physical phenomenon effected to the signal measurement and the results have not decreased (data can be found in AppendixB.3). Therefore signals upon contact with the container walls generated a magnetic field over the metallic container that is called an eddy current (Yamane et al., 2000). However, according to Yamane et al, (2000), the magnetic dipole induced from an eddy current flowing on the surface of a metal particle contributes to the absorption of an electromagnetic wave. The eddy current generates a magnetic field in the wall of the aluminium container, which eliminates the effect of the reflections caused by the aluminium container. Grounding the metallic enclosure eliminates the reflections of the EM wave because of the eddy current magnetic shielding (Cross, 2014). Figure 3-9. shows the schematic of the eddy current generated on a conductive material (i.e. aluminium).

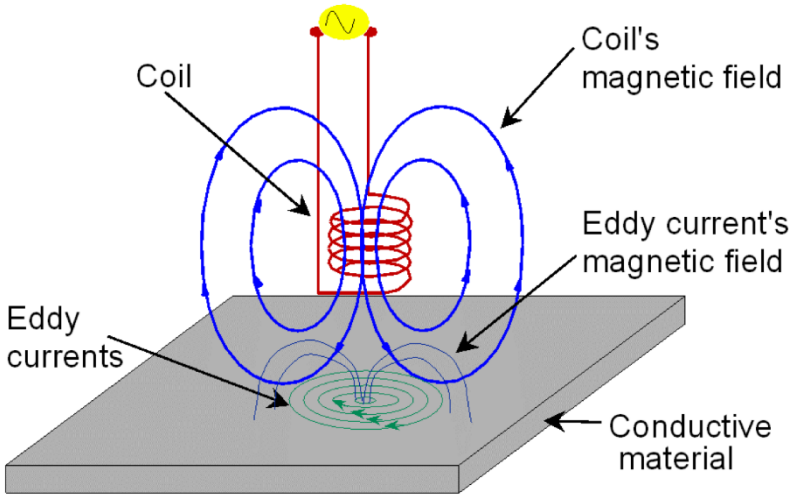

Figure 3-9 Schematic of the eddy current generated due to the electromagnetic field on the surface of a conductive material (http://www.microwavesoft.com/eddycurrent.html)

The earthing of the conductive material (aluminium container) and generating eddy currents is not the basis of this study and it is assumed to be an effective method of absorbing the EM reflections in the aluminium container. In order to test the effectiveness of the grounding of the aluminium container, a simple test was set up. The container was closed at both ends but was not filled with soil. Thus the signal in the container was travelling through the air. The antennas were inserted into the container and a received signal strength obtained at the specific distances along the container.

The results from the metallic container with the earth connection appeared to not be affected by the reflection and waveguide effect, as they follow the expected trend. Figure 3-10 shows the consistency of the results for signal strength with both 434MHz and 868MHz frequencies from the empty aluminium container compared to in just air and also a soil filled container filled with soil.

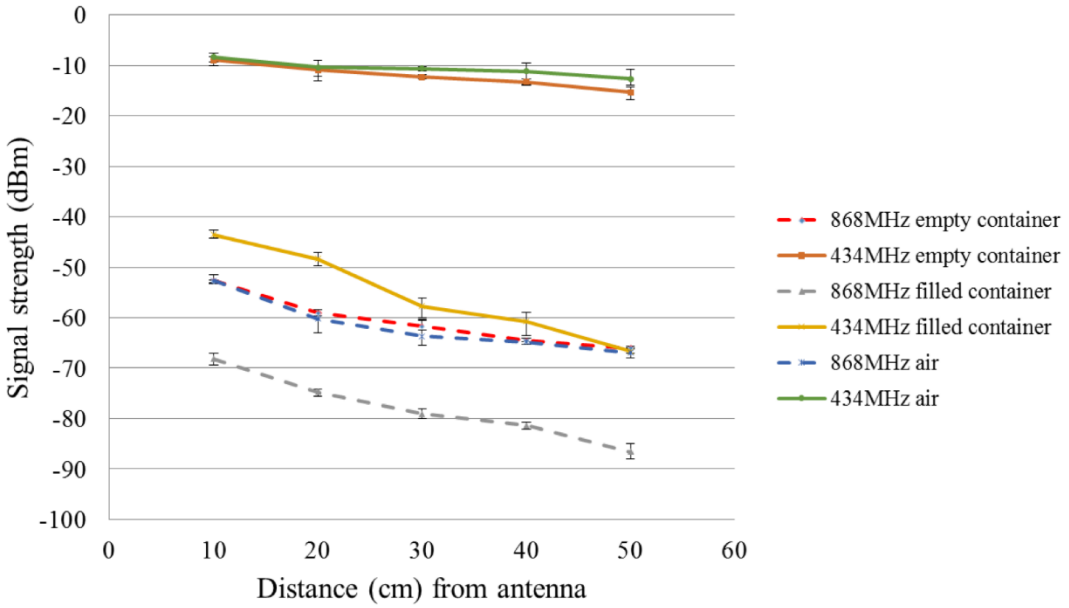

Figure 3-10 Received signal strength with distances from the antenna for the earthed aluminium container for 434 and 868 MHz frequencies

The data plotted in Figure 3-10 are the average of three repetitions each of the signal strength at the five fixed positions along the container and the error bars shows the range of minimum and maximum measured values. The signals were generated by the signal generator nodes that were designed by a previous researcher at the University of Birmingham (Sadeghioon, 2014). The node was designed for the specific frequencies of 434MHz and 868MHz. As shown in Figure 3-10. the correlation found between the signal strength results from the empty container follows the same trend as the air measurement at similar distances for the 434MHz; but the results show the measurements after the 20cm distance diverge, which was expected due to the signal generator output error (±3dBm) which create non uniform output. From Figure 3-10, the signal strength results from the empty container compared to in just air follow a decreasing trend with distance; but it is clear in Figure 3-10 that the measured data for the 868MHz air drops sharply at a distance of 20cm and becomes more deviated from the 868MHz empty container trend. The difference between the measurements for the 868 MHz signal strength is due to the signal generator nodes, which can have an inconsistent output power. The expected

decreasing trend is observed in Figure 3-10 is due to the attenuation (-6dBm) of the signal at the specific distances for both 434MHz and 868MHz. These trials showed that the effect of the waveguide due to the reflection of the signal was cancelled by earthing the aluminium container, which resulted in the consistency of measurements with errors in measurements of less than 0.5%. Therefore, the earthed aluminium container was being used for all future tests. Found all used data in Appendix B.4.

To ensure that the output power effect of the signal generator nodes was not affecting the measurement data, a signal generator was replaced instead of the nodes. The signal generator and the signal spectrum analyser were connected to the antennas with coaxial cable (shielded wire) and the length of the cable was chosen for three meters long to keep signal generator and the signal spectrum analyser about six meters apart from each other. The output power of the signal generator and the response of the antenna at the selected frequencies were measured in order to achieve a base reference for the measurements in Figure 3-11. Figure 3-11. illustrates the measured output of the signal generator and response of the antenna for selected frequencies and distances.

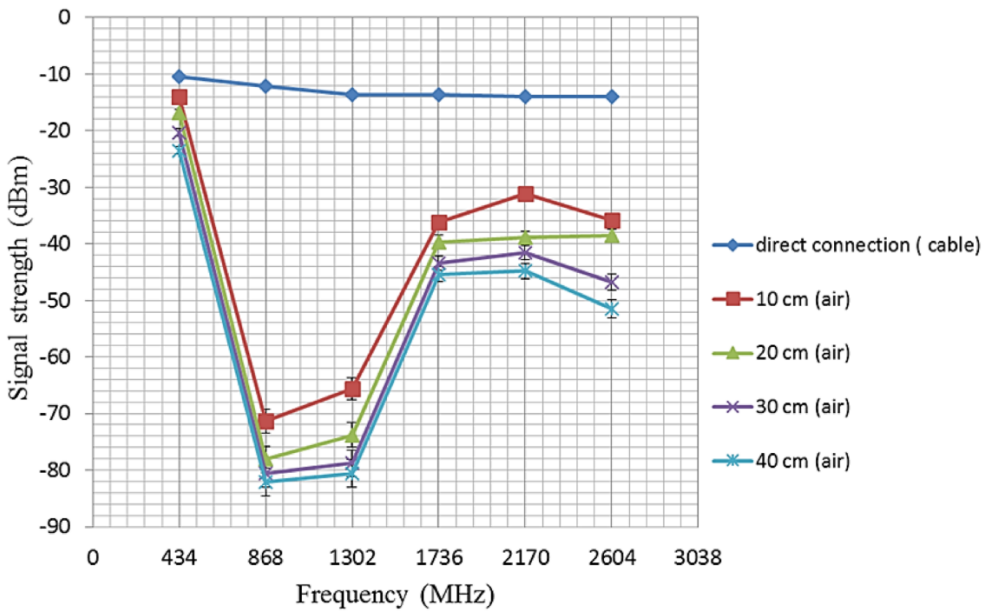

Figure 3-11 Measured power output of the signal generator and the response of the antenna at selected frequencies

It can be seen from Figure 3-11, that the measured signal intensities at the frequency range of 434-2604MHz for direct connection (coaxial cable) showed a relatively constant power output for the signal generator. These data showed that the output of the RF signal generator minimally decreased from its maximum (-10.4dBm) at 434MHz to a constant output level of -13.9dBm for a majority of the frequency range. However, despite the consistent output of the signal generator, when the signals were measured using a 434MHz antenna, the received signal intensity was not uniform and the antenna performed differently across the frequency range. The best performance of the antenna was measured at 434MHz (at all measured distances); this was to be expected as the antenna was specifically tuned for 434MHz (half wavelength). It was expected that with an increase in the frequency of the signal the received signal intensity would decrease (due to higher attenuation in air). However, the received signal intensity at 868MHz and 1300MHz was significantly lower than the expected range of -20 to -30dBm. This unexpected drop was caused by incompatibility between the design (tuned inductive load) of the antenna and the affected frequencies. Although the signal strength for frequencies

(>1300MHz) was lower compared to 434MHz, unlike 868MHz and 1300 MHz, this was within the expected range due to attenuation in air and therefore was not highly affected by the design of the antenna. In addition, it can be seen from Figure 3-11. that, as expected, as the distance increases the received signal intensity decreases.

3.2.3 Signal transmission equipment

An RF signal generator (RF Explorer, RFE6GEN) was used to generate RF signals at the desired frequency range (434MHz-2.6GHz). This frequency range was selected as most commercial wireless sensor networks operate in this range. An RF spectrum analyser (Aim-TTi PSA-2702) was used to measure the intensity of the generated signals at each test frequency. The range of the spectrum analyser was approximately from 1MHz to 2700MHz and it had a limit of -96dBm at the -20dBm reference level. Therefore, the signal strength of the frequency 868MHz and above were not measurable in some trials. A three metre long coaxial cable used to connected the signal generator (Figure 3-12), and spectrum analyser with six meters distance apart to decrease the effect of signal noise on both.

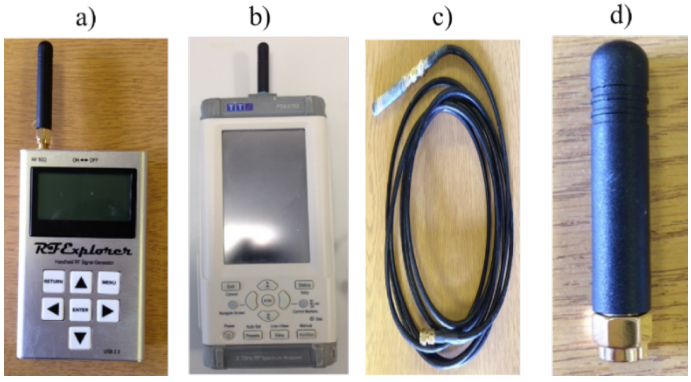

Figure 3-12 The signal generator, b) The RF spectrum analyser, c) Three metre coaxial cable and d) The 434MHZ antenna

3.2.4 Geophysical soil testing equipment

A TDR100 was used to measure the dielectric properties of the soil, such as apparent permittivity and bulk electrical conductivity. The dielectric properties of the soil were used to determine its geotechnical properties e.g. the volumetric water content (VWC) of the soil. The reason for using TDR was to compare the existing geophysical models, (i.e. Topp et al. (2000) and Peplinski et al, (1995), in order to validate the accuracy of the input parameters i.e. the complex dielectric properties of the soil and VWC, into existing signal transmission models, e.g. Modified-Friis and Crim-Fresnel.

In addition, the apparent permittivity and electrical conductivity of the soil samples were calculated using the TDR waveform based on the method proposed by Topp and Davis, (1985). The TDR waveform analysis was carried out based on the MATLAB software scripts developed by Curioni, (2013) to calculate the apparent permittivity and bulk conductivity, with an attempt made to further develop the existing methods (Curioni, 2013). The apparent permittivity and bulk conductivity were determined based on the first estimation of the apparent length of the TDR (Curioni, 2013). Topp et al., (2000) suggested a method to estimate the effective frequency of the signal by considering the rise time (t_r) at the end of the probe reflection coefficient. It recommended that the 10% to 90% range of the end of the probe is the best approximation of the effective frequency (f_{eff}), which is given by Equation (3-3) (Robinson et al., 2003).

$$f_{eff} = \frac{ln\left(\frac{0.9}{0.1}\right)}{2\pi t_r} \tag{3-3}$$

Figure 3-13shows a TDR waveform with conductivity line and also the location of the rise time which used as an input into the Topp model to extract the real and imaginary part of the complex permittivity.

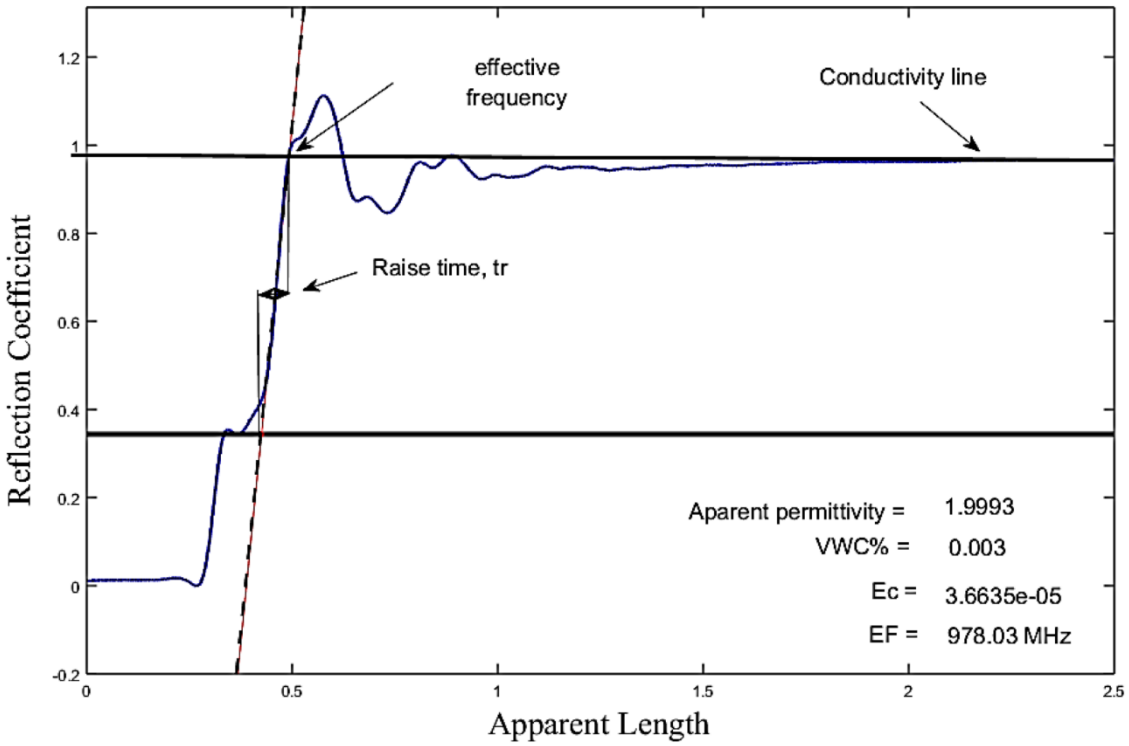

Figure 3-13 Shows a random TDR waveform and the location of the rise time

The real and imaginary parts of the soil were calculated based on Topp model (Topp et al., 2000) method. Moreover, the attenuation of the signal was analysed based on the new real and imaginary component of the complex dielectric permittivity from the TDR and existing models, i.e. Peplinski et al. (1995), in order to investigate the effect of the estimated real and imaginary parts of dielectric permittivity on the signal transmission models.

The TDR measurement was tested using three repetitions in a controlled soil sample, which was prepared in a cylindrical container with dimensions of 10cm x 10cm Figure 3-14. A probe

of 7.5cm length and 3cm width was used with the TDR100 unit and the probe calibration was carried out based on the method developed by Curioni (2013).

Plastic was chosen for the material of the container instead of metal to eliminate the influence of signal reflection via the container wall interference.

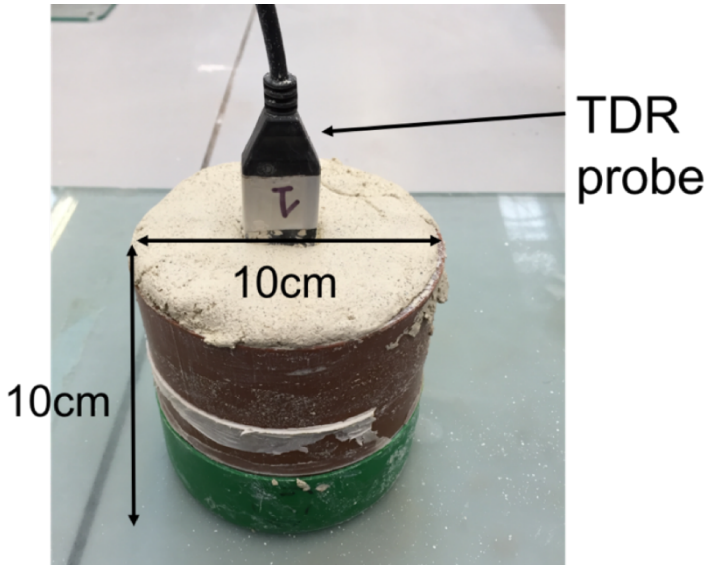

Figure 3-14 Installation of the TDR probe into the soil sample

Figure 3-14. shows that the TDR probe was placed at the centre of the container in order to ensure the TDR probe was surrounded equally on all sides to control the effect of the signal reflection of the signal from hitting the container walls.

3.2.5 Final test setup

The final test setup can be seen in Figure 3-15. The main difference between this test arrangement compared to the previous version was that the antennas were directly connected to the transmission node and the spectrum analyser without the need for an extension cable. It

was decided not to use a cable extension as the cables were not fully shielded and thus may have affected the accuracy of the tests.

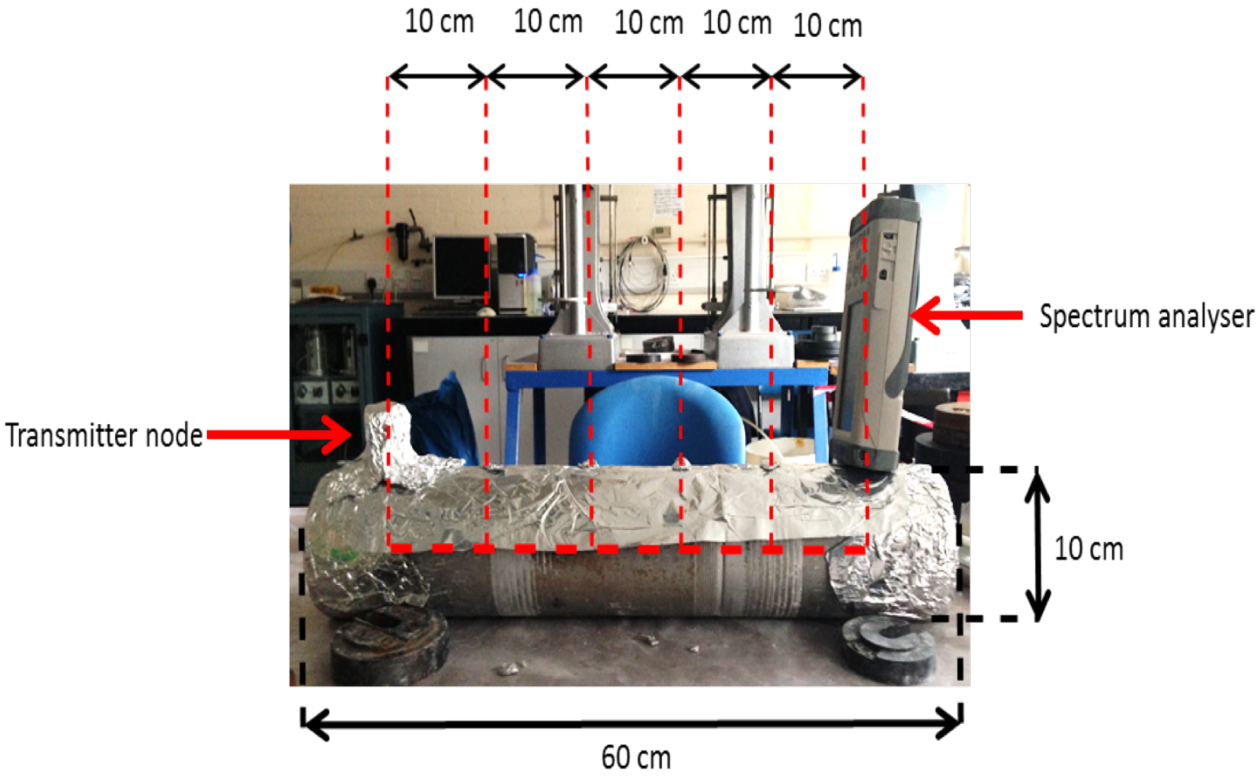

Figure 3-15 Final test setup

The antennas were placed in the vertical direction during the tests because the position of the antenna could affect the received signal (Silva, 2010). The container was placed in the same location for all the tests and attempts were made to keep the room temperature in the range of 24 ℃ ±1 degrees for the entire duration (approximately 4 hours) of the tests. The reason for this was to keep the water content constant during the test. However, because of the limitation of the laboratory cooling system in the temperature controlled room varied between 23 and 26℃.

3.3 Soil used in the experiment

As demonstrated in section 2.5 of literature review the mineralogy of the soil significantly influences the behaviour of the soil mixture. For clay minerals, the mineralogy is the primary factor that controls the size, shape and properties of the soil particles. The mineralogy has a major influence due to the soil particle interaction with the water molecules, which can be strongly attracted to and absorbed by the surface of the soil particles. The particle shape and size are essential characteristics controlling the bulk density, gravimetric water content and void ratio, and these factors also detail the compaction procedure applied to the soil mixtures. The dielectric properties of the soil are also critically dependent on the soil mineralogy, which affects the attenuation of the RF signal.

In these experiments, the soil composition was defined in terms of the percentages of sand (Leighton Buzzard sand was used in these experiments), and the clay content (English China clay was used in these experiments) which is a standard clay type used in laboratory experiments. Details of these soils are presented in section 3.3.1.

3.3.1 Soils used in the experiments

The clay used in these experiments, English China clay also called kaolin clay (Thomas, 2010), is defined as all constituents of the soil smaller than 0.002mm (BSI 1377, 1990). Clay has a much higher surface area compare to the sand due to the small particle size and platy or elongated morphology of the minerals. The surface area of clay particle has a major influence on the liquid solid interface resulting in the cohesive properties of clay. Generally, the smaller the particle, the smaller the pores between the particles; thus clay will have a small capillary size (Curioni, 2013).

To show the influence of granular soil in signal transmission in the soil, Leighton Buzzard sand was used in this study. Leighton Buzzard sand is a natural uncrushed silica that is free from silt, clay or organic matter (Kingston et al., 2008). It is a relatively uniform sand of sub-angular particles. Sand was used in this experiment to investigate the influence of bound and free water in the mixture of sand and clay.

The particle size distribution (PSD) of the sand was determined by dry sieving based on the BSI (1990) to ensure the uniformity of the sand particle size and it shows in Figure 3-16.

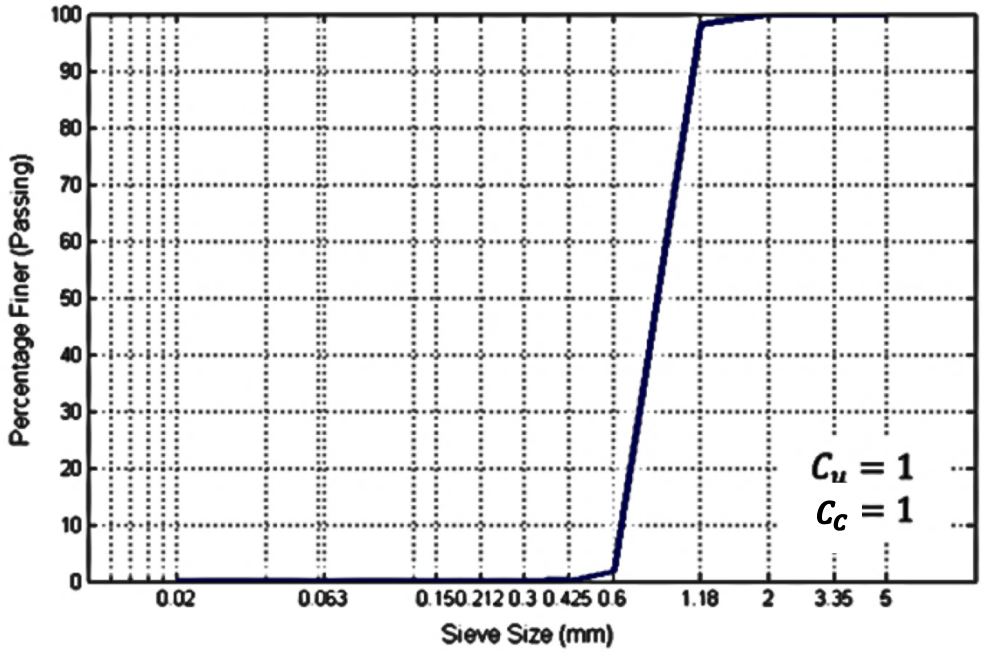

Figure 3-16 Particle size distribution for the Leighton Buzzard sand

Figure 3 17 Particle size distribution for the Leighton Buzzard sand, the uniformity coefficient (C_U) and coefficient of gradation (C_C) are both equal to 1, which indicates that the sand used in the tests can be classified as a single-sized soil. The uniformity of sand is an important factor in this experiment in order to minimise the effect of different sand particle sixe into the signal and also the effect of sand particle on water.

Figure 3-17 shows the PSD for the clay (English China clay) obtained by the wet sieving method (BSI 1377, 1990).

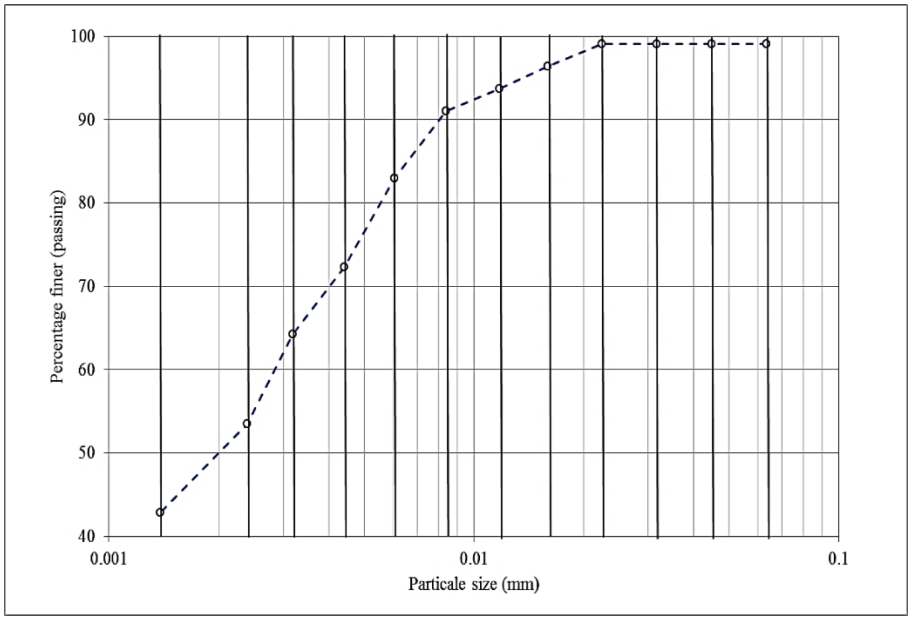

Figure 3-17 Particle size distribution for English China clay (kaolin)

As can be seen from the Figure 3-17, the Particle size distribution for English China Clay (kaolin) shows the clay particle size is distributed uniformly and as the clay definition state, a 43% of clay particles are less than <0.002 (Clayey Silt).

Both of the described sand and clay have used for this experiment for soil mixtures. Found data in Appendix B.5.

3.3.2Soil preparation

In order to understand the effect of sand and clay on the propagation of electromagnetic signals in the soil, it was decided to use a range of sand and clay mixtures based on their different specific surface areas and water absorption potentials. There is a major drop in the signal

strength with an increase in water content above 20% and minimal change in path loss after 30% (Yu et al., 2013). It was thus decided to use different fractions of sand and clay at three gravimetric water covering the common range of water contents (GWC) to investigate the effect of the soil composition and condition on the signal propagation i.e. 0%, 10%, 20% and 30%. Table 3-2 presents the soil mixtures used in these experiments, Samples of 12kg of the soil was prepared for each test to ensure a sufficient quantity of the soil sample was available to fill the container and use for classification testing.

The mixing of the soil was carried out based on BSI (1990), which is standard practice for a laboratory experiment. A mechanical mixer was used to speed up the mixing process and ensure a uniform mixture. Initially, the required proportion of sand and clay was mixed together and then the required water was gradually added to the sample in order to ensure a uniform distribution the sample was then left to stabilise for 24 hours.

There was difficulty in mixing all the soil mixtures by the same procedure. The soil samples with the higher GWCs and higher clay contents were very difficult to mix and ensure a homogeneous sample (water was absorbed locally by the clay particles creating small clumps of material) Table 3-2. indicate soil mixture that caused a problem during mixing procedure.

Table 3-2 Soil mixtures used in the experiment

Soil mixtures By composition		**Aimed GWC (%)**			**Achieved GWC (%)**			**Soils mixtures caused problem**
Sand (%)	Clay (%)							
0	100	0	N/A	N/A	0	N/A	N/A	N/A
10	90	10	20	30	N/A	19.1	30.3	10,20
30	70	10	20	30	9.3	20.3	30.1	10,30
50	50	10	20	30	10.1	19.9	29.1	10,30
70	30	10	20	30	9.9	20	28.8	20,30
90	10	10	20	30	9.9	19.4	N/A	20,30
100	0	0	N/A	N/A	0	N/A	N/A	N/A

As can be seen from Table 3-2 the GWC of the soil mixtures was determined (using oven drying method) using samples taken from three different locations of the container at the beginning of mixing procedure and after finishing the experiment then the average of the GWCs were determined as it can be seen from Table 3-2. Table 3-2. shows the uniformity of the soil mixtures for this experiment. For example, the soil mixture with a composition of 10% sand and 90% clay of 10% and 20 % water contents were difficult to mix homogenously because of the high proportion of clay as the clay absorbed the water and made clumps of the material.

Placing the soil mixtures in the test chamber was one of the most important stages in the experiments in order to ensure as homogeneous a sample as possible. The compaction method was carried out based on BSI (1990). The prepared soil mixture was compacted in three layers using 15 blows per layer, with a 4.5kg standard rammer with the 90mm base plate is

(Figure 3-18. a), in order to ensure uniform soil sample on each layer. An effort was made to scarify the face of each layer to have a good bond with the other layers. After the compaction was completed, the container was weighed to determine the total mass and bulk density of the soil. These steps were repeated three times to ensure repetitions of each mixture was in the same range of GWC and bulk density.

Table 3-3 shows the bulk density of the soil mixtures used in this experiment and includes the number of repetition of each soil mixture.

Table 3-3 Soil mixtures with bulk densities used in this experiment

Soil **mixtures**	Bulk density	**Dry Density (Mg/m^3)**
90% sand 10%clay 10% water	1.843	1.675
90% sand 10%clay 20% water	1.644	1.370
70% sand 30%clay 10% water	1.779	1.617
70% sand 30%clay 20% water	1.626	1.355
70% sand 30%clay 30% water	1.373	1.056
50% sand 50%clay 10% water	1.564	1.422
50% sand 50%clay 20% water	1.627	1.356
50% sand 50%clay 30% water	1.228	0.945
30% sand 70%clay 10% water	1.347	1.225
30% sand 70%clay 20% water	1.470	1.225
30% sand 70%clay 30% water	1.279	0.984
10% sand 90%clay 20% water	1.236	1.030
10% sand 90%clay 30% water	1.325	1.019

For the soil mixtures which were excessively dry or wet, the aforementioned compaction method was not suitable. Therefore, an attempt was made to use a vibrating table to get the soil mixture into the container and minimise the void ratio and create a homogeneous soil mixture. Figure 3-18, b) shows the vibrating table used for mixtures that were difficult to compact.

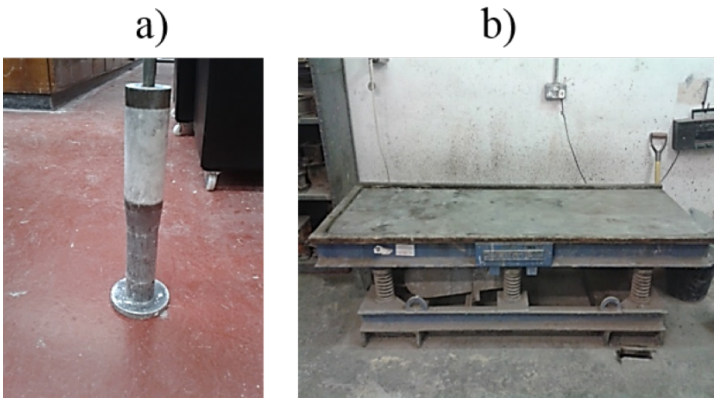

Figure 3-18 a) Rammer, b) Vibrating table

Overall, the placing of the soil mixture into the container was critical to its performance in estimating the signal through the soil sample. The placing of the soil into the container was difficult due to the length of the container. Both mechanical ramming and a vibrating table were used to create the soil surface homogenously and eliminate the void ratio between the soil surface and the container wall.

3.4 Field Trials

Although the laboratory tests provided a good opportunity to study the RF propagation in soil in a controlled environment, it was crucial to assess the performance of the estimation models in a realistic environment. In addition, the physical constrains (i.e. amount of soil sample and available space) did not allow RF tests to be carried out in the laboratory at long distances. In order to address these concerns, field trials were conducted in an industrial test facility at near Blagdon, UK. The methodology used in these trials were derived from the methodology developed by Sadeghioon, (2014) for measurement of electromagnetic signals in the soil. Three 433MHz commercial waterproof Omni-directional antennas were buried at a depth of 60cm below the ground surface **Error! Reference source not found.**. A coaxial cable was used to

connect each of the antennas to an access box at the surface. As the condition of the soil (i.e. water content) could not be controlled, Time Domain Reflectometry (TDR) probes were also placed at close proximity of the antennas in order to measure the geophysical soil properties before each test. The same signal generator and spectrum analyser which were used for the laboratory tests were also used for the field tests. **Error! Reference source not found.**. shows a schematic of the field test setup.

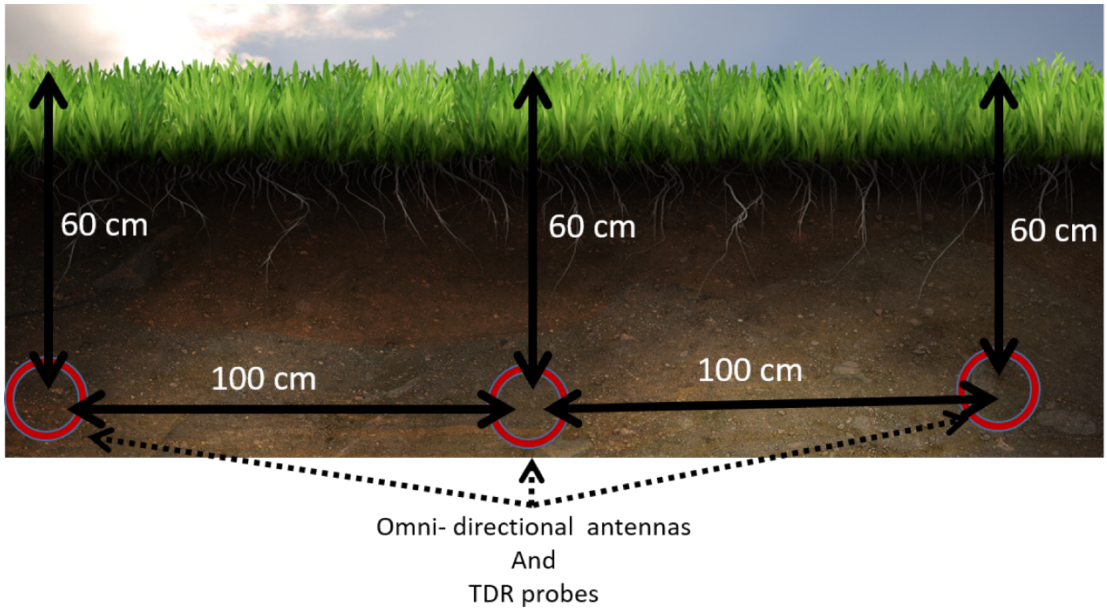

Figure 3-19 Schematic of the field test setup

3.5 Summary

This chapter has described the methodology developed for the experiments conducted in this thesis. Key issues discussed were:

- Development of the requirements for measuring the signal attenuation in soils under laboratory conditions and developing of an appropriate container for the soil samples and also determing the spacing of the antenna and receiver in order to measure the signal attenuation at different distances.

- the design of the experimental arrangement was modified in the laboratory to cope with issues such as eddy currents and earthing to eliminate the effect of the reflected signals into the container.
- The soil mixtures used in the experiments and the sample preparation procedures to ensure homogeneous samples.

The next chapter describes details of the experiments that were conducted and the results from these experiments.

Chapter 4 RESULTS AND DISCUSSION

4.1 Introduction

This chapter presents the results from the experiment to investigate the behaviour of EM signal propagation in a range of soil mixtures and water contents. The experiments were carried out on seven different soil mixtures with different fractions of sand (Leighton Buzzard) and clay (English-China clay) with four desired gravimetric water contents (0%, 10%, 20% and 30%) as shown in Table 3-2 in the previous chapter.

The preparation of the soil mixtures has been described in chapter 3 as part of the methodology and this highlighted that when there was a high amount of sand or clay (>90%) and a water content of less than 10% the mixtures were challenging to prepare and place in the test container this caused inconsistency in the measured signal intensity which is discussed further in the Sections 4.2-4.4.

4.2 Effects of soil composition and condition on permittivity measurements

Initially, TDR measurements and signal transmission were carried out in air dried samples of the sand (Leighton Buzzard) and clay (English-China clay as powder) to investigate the dielectric properties (dielectric permittivity, electrical conductivity) and VWC of each of the primary components of the soil mixtures. Figure 4-1. shows the measured TDR waveform for

the sand and the clay (air dry), these materials were slowly poured into the container and a vibrating table was used for the compaction.

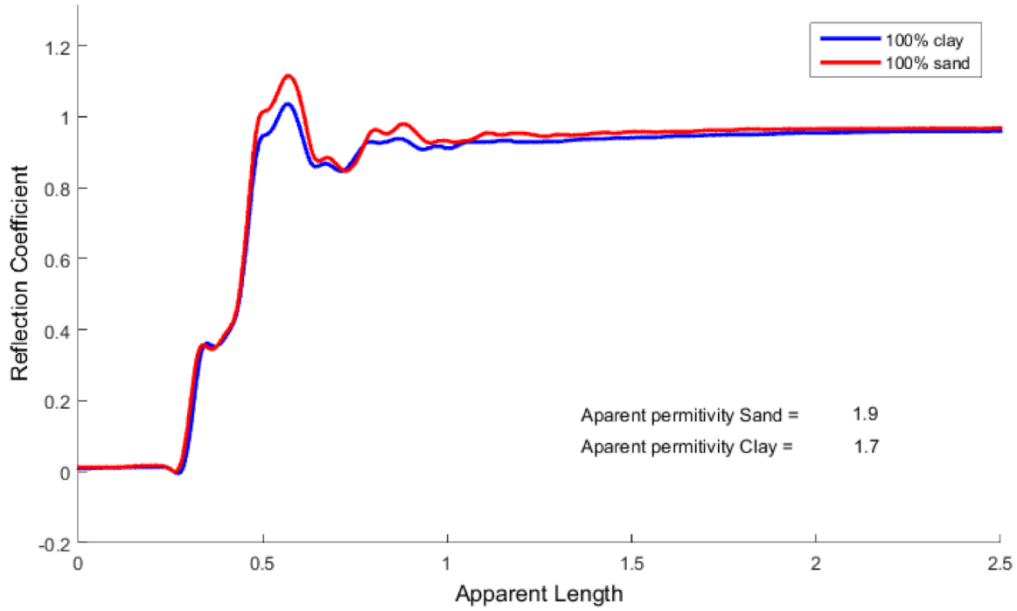

Figure 4-1 Measured TDR waveform for 100% air dried sand and clay samples used in the experiment

Figure 4-1shows a small difference between the apparent permittivity of the air dried and not compacted sand and clay. This similarity is due to the lack of water in these samples. As the water content in the samples increases the difference between the clay and sand becomes more apparent. This is caused by the difference in the amount of free and bound water in these samples that is related to the size of the particles and water absorption ability of the sand and clay, which will affect the apparent permittivity, because the energy of signal was attenuated by passing through the water molecules and (due to higher apparent permittivity).

By increasing the clay content in the sample of sand, it will result in a higher surface area of particles (smaller size of particles) which results in a higher portion of bound water compared to free water in some samples. As it was discussed in the literature review (see Section 2.3), the dielectric permittivity of the soil is tightly related to the amount bond and free water. Unlike

the free water the permittivity of bound waters attached tightly to soil particles is closer to the value of permittivity of ice and is in the region of 3.5-3.8 (Saarenketo, 1998). This results in lower combined permittivity for samples with higher bond water compared to those with higher ratio of free water (for a given water content).

The Table 4-1. presents the average results from the TDR waveform analysis (three repeats) which was calculated based on the existing method as described in methodology.

Table 4-1 Results from the TDR waveform of air dried sand and clay

	Air dry sand (Leighton Buzzard)	Air dry clay (English-China clay)
Apparent Dielectrically permittivity ($\boldsymbol{\varepsilon_a}$)	1.9	1.7
Electrical conductivity ($\boldsymbol{E_c}$) mS/cm	3.6	5.3
Effective frequency ($\boldsymbol{f_{eff}}$) MHz	978	902
Real part of **dielectrical** permittivity	1.9	1.7
Imaginary part of **dielectrical** permittivity	0.004	0.006

Figure 4-2. shows the effect of an increasing clay content on the measured real part of permittivity using TDR waveform for samples at achieved GWC as can be found the values in Table 3-2.

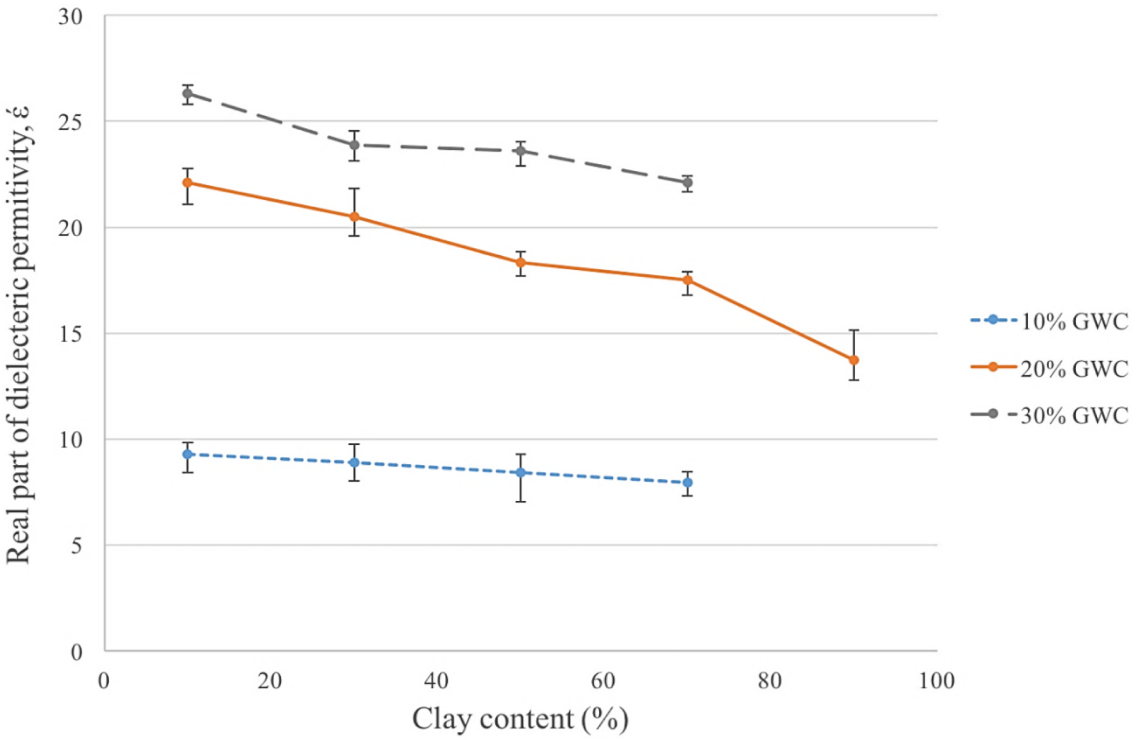

Figure 4-2 The effect of clay content on the real part of dielectric permittivity measured by TDR based on the Topp model. The legend of the figure is aimed GWC of the samples

The test was repeated three times to investigate the repeatability and variability of the measured results. The range of measurements (min-max) are noted in Figure 4-2 as error bars. Data used cab be found in Appendix A.1.

As can be seen from the Figure 4-2. the real permittivity decreases with increasing clay content as more portion of the water content is bound water therefore, reducing the combined relative permittivity of the mixture. This is in line with findings by Topp et al., (2000) and Gong et al., (2003). For the samples with 10% GWC due to lack of water the differences of the real parts of permittivity are small as there is very little free water available.

The effect of water content on the real and imaginary part of the permittivity is related to the proportion of bound and free water content of the soil as the free water increases in the sample the signal loss due to energy absorption of the water increases therefore, increasing the (real) dielectric permittivity. In addition, due to high permittivity of free water (81) the combined

permittivity of the soil increases. As mentioned in Section 2.3, increases in the amount of clay in the soil forms more bound water due to the high surface area of the clay particles in comparison to the sandy soil, resulting in the combined dielectric permittivity (real) of the soil to decrease (Figure 4-3) as the permittivity (real) of the bound water is significantly lower (3.5-3.8) than free water.

In contrast, the imaginary part of the dielectric constant of the soil increases as the clay content increases in the soil mixture. The imaginary part of the dielectric permittivity of wet soils is mainly formed by the bound water in the soil mixture (Saarenketo, 1998). Figure 4-3 shows the average imaginary part of dielectric permittivity values (three repetitions) measured by TDR model as described in the literature review for soil compositions at 10%, 20% and 30% GWC.

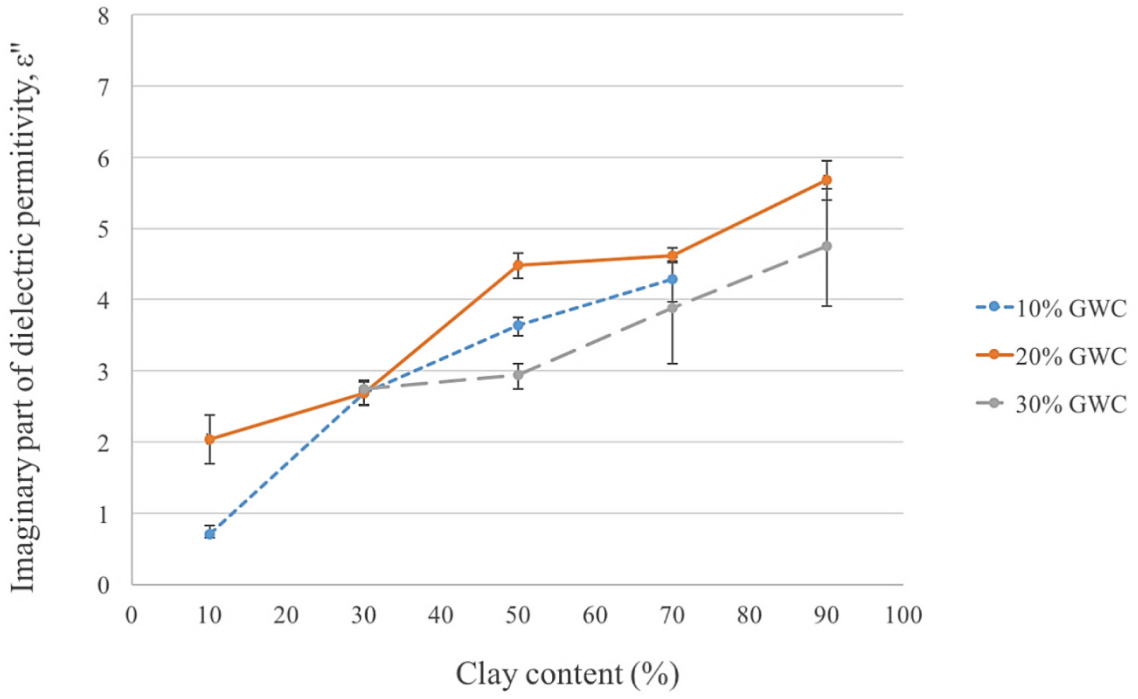

Figure 4-3 Effect of clay content on the imaginary (ε") parts of the dielectric permittivity.

From Figure 4-3 the imaginary part of the complex dielectric permittivity increases with an increase in the clay content of the soil. This is expected as with the increase in the clay content

of the soil the ration of bound water to free water increases (for a given water content) therefore, increasing the imaginary part of the dielectric permittivity of the soil. The TDR measurements were repeated three times for each soil samples on a different location of the test container and the average of the measurement have plotted in Figure 4-3. with the range (maximum-minimum) demonstrated as error bars in the figure. Values used in Figure 4-3 can be found from Appendix A.2.

4.3 Effects of soil composition and condition on RF attenuation

Following the investigation into the effects of soil composition and condition on the dielectric properties of soil, their effect on the attenuation of EM signal in soil was also studied. As mentioned in the literature review (Section 2.4), the attenuation of EM signals in soil is scientifically dependent on the dielectric properties of the soil (i.e. permittivity, conductivity and magnetic permeability), in particular the imaginary part of the dielectric permittivity. It was demonstrated in Figure 4-2 and Figure 4-3.that an increase in the clay content of the soil results in an increase in the imaginary part of the dielectric permittivity and a reduction in the real part of the permittivity. Figure 4-4 shows the change in the attenuation of the EM signal with an increase in clay content of the soil. The GWC was 20% and the distance between the antenna and the signal receiver was 10cm. The frequency used was 434MHz.

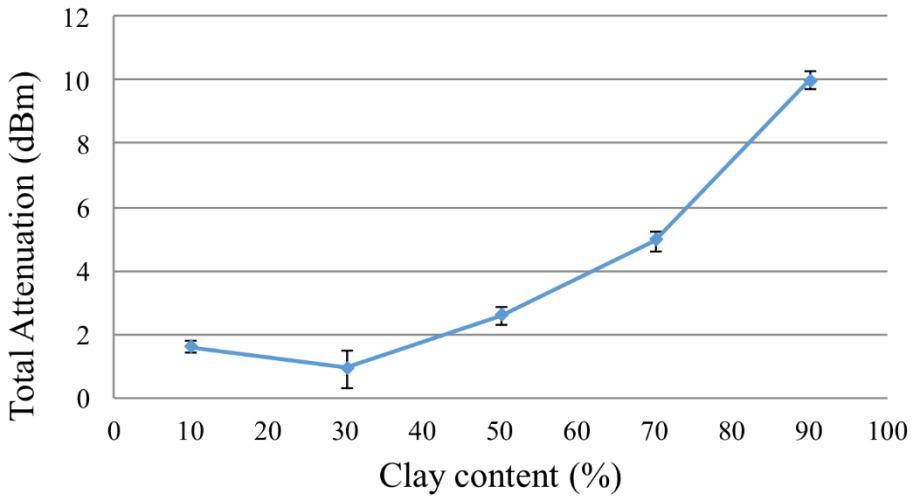

Figure 4-4 Effect of soil composition on signal attenuation through 10cm

It can be seen from Figure 4-4 that the attenuation of the electromagnetic signal increases with an increase in the clay content of the soil mixture with a GWC of 20%. This is mainly caused by the increase in the imaginary part of the dielectric permittivity, which corresponds to signal in the medium. The error bars represent the range of the readings (min-max) from three repetitions for each sample. The large error bar for the sample in 30% clay content was due to the soil preparation difficulties as the 30% clay content with 20% GWC was challenging to be mixed homogeneous and place in the soil container. Another factor which greatly contributes to the permittivity of the soil is its water content (Topp and Davis, 1985; Topp et al., 1980). Figure 4-5. shows the effect of the gravimetric water content on the attenuation of the signal for a soil mixture of 50% sand and 50% clay. The transmission distance was 10cm and the frequency of the signal was 434MHz.

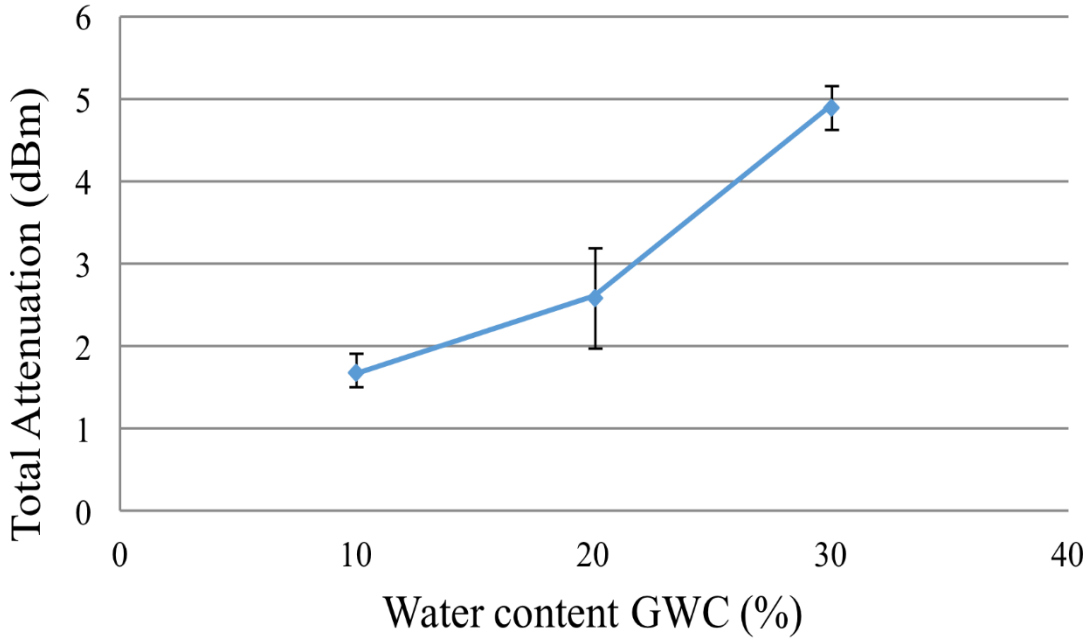

Figure 4-5 Effect of Gravimetric Water Content (GWC) on the attenuation of the signal in 50 % sand and 50 % clay soil sample by the 434MHz carrier frequency

As can be seen from Figure 4-5, the signal attenuation increases with an increase in the water content which is similar to results demonstrated by Li et al., (2007). This is due to increase in permittivity of the soil caused by the increases in the free water content of the soil moisture. As was presented in the literature review (section 2.3), increasing the free water content of a soil sample, raises the permittivity (real part) of the soil which causes more energy absorption of the water molecules. From Figure 4-5 can be seen that the error bars (based on the range of five repetitions) increase as the water content of the soil mixture increases. This is mainly due to the difficulties of taking measurements in the samples with higher water content such as accumulation of water around the antennae when it was placed in the soil. As was mentioned in the literature (section 2.2) review the distance between the transmitter and receiver is one of the main factors which affect the attenuation of RF signals in soil. Estimation of attenuation with respect to distance is one of the main outputs of the RF path loss models (i.e. Modified-Friis). Therefore, it is essential that this effect is also considered when studying RF attenuation.

Section 4.4 (below) presents the results from the tests analysing the effect of distance on path loss. Appendix A.3 and Appendix A.4 show the data used in these figures.

4.4 Effect of distance on attenuation of electromagnetic signals in soil

As mentioned in Section 2.1-2.3 in the literature review, the electromagnetic signals travel through any medium, they become attenuated due to reflection, refraction, and absorption. Figure 4-6 shows the measured signal strength at different distances (10-50 cm) for the soil mixtures at 20% GWC and a carrier frequency of 434MHz. The test was repeated three times for each soil samples and also the soil mixtures prepared three times for each soil composition (error bars represent the range of the measured signals). The raw data can be found in the Appendix A.5.

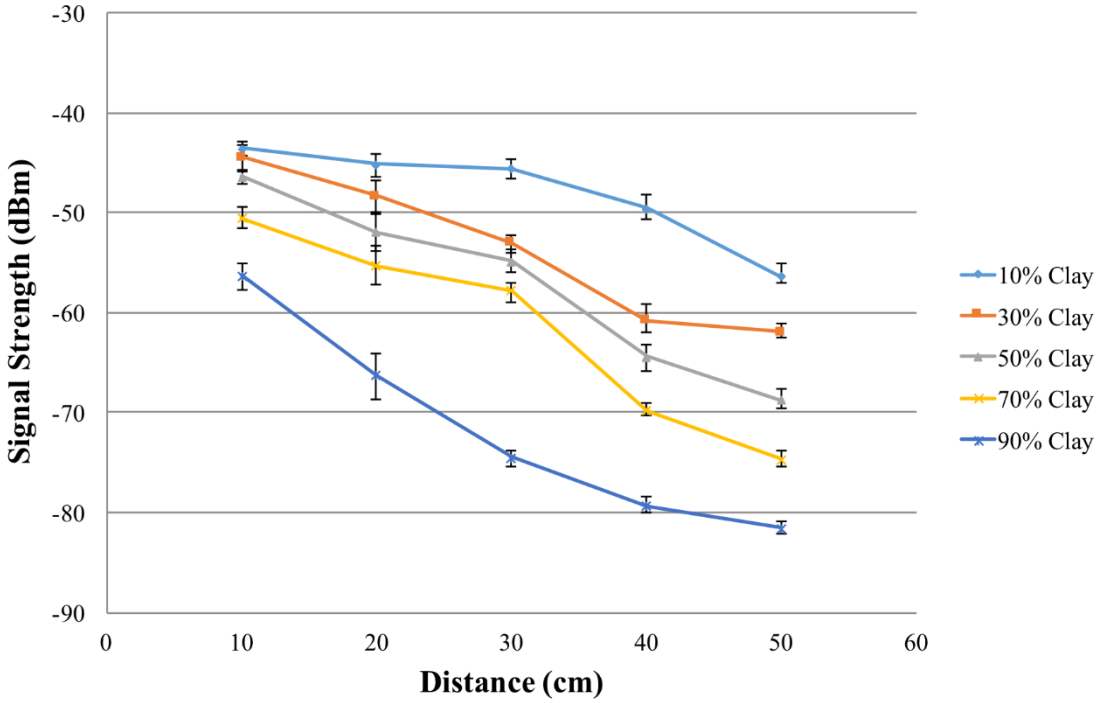

Figure 4-6 Attenuation of electromagnetic signals with the frequency of 434MHz with distance in various soil compositions with a GWC of 20%

As expected it can be seen from Figure 4-6 that the measured signal decreases with an increase in the distance between the antenna and the generator (inter node distance). This effect was expected as it was previously demonstrated in Bogena et al., (2010) and Li et al., (2007). Moreover it can be shown from Figure 4-6 that the signal strength drops more rapidly with distance in samples with higher clay content (i.e. 90%) compared to lower clay content samples (i.e. 10%) this is due to the higher imaginary part of the permittivity of these samples which results in larger attenuation of the signal. Also as can be seen from Figure 4-6 that all samples followed a similar decreasing trend in signal intensity with distance. The measured results are in line with those measured by Bogena et al., (2010). In fact, the signal strength decreases more rapidly after the distance increases to the 30cm and more and it is due to the faster energy losses of the signal.

The transmitter used during the tests for transmissions with a carrier frequency of 868MHz showed unreliable consistency in its performance due to a fault of the transmission nodes resulting in the node not transmitting the 868MHz frequency with a fixed output power over the time of the test. Therefore, it cannot be compared with the results from the signal transmission with a carrier frequency of 434MHz and are not presented here. As was mentioned in section 2.2 from literature review various models have been developed to estimate the attenuation of the electromagnetic signals in soil based in the soil characteristics (i.e. dielectric values) and transmission properties (i.e. distance and frequency). Section 4.5 compares two of the commonly used models with measured values from laboratory test to investigate their performance.

4.5 Comparison of measured attenuation with existing models

In this section, the measured attenuations in the laboratory tests are compared with the estimated values from the modified-Friis and Crim-Fresnel models. The effect of soil composition (clay/sand ratio) and GWC on the accuracy of these models is also analysed in this section. Figure 4-7. shows the measured attenuation values for a carrier frequency of 434MHz in samples with varying soil composition at 20% GWC in order to investigate the effect of the soil composition on the prediction accuracy of the models. Table 4-2presents the complex permittivity values of the soil samples used in theis comparison.

Table 4-2 Permittivity and water content values for different soil samples

Soil mixture compositions	**GWC %**	**E' (real part of permittivity) based on TDR**	**E" (imaginary part of permittivity) based on TDR**	**E' (real part of permittivity) based on Peplinski**	**E" (imaginary part of permittivity) based on Peplinski**
10% sand & 90% clay	20	13.44	5.68	15.2	6.94
30% sand & 70% clay	20	16.38	4.61	17.4	5.1
50% sand & 50% clay	10	8.25	3.64	9.9	4.46
50% sand & 50% clay	20	17.04	4.48	18.1	5.5
50% sand & 50% clay	30	23.50	2.93	24.8	4.8
70% sand & 30% clay	20	20.17	2.69	22.69	3.47
90% sand & 10% clay	20	21.91	2.04	23.7	2.89

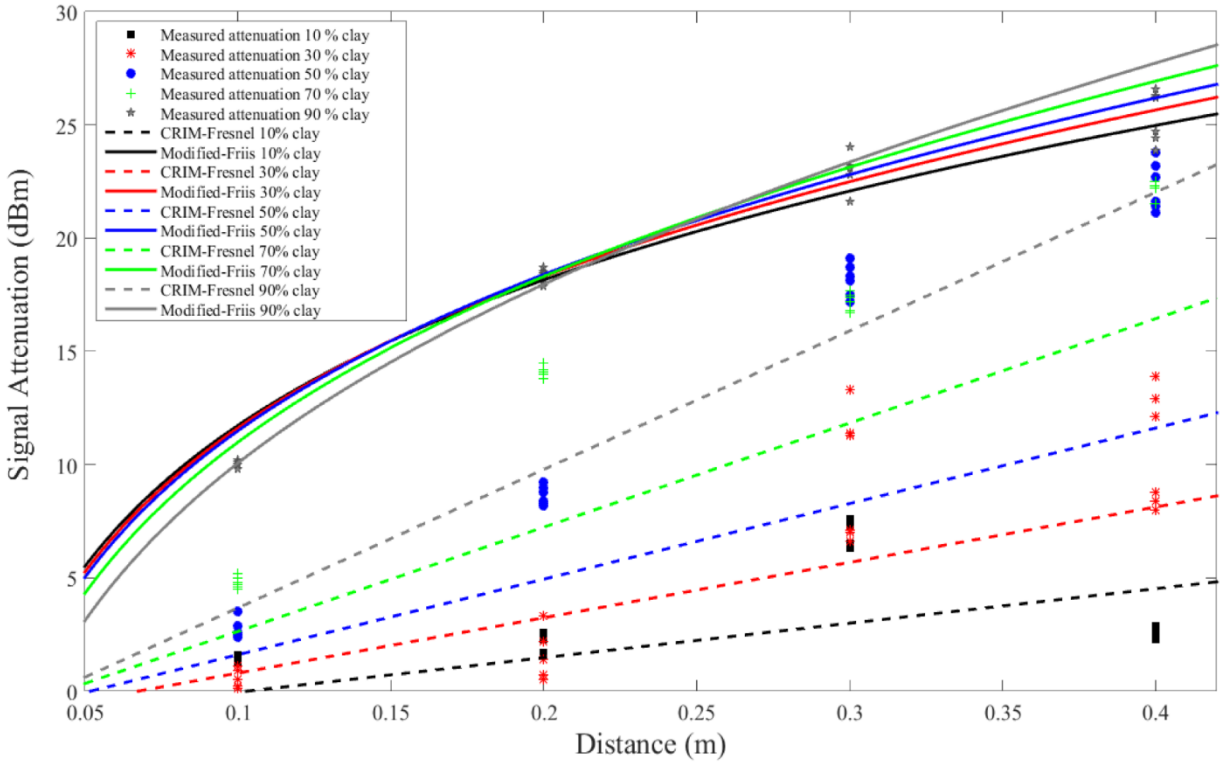

Figure 4-7 Effect of soil composition on the attenuation of the signal and comparison of the Modified-Friis and Crim-Fresnel model (20% GWC, 434MHz carrier frequency)

As can be seen from Figure 4-7. the amount of clay content in the soil has a direct effect on the attenuation of the signal with the increase in clay content resulting in a rise in the attenuation of the signal which is line with the literature (Mironov et al., 2008; Peplinski et al., 1995b). This is mainly due to the increase in the imaginary part of the dielectric permittivity of soil with an increase in clay. It can also be seen from Figure 4-7 that both the Crim-Fresnel and modified-Friis models fail to estimate the attenuation of the signal accurately for all soil compositions. However, it can also be seen from Figure 4-7 that the Crim-Fresnel model provides a better estimation of the signal attenuation through soil with a lower clay content compared to the modified-Friis model. In order to quantify the goodness of fit the root mean square error (RMSE) was calculated based on the average if the measured values at each point for all the different soil compositions for both models (**Error! Reference source not found.**) shows that modified-Friis model estimated the attenuation of the signal at higher clay content

(90% clay) samples with higher accuracy compared to the Crim-Fresnel model. In contrast the Crim-Fresnel model provide a better estimation in lower clay content sample such as 10% clay. This is expected as the Crim-Fresnel model was developed on limited soil samples (mainly sand at different water contents) (Bogena, 2009). For the soil mixtures studied, there also appears to be a transition between approximately 30% and 70% clay when the Crim-Fresnel model produces better signal attenuation estimates at the shorter distances and the modified-Friis model produces better estimates the signal attenuation at the longer distances. This is assumed to be due to the fact that the CRIM- Fresnel model was developed based on tests on a shorter internode distance compared to Modified-Friis model. Comparison of the Modified-Friis model using the Peplinski model as an input with values extracted from TDR (using Topp model) is presented in Figure 4-8.

Table 4-3 Root Mean Square Error (RMSE) for all soil mixtures at a 20% GWC

	RF Models	**10% Clay**	**30% Clay**	**50% Clay**	**70% Clay**	**90% Clay**
RMSE	Crim-Fresnel	2.35	4.03	7.66	5.18	6.67
RMSE	Modified-Friis based on TDR	16.66	12.33	7.20	5.36	1.13
RMSE	Modified-Friis based on Peplinski	17.07	12.86	7.29	5.42	1.16

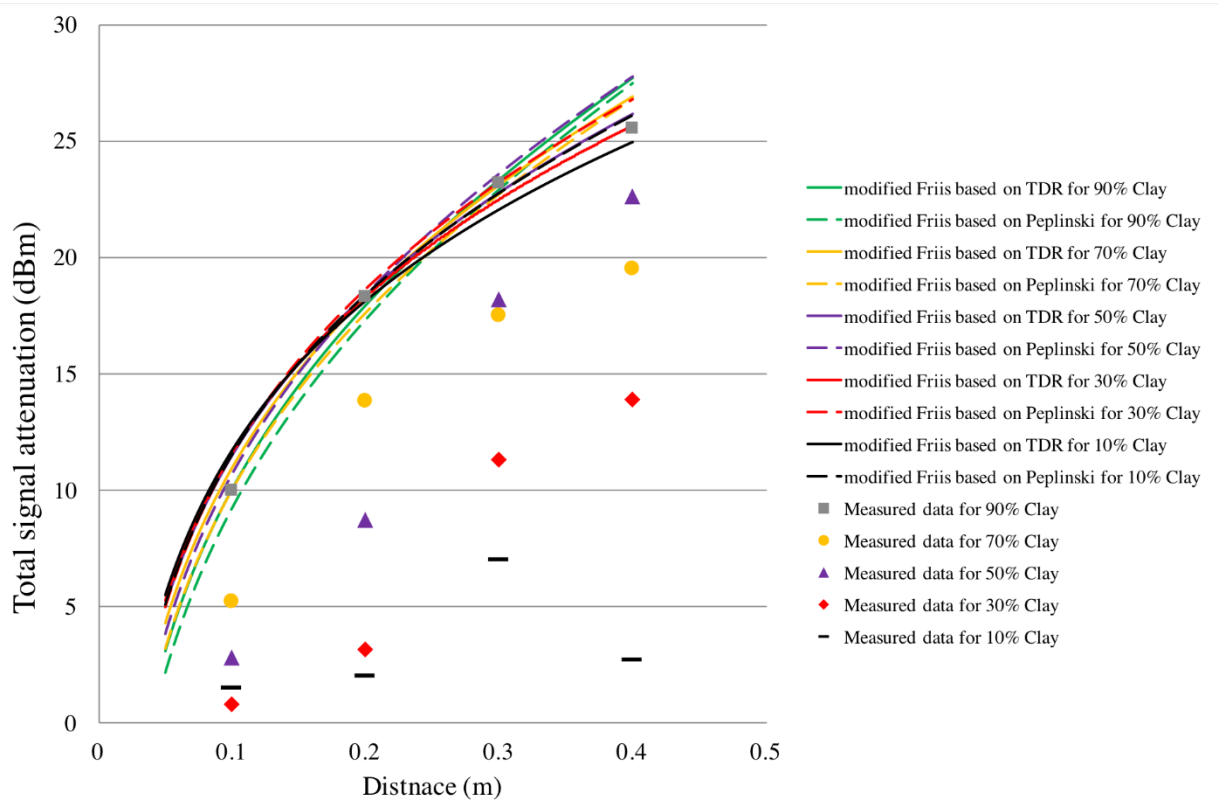

Figure 4-8 Comparison of Modified-Friis based on TDR and Peplinski methods

As can be seen from Figure 4-8 the modified models using the extracted values form the TDR waveform provided a similar estimation to the Modified-Friis model using the Peplinski to calculate the real and imaginary values of the permittivity based on soil compositions. Despite their similarity the estimated values from these methods differ from each other due to difference in the real and imaginary permittivity values which are used in each of these methods.

The calculated RMSE for the mixtures with the 30, 50, 70 % clay content for both of the Modified-Friis models and the CRIM Fresnel model are illustrated in **Error! Reference source not found.** and all the raw data used, can be found in Appendix A.6.

It can be concluded from **Error! Reference source not found.** that all of the models performed similar to each other (similar RMSE values) at mid-range composition values (i.e. 50% Clay).

It can also be concluded from **Error! Reference source not found.** that the RMSE value of the models diverges at the limits of the composition range (i.e. at 90% clay and at 10% clay) with each model performing significantly better than the other (based on the RMSE values). This clearly shows that none of the models is suitable for estimating the RF attenuation in all types of soil and further highlights the importance of comparison of these models in a wide range of soil types and conditions. It also shows that each model should be used in a specific range of soil types and conditions in order to have an acceptable accuracy. From Table 4-3 and Figure 4-9 it can be concluded that the both of the modified-Friis model are more suitable for mid to long inter node distance (>30cm) and soils with higher levels of clay content while Crim-Fresnel is more suitable for short internode distances and soil with low or no clay content (high sand content). This is very interesting as it shows that these models are only really suitable for the soil types that are similar to the ones that were used for their development and cannot be accurately used in a larger soil domain (despite their developers' claims). Results of the RMSE studies also showed that the Modified-Friis model based on the values extracted from the TDR measurements performed better than the Modified-Friis model based on the Peplinski mixing model. This is extremely encouraging and further validates the usage of the complex permittivity values extracted from the TDR measurements as an input into RF estimation models. In addition, using the values obtained from the TDR waveform provides a significant practical advantage over the Peplinski method as it eliminated the need for laboratory analysis of the soil (i.e. particle size distribution tests) and enable the RF attenuation to be estimated in the field on the spot using in situ TDR measurements. This is specifically beneficial in time sensitive applications or in applications were access to the site is limited (i.e. no possibility for a return to the site after laboratory analysis) or the requires laboratory equipment are not available.

Another parameter which will affect the performance of the estimation models is the frequency. It is essential to investigate the accuracy of the models within a large frequency range. The attenuation of the signal is measured at 434, 868, 1300, 1736, 2170 and 2604 MHz for the distances of 10 cm and 20 cm between the antenna and the receiver. Figure 4-9 shows the comparison of the average measured attenuation values (three repetitions with the range shown as error bars) in the frequency range of 434MHz to 2.6GHz with estimated values based on Crim-Fresnel and Modified-Friis models for soil mixture of 50% clay, 50% sand and 30% GWC. The raw data used in this figure can be found in Appendix A.7.

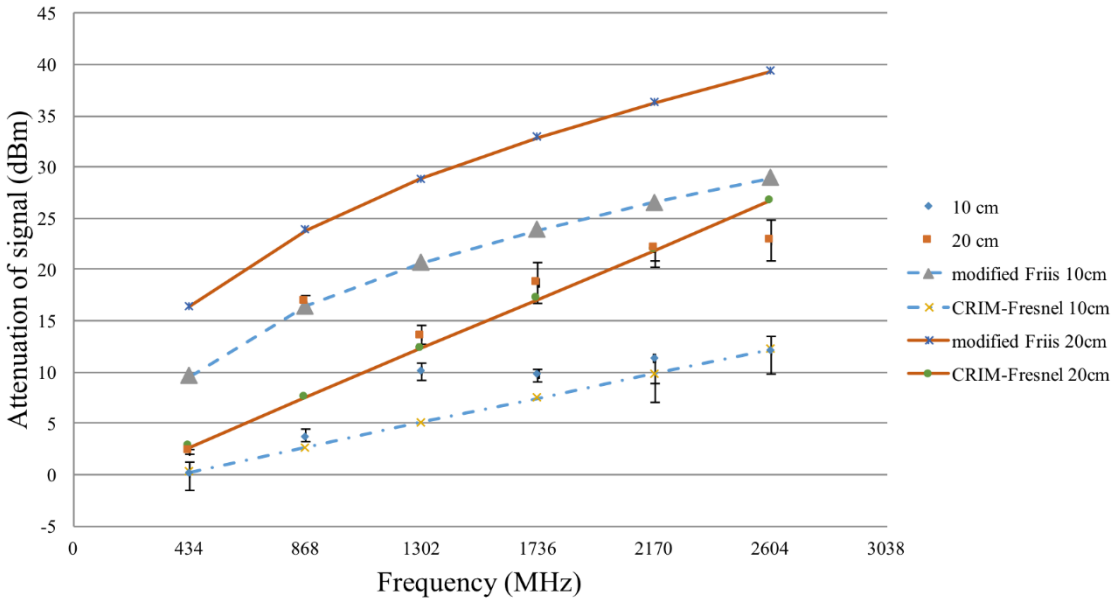

Figure 4-9 Comparison of the measured attenuation values in the frequency range of 434MHz -2.6GHz with estimated values based on Crim-Fresnel and Modified-Friis models in the soil of 50% sand and 50%clay with 30% GWC.

As shown in Figure 4-9 there is a discrepancy between the estimated values by the modified-Friis and Crim-Fresnel models. This is similar to the results obtained by Chaamwe et al., (2010). The root mean squared error of both of the models was calculated based on the average

of the measured values in order to compare their signal attenuation estimation capability. Table 4-4. presents the calculated RMSE values for both of the models.

Table 4-4 Calculated RMSE values for measured values respect to the RF models

	RF Models	**10 cm**	**20 cm**
RMSE	Crim-Fresnel	0.98	1.70
RMSE	Modified-Friis	5.47	5.67

As can be shown from Table 4-4 The calculation of the RMSE values at both distances of 10cm and 20cm showed that the Crim-Fresnel model provided a better estimation of the signal attenuation compared to the Modified-Friis model (RMSE).

As the mentioned earlier water content of the soil has a significant effect on its dielectric properties (specifically permittivity) and in turn has a large effect on the attenuation of the signal in the soil. Therefore, it is crucial to investigate the accuracy of the attenuation estimation models with respect to the water content of the soil. During this research the attenuation of the signal was measured in different soil samples with varying water contents (10% 20% and 30%) and soil composition of 50% clay and 50% sand. This soil composition was selected as the models had a close performance in the previous tests at this soil composition (at 20% GWC). Figure 4-10 shows the results from these tests with three repetitions (the raw data from these tests is presented in Appendix A.8).

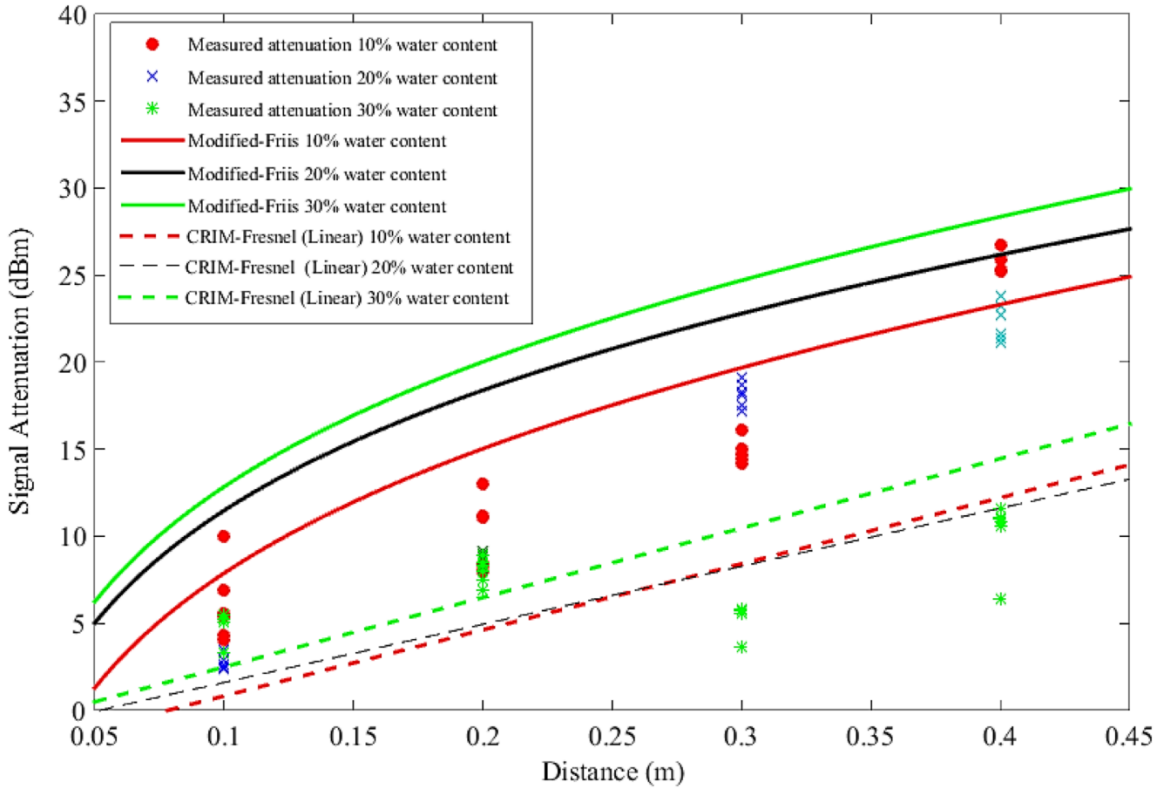

Figure 4-10 Effect of GWC on the prediction accuracy of RF transmission models for a 50% Clay and 50% Sand sample (434MHz carrier frequency).

As can be seen from Figure 4-10. both of the models failed to provide an accurate estimation for samples over the full range of GWC. However, based on the calculated RMSE values (**Error! Reference source not found.**) of the models at different gravimetric water contents, he modified-Friis model provided a better estimation at lower GWC compared to the Crim-Fresnel model. As an example at 10% water content (Table 4-5) the Modified-Friis (based on TDR) had an RMSE value of 3.54 while the Crim-Fresnel model had an RMSE of 8.59. In contrast at 30% GWC the Modified-Friis (based on TDR) model had an RMSE value of 14.85 while the Crim-Fresnel model had an RMSE of 3.52 which shows that the Crim-Fresnel model provides a better estimation at higher water content values.

Table 4-5 RMSE values for the Crim-Fresnel and modified-Friis model

	RMSE		
GWC (%)	**modified-Friis based on TDR**	**modified-Friis based on Peplinski**	**CRIM- Fresnel**
10	3.54	3.85	8.59
20	7.20	7.27	7.60
30	14.85	15.13	3.52

The Modified-Friis model using the values from Peplinski is also compared with the proposed Modified-Friis model using the extracted permittivity values from TDR measurements (using Topp model). Figure 4-11 shows the comparison between estimated values from the Modified-Friis model using Peplinski and TDR measurements at different water contents.

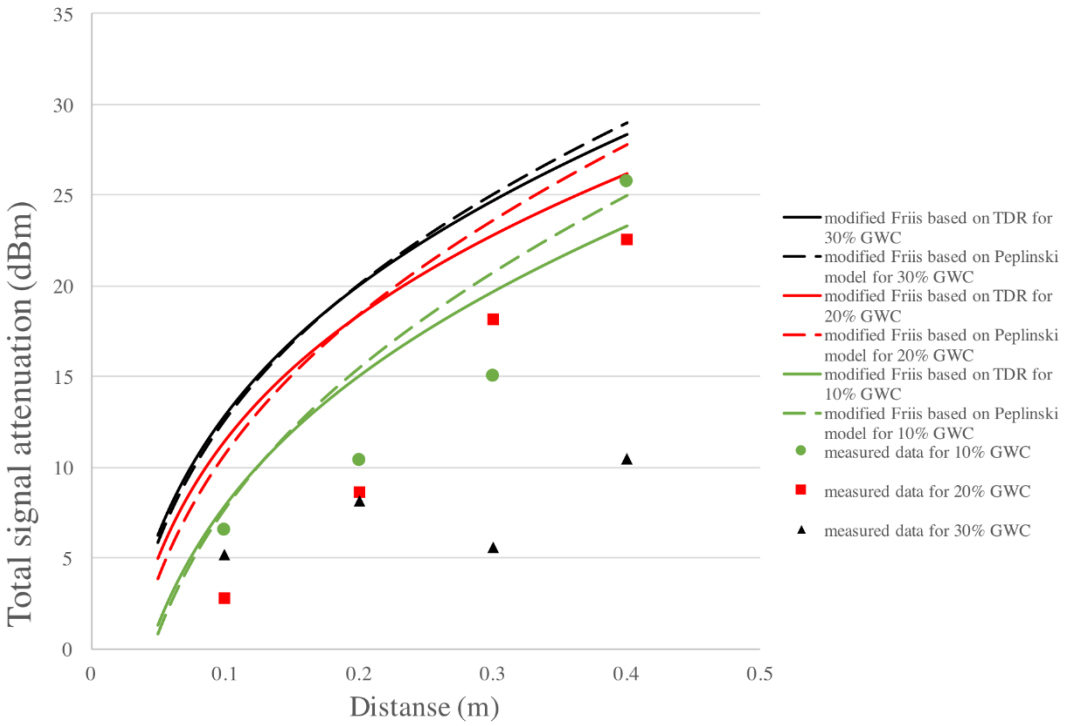

Figure 4-11 Effect of water content on Modified-Friis model based on extracted values from TDR and Peplinski

As can be seen from Figure 4-11 both of the Modified-Friis models provided a similar estimation of RF attenuation in soil. However, there is small discrepancy between the two estimated values at each water content. The accuracy of these two methods is compared using the calculated RMSE values presented in Table 4-5. These values shows that the Modified-Friis model using the values extracted from TDR measurements provided a more accurate estimation of attenuation compared to the Modified-Friis method based on the permittivity values obtained from Peplinski mixing model. From results shown in Table 4-5, Figure 4-7 and Table 4-3 it can be concluded that the Crim-Fresnel model is more suitable for the approximation of attenuation in soils with high water content (>20%) and lower clay content (<50%) while the modified-Friis model (based on TDR) provides a better approximation for samples with lower water content (<20%) and high clay content (>50%). This is mainly caused by the effect of the imaginary part of the dielectric permittivity on the estimation values of the Crim-Fresnel model as it follows a linear approximation equation which is more sensitive to imaginary part of the permittivity compared to the modified-Friis (based on TDR) model. In addition, this linear estimation of attenuation of the signal with an increase of distance is not similar to the fundamental behaviour of the signal (Equation 2-9) and will result in large errors in estimation of the signal attenuation (over estimation) at larger distances. One of the limitation of the laboratory tests presented in this research is the limited range between the transmitter and receiver (due to practical limitations of RF tests). Therefore, it is essential to investigate the attenuation RF signals and the performance of the estimation models at larger distances. Section 4.6 presents the results from RF attenuation tests carried out in the field at larger distances and more realistic environment.

4.6 Field tests

Although the laboratory tests provided a good opportunity to study the RF propagation in soil in a controlled environment, it was crucial to assess the performance of the estimation models in a realistic environment. The methodology used for these tests is described in section 3.4. The representative classification of the soil at this location based on soil classification tests carried out in the laboratory on the sample taken at the same depth as the antennas is presented in Table 4-6 and Table 4-7 shows the volumetric water content and dielectric constant from each visit**Error! Reference source not found.Error! Reference source not found.**.

Table 4-6 Soil classification by measuring particle size distribution and Plastic and liquid limits

Soil classification	**MH - slightly sandy clayey SILT of high plasticity**
Gravel (%w)	13
Sand (%w)	19
Silt (hydr) (%w)	48
Clay (hydr) (%w)	20
Fines (%w)	68
Plastic Limit (%)	29
Liquid Limit (%)	64
Plasticity Index (%)	24
Linear Shrinkage (%)	14

Table 4-7 Soil difference VWC at different time of visit

Measurement Date	VWC(%)	Apparent permittivity	Real part of dielectric permittivity	Imaginary part of dielectric permittivity
25/02/2015	22.5	25.1	23.8	4.63
01/05/2015	16.1	13.6	12.7	2.93
25/06/2015	15.5	11.7	11.1	2.26

The attenuation of the electromagnetic (EM) signals in the soil was also measured in the field and the comparison of the measured signal strength with estimated values by the modified-Friis and Crim-Fresnel models at each visit is shown in Figure 4-12 to Figure 4-14 The measurements were repeated three times at each location and frequency and error bars in these figures represent the range of measurements (Minimum and Maximum). The raw data from these tests is presented in Appendix A.9.

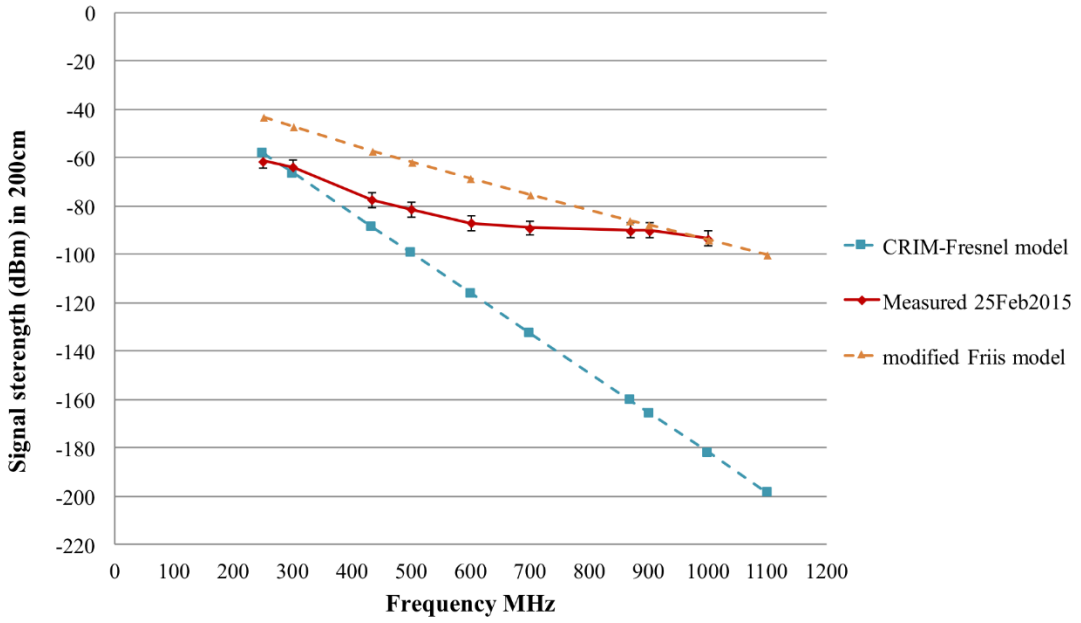

Figure 4-12 Comparison of the measured signal strength to the modified-Friis and Crim-Fresnel models for the 25th February 2015

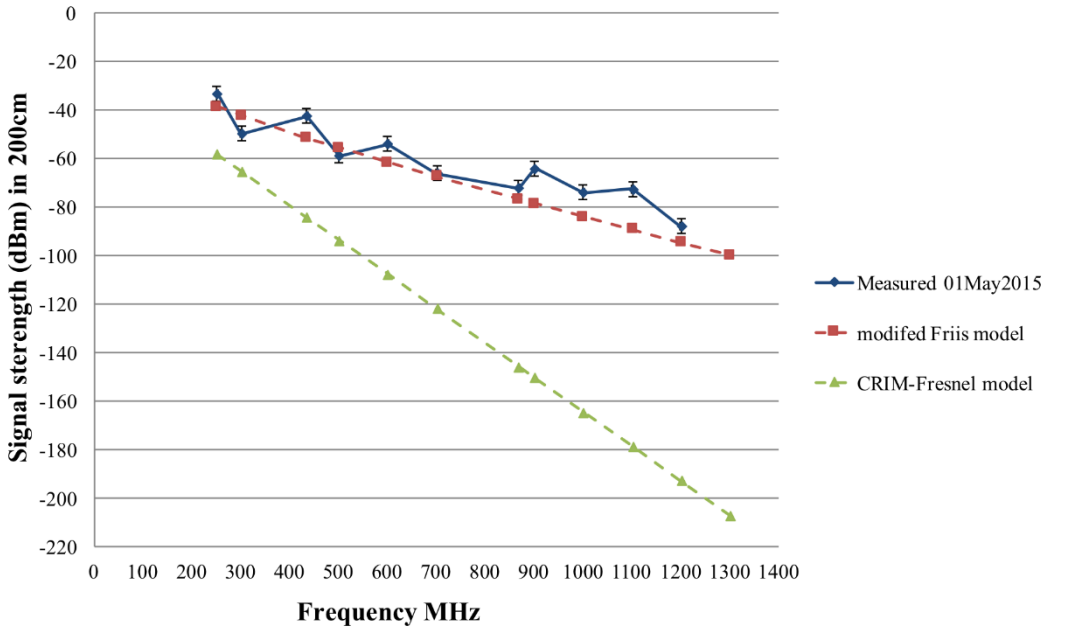

Figure 4-13 Comparison of the measured signal strength to the Modified-Friis and Crim-Fresnel models for the 1th of May 2015

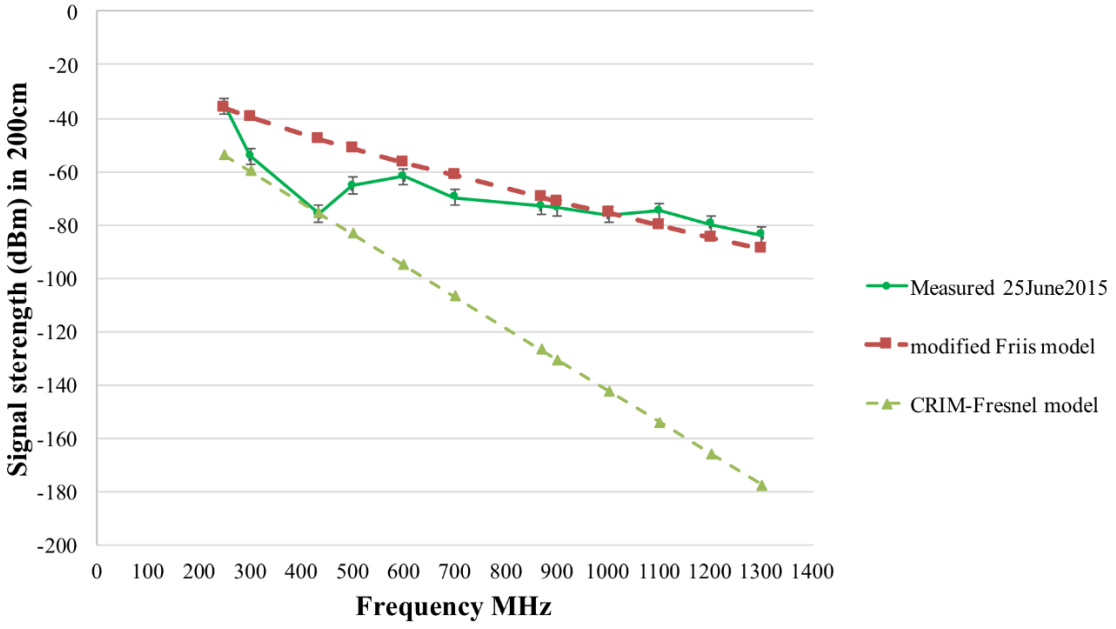

Figure 4-14 Comparison of the measured signal strength to the Modified-Friis and Crim-Fresnel models for the 25th June 2015

The RMSE values of the Modified-Friis and Crim-Fresnel models were calculated in order to compare the results and accuracy of the models. Table 4-8 shows the calculated RMSE values for the results from the field trials. As can be seen from Figure 4-12 to Figure 4-14 and Table 4-8 and as mentioned before the condition of the soil in the field were not controllable, therefore inform**Error! Reference source not found.**ation regarding the condition of the soil before each measurement was required in order to compare the results. The calculated Volumetric Water Content (VWC %) and permittivity of the soil based on the TDR measurements and Topp (1985) model (at each visit) are presented in the **Error! Reference source not found.**.

Table 4-8 The calculated RMSE values for the measured signal strength with respect to the modified-Friis and Crim-Fresnel models

Measurement Date	RMSE Modified-Friis	RMSE Crim-Fresnel
25/02/2015	14.68	49.03
01/05/2015	10.53	76.15
25/06/2015	10.80	54.84

As can be seen from Figure 4-12 to Figure 4-14 and also from the calculated RMSE values presented in Table 4-8. Modified-Friis Model had a significantly better estimation of the RF signal attenuation compared to the Crim-Fresnel Model. As mentioned before this is mainly due to the linear approximation of CRIM Fresnel model which lead to large errors at larger distances and higher frequencies. Comparison of the measured attenuation values presented in Figure 4-12 to Figure 4-14that the variation in the measured signal strength were significantly lower for the February measurement compared to other two measurement sets. This is believed to be caused by the higher attenuation of the soil (due to higher water content) during these measurements which reduced the effect of reflection from the surface/environment as these

signals needed to travel longer distances compared to the direct path and an increase in attenuation of the soil affect them more than the direct path. Only three visits were made due to a limitation in accessing the site. These visits were made in different seasons, with significantly different soil conditions due to seasonal rainfall. Results from all of the visits strongly showed that the modified-Friis is a better model for the approximation of RF attenuation in the soil.

4.7 Model performance comparison and suitability matrix

Comparison of the estimated values of attenuation with measured values both in the laboratory and filed tests showed that neither of these models is can provide an accurate estimation of attenuation of RF signals in all soil types or conditions. A key finding of this research is identification of ranges and conditions in which each models is more accurate. Table 4.9 details the suitability of each model based on the results from laboratory and field trials. Despite the simplicity of this table it can provide valuable information as to which model is more suitable at each scenario.

Table 4.9 Suitability table for CRIM-Fresnel and Modified-Friis based on soil composition and water content (GWC)

	Low water content GWC (<20%)	**High water content GWC (>20%)**
Low clay content (<50%)	Modified-Friis	CRIM-Fresnel
High clay content (>50%)	Modified-Friis	Modified-Friis

In addition to the Table 4.9 results from this study showed that the CRIM-Fresnel model is only suitable for soils with high (>20%) water content where, most of the water content is in the form of free water.

Chapter 5 CONCLUSIONS AND RECOMMENDATIONS FOR FURTHER WORK

5.1 Conclusions

This thesis presented the development of a methodology for measurement of signal attenuation in the soil at the frequency of 434MHz in the laboratory. In addition, the measurements of attenuation at the range of frequency of 250MHz to 2604MHz in one the field test were presented. The methodology was developed based on a review of the literature on measuring the signal attenuation in different soil mixtures and conditions the main aim of the research was to compare different attenuation estimation models in different soil conditions and compositions. It was apparent that none of the existing RF models used to estimate the attenuation of the signal in soil mixtures provided an accurate estimation in the soil range studied in this research. A comparison of the Modified-Friis and Crim-Fresnel models which, are the two most commonly used RF propagation models, showed that their estimated values for attenuation of a signal were different from each other. The Modified-Friis model estimates the signal attenuation nonlinearly as the distance increases with a logarithmic pattern. This is similar to the pattern of RF attenuation in open space. In contrast, the Crim-Fresnel model follows a linear estimation of signal attenuation with increasing distance. This results in the Crim-Fresnel model to significantly overestimate the attenuation of the signal at larger distances. This shows that neither of the models are suitable to estimation of RF attenuation across all soil types and conditions. Both of the models use the link budget equation, but the parameters which are used in these models are different as the Modified-Friis model uses the

general relationship between the transmitted and received power by considering the loss in free space, gains at the receiver and transmitter and the loss caused by the medium. In contrast the Crim-Fresnel model only consider the attenuation of the signal due to reflection into account.

From the review of the literature, it was established that the behaviour of the electromagnetic signals in soil is mostly dependent on the geotechnical properties of the soil in particular the percentage of clay content, volumetric water content and the bulk density of the soil sample, in addition, the dielectric properties of the soil have an effect on the signal propagation such as the dielectric permittivity, electric conductivity and magnetic permeability (these are also affected by the geotechnical parameters of the soil). The water content of the soil is the most important parameter that can affect the soil dielectric properties due to the high energy absorption ability of the water molecules. The amount of water in the soil sample can be divided into free water or bound water which have a specific influence on the signal attenuation. This is determined by the composition of the soil. In soil mixtures with high clay content larger portion of the water will be in the form of bound water compared to a soil mixture with lower clay content and the same total water content. This greatly affect the combined dielectric permittivity of the soil as the real part of the permittivity of the bound water is significantly lower than of free water. This is also significant as the performance each of analysed models also highly depends on the dielectric permittivity of the soil.

A methodology was developed to measure the signal attenuation in the soil. The signal attenuation was measured at 10cm steps up to 50cm from the signal transmitter antenna that was placed initially into the plastic container (which caused unwanted reflections) and then into the aluminium container. Finally, the signal intensity was measured at the holes placed at different distances along the container, 10cm apart from each other up to 50cm and then the signal intensity was deducted from the signal intensity at the origin to calculate the attenuation at each point.

The results from the experiments showed that neither of the models investigates in this research can accurately estimate the attenuation of the signal in the soil in all of the studied soil mixtures. At a fixed water content (i.e. 20% GWC) These results showed that the Crim-Fresnel model provides a better estimation in soil mixtures with no or low (<30%) clay content. While both models performed very similar at 50% clay content, the Modified-Friis model provides a significantly better estimation for attenuation of signals in samples with high (i.e. >50%) clay content. Based on these findings and soil samples studied in this research a suitability matrix is developed (see Section 4.7) which identifies which model provides a better estimation for different soil compositions and conditions. This can greatly assist researcher in the field of electromagnetic propagation in soil (i.e. underground wireless sensor networks).

Comparison of the results from the test carried out in this research also showed that the Crim-Fresnel model is more suited for shorter inter node distances (<30cm) as it has a higher accuracy in estimating the attenuation compared to Modified-Friis model. However, the Modified-Friis model has a better estimation accuracy at longer internode distances. This is also an important finding as it identifies suitability of each models for different application were distance is an important factor (i.e. research in ground penetrating radars).

The water content of the soil mixture plays a major role in its dielectric properties and in turn attenuation of signals in the soil. Results of the tests carried out on samples at varying water content showed that the Modified-Friis model has a higher estimation accuracy in low to moderate water contents (<20% GWC) while the CRIM Fresnel model provided a better estimation for samples with high water content (>20% GWC).

This research also investigated the usage of complex permittivity values obtained from the TDR measurements (using the Topp model) as an input to the RF estimation models (specifically Modified-Friis model). The results from this comparison showed that the values extracted from the TDR measurements (using the Topp model) can be used to as an input to

the Modified-Friis model. In addition, results from these comparisons showed that the estimated values of the Modified-Friis model using the values extracted from the TDR had higher accuracy compared to the estimated values from the Modified-Friis model using the Peplinski model. As was mentioned using the values obtained from the TDR waveform provides a significant practical advantage over the Peplinski method as it eliminated the need for laboratory analysis of the soil (i.e. particle size distribution tests) and enable the RF attenuation to be estimated in the field on the spot using in situ TDR measurements which benefits time sensitive applications or where laboratory equipment for soil classification is not available or the access to the site is limited (i.e. no possibility of return visits).

In order to analyse the performance of these models further attenuation measurements were also carried out in the field. The tests were carried in three different times of the year to see the effect of different water content (due to seasonal changes and rain). The results of the field tests showed that the Modified-Friis model provided a significantly better estimation of RF attenuation at all volumetric water contents (i.e. different visits) compared to the CRIM Fresnel model. This is due to the linear approximation nature of the CRIM Fresnel model which significantly overestimates the attenuation of the signal at longer (>30cm) internode distances. From comparing all of the results obtained in this research it can be concluded that based on the soil samples studied in this research and the results from the field trials the Modified-Friis model is a clearly more accurate estimation model for internode distances. However, at shorter internode distances the choice of the path loss model depends on the soil mixture composition and water content. This research can specifically provide valuable information in deciding which model to use based on the soil type and condition in application were the distance between the transmitter and receiver is small.

5.2 Recommendation for future work

The research detailed in this thesis can only be considered a starting point on a quest of discovery through soil electromagnetic properties soil and their relationships to signal propagation therefore, a number of recommendations are identified in this section based on the research presented in this thesis.

- The methodology for the signal attenuation measurement can still be improve by further eliminating the effect of environmental signals on the measurements. Therefore, further developments like the introduction of an electromagnetic signal chamber are necessary to minimise the measurement errors.
- The effect of temperature on the attenuation of signals in soil was not investigated in this research. Therefore, it is recommended that this effect is studied in more detail to provide a better understanding of attenuation of signals at varying soil temperatures.
- Due to time and resource limitation only two types of soil and various compositions of them were tested in this research. However, for future experiments it would be constructive to use larger variety of soil types to discover the effect of the soil mineralogy and relative magnetic permeability (i.e. iron oxide rich soils) on signal propagation.
- For field experiments it is recommended that further test are carried out in different locations with different soil types and at a longer period (larger seasonal variations) to obtain a better understanding of the signal attenuation and the accuracy of estimation models.
- TDR was used in this research for measuring the volumetric water content and to measure the permittivity of the soil. It is suggested that further tests be undertaken using vector network analyser in parallel with TDR to validate the results obtained from the

TDR. This can help to further validate the use of TDR for extracting the real and imaginary parts of permittivity.

References

Akyildiz, I.F. (2002) A survey on sensor networks. IEEE Communications Magazine, 40 (8): 102–105

Akyildiz, I.F., Pompili, D. and Melodia, T. (2005) Underwater acoustic sensor networks: research challenges. Ad Hoc Networks, 3 (3): 257–279

Akyildiz, I.F., Sun, Z. and Vuran, M.C. (2009) Signal propagation techniques for wireless underground communication networks. Physical Communication, 2 (3): 167–183

Bittelli, M., Salvatorelli, F. and Pisa, P.R. (2008) Correction of TDR-based soil water content measurements in conductive soils. Geoderma, 143 (1–2): 133–142

Bogena, H.R. (2009) Hybrid Wireless Underground Sensor Networks: Quantification of Signal Attenuation in Soil. Vadose Zone Journal, 8 (3): 755

Bogena, H.R. (2010) Potential of Wireless Sensor Networks for Measuring Soil Water Content Variability. Vadose Zone Journal, 9 (4): 02–08

Bradford, J.M. (1976) Fundamentals of Soil Behavior. Soil Science Society of America Journal. 40 p. :3-4

BSI 1377 (1990) Methods of test for soils for civil engineering purposes. London: British Standards Institution, Part 2.

Campbell, J.E. (1990) Dielectric Properties and Influence of Conductivity in Soils at One to Fifty Megahertz. Soil Science Society of America Journal, 54 (2): 332

Chaamwe, N. (2010) “Wave Propagation Communication Models for Wireless Underground Sensor Networks.” In 2010 IEEE 12th International Conference on Communication Technology, Proceedings, ICCT, Department of Electronics and Information Engineering Huazhong University of Science and Technology. 2010. pp. 9–12

Chehri, A. (2006) Application of Ad-hoc sensor networks for localization in underground mines. IEEE Wireless and Microwave Technology Conference, WAMICON 2006, p. :1-4

Chudinova, S.M. (2009) Dielectric characteristics of soils and categories of soil water. Eurasian Soil Science, 42 (4): 405–414

Craig, R.. (2004) Craig's Soil Mechanics, Seventh Edition. 7th ed.

Cross, J.D. (2014) Low-frequency electromagnetic fields for the detection of buried objects in the shallow sub-surface. PhD Thesis University of Birmingham

Curioni, G. (2013) Investigating the seasonal variability of electromagnetic soil properties using field monitoring data from Time-Domain Reflectometry probes. Phd Thesis University of Birmingham

Dam, R.L. Van, Borchers, B. and Hendrickx, J.M.H. (2005) Methods for prediction of soil dielectric properties. Defense and Security, 5794: 2

Dam, R.L. Van, Hendrickx, J.M.H., Cassidy, N.J., et al. (2013) Effects of magnetite on high-frequency ground-penetrating radar. Geophysics, 78 (5): 2–3

Friis, H.T. (1946) A Note on a Simple Transmission Formula. Proceedings of the IRE, 34 (5): 254–256

Gershun, A. (1945) Fresnel Reflection of Diffusely Incident Light. Journal of the Optical Society of America, 35 (2): 162

Giese, K. and Tiemann, R. (1975) Determination of the complex permittivity from thin-sample time domain reflectometry improved analysis of the step response waveform. Advances in Molecular Relaxation Processes, 7 (1): 45–59

Gong, Y., Cao, Q. and Sun, Z. (2003) The effects of soil bulk density , clay content and temperature on soil water content measurement using time-domain reflectometry., 3614 (May 2002): 3601–3614

Gupta, V.K. (2011) The Effect of Bulk Density on Emission Behavior of Soil at Microwave Frequencies. International Journal of Microwave Science and Technology, 2011: 1–6

Heimovaara, T.J., Winter, E.J.G. De, Loon, W.K.P. Van, et al. (1996) Frequency-dependent dielectric permittivity from 0 to 1 GHz: Time domain reflectometry measurements compared with frequency domain network analyzer measurements. Water Resources Research, 32 (12): 3603–3610

Jenny, H. and Amundson, R. (1941) Factors of Soil Formation a System of Quantitative Pedology, 28-50

Jones, S.B., Wraith, J.M. and Or, D. (2002) Time domain reflectometry measurement principles and applications. Hydrological Processes, 16: 141–153

Kennedy, G.A. (2006) High resilience wireless mesh networking characteristics and safety applications within underground mines High resilience wireless mesh networking characteristics and safety applications within underground mines. PhD Thesis University of Exeter

Kingston, E., Clayton, C., Priest, J., et al. (2008) "Effect of grain characteristics on the behaviour of disseminated methane hydrate bearing sediments." In Proceedings of the 6th International Conference on Gas Hydrates (ICGH 2008), Vancouver, British Columbia, CANADA, July 6-10, 2008. 2008. p. :1-9

Li, L., Vuran, M.C. and Akyildiz, I.F. (2007) "Characteristics of Underground Channel for Wireless Underground Sensor Networks." In 6th annual Mediterranean Ad Hoc Networking Workshop. 2007. p. :92-99

Martinez, A. and Byrnes, A. (2001) Modeling dielectric-constant values of geologic materials: An aid to ground-penetrating radar data collection and interpretation. Kansas Geological Survey, 1930 Constant Avenue, Lawrence, KS 66047

Menziani, M. and Rivasi, M.R. (1996) Soil volumetric water content measurments using TDR technique. Annali de Geofisica, p. :91-96

Mironov, V.L. (2004) Generalized Refractive Mixing Dielectric Model for Moist Soils. Geoscience and Remote Sensing, IEEE Transactions, 42 (4): 773–785

Mironov, V.L., Kosolapova, L.G. and Fomin, S. V (2008) Soil Dielectric Model Accounting for Contribution of Bound Water Spectra through Clay Content. PIERS online, (1): 1157–1161

Mironov, V.L., Kosolapova, L.G. and Fomin, S. V. (2009) Physically and mineralogically based spectroscopic dielectric model for moist soils. IEEE Transactions on Geoscience and Remote Sensing, 47: 2059–2070

Mironov, V.L., De Roo, R.D. and Savin, I. V (2010) Temperature-Dependable Microwave Dielectric Model for an Arctic Soil. IEEE Transactions on Geoscience and Remote Sensing, 48 (6): 2544–2556

Peplinski, N.R., Ulaby, F.T. and Dobson, M.C. (1995a) Corrections to "Dielectric Properties of Soils in the 0.3-1.3-GHz Range." IEEE Transactions on Geoscience and Remote Sensing, 33 (6): 1340

Peplinski, N.R., Ulaby, F.T. and Dobson, M.C. (1995b) Dielectric properties of soils in the 0.3-1.3-GHz range. IEEE Transactions on Geoscience and Remote Sensing, 33 (3): 803–807

Robinson, D.A. (2002) A Review of Advances in Dielectric and Electrical Conductivity Measurement in Soils. Vadose Zone Journal, 2: 444–475

Robinson, D.A. (2005) On the effective measurement frequency of time domain reflectometry in dispersive and nonconductive dielectric materials. Water Resources Research. 41 p. :1-9

Robinson, D.A., Schaap, M., Jones, S.B., et al. (2003) Considerations for Improving the Accuracy of Permittivity Measurement using Time Domain Reflectometry. Soil Science Society of America Journal, 67: 62–70

Saarenketo, T. (1998) Electrical properties of water in clay and silty soils. Journal of Applied Geophysics, 40 (1–3): 73–88

Sabey, B.R. (1966) Fundamentals of Soil Science. Soil Science Society of America Journal. 30 p. iv

Sadeghioon, A., Metje, N., Chapman, D., et al. (2014) SmartPipes: Smart Wireless Sensor Networks for Leak Detection in Water Pipelines. Journal of Sensor and Actuator Networks, 3 (1): 64–78

Sadeghioon, A.M. (2014) Design and Development of Wireless Underground Sensor Network. PhD Thesis University of Birmingham

Silva, A.R. (2010) Channel Characterization for Wireless Underground Sensor Networks. Master Thesis University of Nebraska

Silva, A.R. and Vuran, M.C. (2010) Communication with Aboveground Devices in Wireless Underground Sensor Networks : An Empirical Study. Communications (ICC), 2010 IEEE International Conference on, pp. 1–6

Stoianov, I., Nachman, L., Madden, S., et al. (2007) PIPENET: A Wireless Sensor Network for Pipeline Monitoring. 2007 6th International Symposium on Information Processing in Sensor Networks, p. :264-273

Stuntebeck, E.P. and Akyildiz, I.F. (2006) Wireless underground sensor networks: Research challenges. Ad Hoc Networks, 4: :669-686

Sun, Z.S.Z. and Akyildiz, I.F. (2010) Channel modeling and analysis for wireless networks in underground mines and road tunnels. IEEE Transactions on Communications, 58 (6): 1–5

Thomas, A. (2010) MEASUREMENT OF ELECTROMAGNETIC. PhD Thesis University of Birmingham

Topp, C., Resource, L. and Canada, A. (1980) Electromagnetic Determination of Soil Water Content. Water resources research, 16 (3): 574–582

Topp, G.C. and Davis, J.L. (1985) Measurement of Soil Water Content using Time-domain Reflectometry (TDR): A Field Evaluation. Soil Science Society of America Journal, 49: 19–24

Topp, G.C., Zegelin, S. and White, I. (2000) Impacts of the Real and Imaginary Components of Relative Permittivity on Time Domain Reflectometry Measurements in Soils. Soil Science Society of America Journal, 64 (4): 1244

Vuran, M.C. and Akyildiz, I.F. (2010) Channel model and analysis for wireless underground sensor networks in soil medium. Physical Communication, 3 (4): 245–254

Wang, J.R. and Schmugge, T.J. (1980) An Empirical Model for the Complex Dielectric Permittivity of Soils as a Function of Water Content. IEEE Transactions on Geoscience and Remote Sensing, GE-18: 288–295

Yaghjian, A., Yaghjian .D and Yaghjian, A. (1986) An overview of near-field antenna measurements. IEEE Transactions on Antennas and Propagation, 34 (1): 30–45

Yamane, T., Nishikata, A. and Shimizu, Y. (2000) Resonance suppression of a spherical electromagnetic shielding enclosure by using conductive dielectrics. IEEE Transactions on Electromagnetic Compatibility, 42 (4): 441–448

Yoon, S.-U., Cheng, L., Ghazanfari, E., et al. (2011) A Radio Propagation Model for Wireless Underground Sensor Networks. 2011 IEEE Global Telecommunications Conference GLOBECOM 2011, pp. 01–05

Yu, N.W. (2013a) Electromagnetic Wave Propagation In Soil For Wireless Underground Sensor Networks., 5794: 12–22

Yu, N.W. (2013b) Progress In Electromagnetics Research M, Vol. 30, 11–23, 2013., 30 (November 2012): 11–23

Zhang, Z. and Satpathy, S. (1990) Electromagnetic wave propagation in periodic structures: Bloch wave solution of Maxwell's equations. Physical Review Letters, 65 (21): 2650–265

Appendix A:

Appendix A included of raw data was figured in result and discussion chapter. Each table was addressed to the figure.

A. 1 Data used for figure 4-2

Clay (%)	10% GWC	20% GWC	30% GWC
10	9.28	22.1	N/A
30	8.9	20.51	26.31
50	8.4	18.32	23.88
70	7.95	17.5	23.62
90	N/A	13.74	22.1

clay	r1	r2	r3	10% average	(-)	(+)
10	8.4	9.6	9.85	9.28	0.88	0.57
30	8.1	9	9.8	8.97	0.87	0.83
50	7.1	9	9.35	8.48	1.38	0.87
70	7.3	8.1	8.45	7.95	0.65	0.50
90	N/A	N/A	N/A	N/A	N/A	N/A

clay	r1	r2	r3	20% average	(-)	(+)
10	21.1	22.5	22.8	22.13	1.03	0.67
30	19.6	20.1	21.83	20.51	0.91	1.32
50	17.7	18.4	18.85	18.32	0.62	0.53
70	16.9	17.9	17.98	17.59	0.69	0.39
90	12.8	13.3	15.13	13.74	0.94	1.39

clay	r1	r2	r3	30% average	(-)	(+)
10	N/A	N/A	N/A	N/A	N/A	N/A
30	25.8	26.41	26.73	26.31	0.51	0.42
50	23.12	24	24.53	23.88	0.76	0.65
70	22.9	23.9	24.05	23.62	0.72	0.43
90	24.2	24.68	24.95	24.61	0.41	0.34

A. 2 Data used for figure 4-3

Clay (%)	10% GWC	20% GWC	30% GWC
10	0.71	2.04	
30	2.68	2.69	2.74
50	3.64	4.48	2.94
70	4.29	4.61	3.88
90		5.68	4.75

Clay (%)	r1	r2	r3	10% average	(-)	(+)
10	0.66	0.65	0.83	0.71	0.05	0.12
30	2.53	2.65	2.88	2.69	0.16	0.19
50	3.5	3.69	3.75	3.65	0.15	0.10
70	3.98	4.31	4.6	4.30	0.32	0.30
90	N/A	N/A	N/A	N/A	N/A	N/A

Clay (%)	r1	r2	r3	20% average	(-)	(+)
10	1.7	2.05	2.38	2.04	0.34	0.34
30	2.52	2.71	2.85	2.69	0.17	0.16
50	4.29	4.485	4.65	4.48	0.19	0.18
70	4.52	4.58	4.72	4.61	0.09	0.11
90	5.4	5.7	5.95	5.68	0.28	0.27

Clay (%)	r1	r2	r3	30% average	(-)	(+)
10				N/A	N/A	N/A
30	2.73	2.75	2.76	2.75	0.02	0.01
50	2.74	2.98	3.1	2.94	0.20	0.16
70	3.1	4	4.55	3.88	0.78	0.67
90	3.9	4.79	5.55	4.75	0.85	0.80

A. 3 Data used for figure 4-4

Clay (%)	r1	r2	r3	aver	(+)	(-)
10	1.40	1.54	1.79	1.58	0.21	0.18
30	0.30	0.96	1.51	0.92	0.59	0.62
50	2.30	2.65	2.85	2.60	0.25	0.30
70	4.60	4.98	5.25	4.94	0.31	0.34
90	9.70	9.96	10.27	9.98	0.29	0.28

A. 4 Data used for figure 4-5

GWC (%)	r1	r2	r3	aver	(+)	(-)
10	1.40	1.74	1.94	1.69	0.25	0.29
20	2.50	2.63	2.68	2.60	0.08	0.10
30	3.90	5.05	5.80	4.92	0.88	1.02

A. 5 Data used for the figure 4-6

Distance cm	**10% Clay**	**r1**	**r2**	**r3**	**average**	**(+)**	**(-)**
10.00	-43.56	-42.90	-43.50	-44.28	-43.56	0.66	0.72
20.00	-45.20	-44.20	-45.00	-46.39	-45.20	1.00	1.19
30.00	-45.59	-44.60	-45.51	-46.65	-45.59	0.99	1.06
40.00	-50.56	-48.20	-49.80	-50.67	-49.56	1.36	1.11
50.00	-56.36	-55.17	-56.80	-57.10	-56.36	1.19	0.74
Distance cm	30% Clay	r1	r2	r3			
10.00	-44.43	-45.98	-44.10	-43.20	-44.43	1.23	1.55
20.00	-48.36	-50.10	-46.80	-48.17	-48.36	1.56	1.74
30.00	-53.00	-54.10	-52.70	-52.20	-53.00	0.80	1.10
40.00	-60.76	-59.20	-61.10	-62.00	-60.77	1.57	1.23
50.00	-61.91	-62.50	-61.10	-62.10	-61.90	0.80	0.60
Distance cm	50% Clay	r1	r2	r3			
10.00	-46.43	-47.10	-45.80	-46.40	-46.43	0.63	0.67
20.00	-51.94	-53.90	-49.98	-51.94	-51.94	1.96	1.96
30.00	-54.86	-53.75	-54.82	-56.00	-54.86	1.11	1.14
40.00	-64.43	-64.10	-65.90	-63.30	-64.43	1.13	1.47
50.00	-68.71	-67.60	-68.90	-69.63	-68.71	1.11	0.92
Distance cm	70% Clay	r1	r2	r3			
10.00	-50.56	-50.70	-49.50	-51.48	-50.56	1.06	0.92
20.00	-55.3	-53.29	-55.40	-57.20	-55.30	2.01	1.90
30.00	-57.75	-57.25	-59.00	-57.00	-57.75	0.75	1.25
40.00	-69.76	-69.10	-70.23	-69.95	-69.76	0.66	0.47
50.00	-74.63	-74.59	-75.4	-73.9	-74.63	0.73	0.77
Distance cm	90% Clay	r1	r2	r3			
10.00	-56.26	-55.10	-56.00	-57.67	-56.26	1.16	1.41
20.00	-66.27	-64.10	-66.00	-68.70	-66.27	2.17	2.43
30.00	-74.57	-74.20	-73.90	-75.40	-74.50	0.60	0.90

40.00	-79.32	-78.40	-80.00	-79.55	-79.32	0.92	0.68
50.00	-81.50	-82.10	-80.96	-81.45	-81.50	0.54	0.60

A. 6 Data used for figure 4-7

10 cm	**clay**	**r1**	**r2**	**r3**	**average**	**(-)**	**(+)**
	10	1.30	1.40	1.60	1.43	0.13	0.17
	30	0.10	0.50	1.10	0.57	0.47	0.53
	50	2.40	2.90	3.50	2.93	0.53	0.57
	70	4.50	4.80	5.20	4.83	0.33	0.37
	90	N/A	N/A	N/A	N/A	N/A	N/A
20 cm	clay	r1	r2	r3	average	(-)	(+)
	10	1.60	2.30	2.60	2.17	0.57	0.43
	30	0.70	1.40	2.20	1.43	0.73	0.77
	50	8.20	9.20	8.80	8.73	0.53	0.47
	70	13.80	14.50	14.10	14.13	0.33	0.37
	90	18.70	17.90	18.40	18.33	0.43	0.37
30 cm	clay	r1	r2	r3	average	(-)	(+)
	10	6.30	7.60	7.30	7.07	0.77	0.53
	30	11.40	7.10	6.60	8.37	1.77	3.03
	50	19.10	17.20	18.70	18.33	1.13	0.77
	70	16.70	17.20	17.70	17.20	0.50	0.50
	90	21.60	24.00	23.20	22.93	1.33	1.07
40 cm	clay	r1	r2	r3	average	(-)	(+)
	10	2.30	2.90	2.70	2.63	0.33	0.27
	30	8.00	13.90	12.10	11.33	3.33	2.57
	50	21.10	23.80	22.70	22.53	1.43	1.27
	70	21.50	22.50	22.20	22.07	0.57	0.43
	90	23.90	24.70	26.60	25.07	1.17	1.53

A. 7 Data used for figure 4-8

Soil mixture used

50% clay	6004.10	gr
50 % sand	6000.10	gr
30 % water	3600.40	gr

total Weight mixed	15604.60	gr
container Weight	2610.00	gr
container + soil (Weight)	12615.00	gr
container volume	5365.87	cm³
bulk density	1.86	gr/cm³
dry density	1.34	gr/cm³
VWC	0.52	cm³

GWC for wet soil A		Tray (g)	Tray + WS	Tray + DS	GWC		GWC %
	Tray 1	9.39	50.54	41.46	0.28	0.28	28.14
	Tray 2	9.91	65.16	53.34	0.27		
	Tray 3	9.49	40.55	33.59	0.29		

frequency 434 MHz signal strength					**attenuation**			
	air	t1	t2	t3	air	t1	t2	t3
10.00		-68.40	-69.60	-71.30	0.00	0.11	0.01	-0.39
20.00		-69.50	-69.60	-70.00	0.00	-2.09	-2.09	-2.79
frequency 868 MHz signal strength					attenuation			
	air	t1	t2	t3	air	t1	t2	t3
10.00		-67.80	-69.00	-68.90	0.00	-2.97	-4.27	-3.77
20.00		-71.50	-72.80	-72.30	0.00	-15.27	-17.17	-18.57
frequency 1300 MHz signal strength					attenuation			
	air	t1	t2	t3	air	t1	t2	t3
10.00		-64.70	-65.40	-66.50	0.00	-10.93	-9.03	-10.83
20.00		-76.40	-74.50	-76.30	0.00	-13.03	-12.93	-14.63
frequency 1736 MHz signal strength					attenuation			
	air	t1	t2	t3	air	t1	t2	t3
10.00		-69.10	-70.20	-69.20	0.00	-10.63	-7.93	-11.93
20.00		-80.10	-77.40	-81.40	0.00	-18.13	-19.93	-18.43
	air	t1	t2	t3	air	t1	t2	t3
10.00		-73.70	-71.90	-72.10	0.00	-11.03	-11.23	-11.73
20.00		-80.50	-80.70	-81.20	0.00	-22.13	-21.83	-22.23
frequency 2604 MHz signal strength					attenuation			
	air	t1	t2	t3	air	t1	t2	t3
10.00		-70.40	-74.10	-71.60	0.00	-14.12	-12.92	-10.12
20.00		-85.90	-84.70	-81.90	0.00	-23.02	-22.52	-23.02

	Average signal Strength			Average Attenuation			RFL
error +		error -		error +		error -	-54.50
1.21	-69.61	1.69		1.21	0.09	1.69	
0.19	-69.69	0.31		0.19	2.31	0.31	
							RFL
							-74.20
0.73	-68.53	0.47		0.73	3.63	0.47	
0.67	-72.17	0.63		0.67	16.79	0.63	
							RFL
							-74.40
0.77	-65.47	1.03		0.77	10.17	1.03	
1.14	-75.64	0.76		1.14	13.46	0.76	
							RFL
							-73.20
0.37	-69.47	0.73		0.37	9.83	0.73	
1.90	-79.30	2.10		1.90	18.76	2.10	
							RFL
							-78.40
-2.43	-69.47	4.23		-2.43	11.32	4.23	
-1.20	-79.30	1.90		-1.20	22.06	1.90	
							RFL
							-87.50
1.38	-71.78	2.32		1.38	12.06	2.32	
1.93	-83.83	2.07		1.93	22.85	2.07	

Plot attenuation Vs distance

Distances cm	434.00	868.00	1300.00	1736.00	2170.00	2604.00
10.00	0.09	3.63	10.17	9.83	11.32	12.06
20.00	2.31	16.79	13.46	18.76	22.06	22.85
Friis model	434.00	868.00	1300.00	1736.00	2170.00	2604.00
10.00	9.63	16.39	20.64	23.89	26.57	28.89
20.00	16.39	23.89	28.87	32.87	36.28	39.34
Crim-Fresnel model	434.00	868.00	1300.00	1736.00	2170.00	2604.00
10.00	0.28	2.67	5.06	7.45	9.85	12.24
20.00	2.74	7.53	12.30	17.11	21.89	26.68

A. 8 Data used for figure 4-9

10 cm	**clay/water**	**r1**	**r2**	**r3**	**average**	**(-)**	**(+)**
	50/10	4.10	6.90	4.30	5.10	1.00	1.80
	50/20	2.90	2.40	3.50	2.93	0.53	0.57
	50/30	5.50	3.30	5.10	4.63	1.33	0.87
20 cm	clay/water	r1	r2	r3	average	(-)	(+)

	50/10	13.00	8.00	11.10	10.70	2.70	2.30
	50/20	8.90	8.30	9.20	8.80	0.50	0.40
	50/30	8.00	6.90	8.90	7.93	1.03	0.97
30 cm	clay/water	r1	r2	r3	average	(-)	(+)
	50/10	16.10	14.20	15.00	15.10	0.90	1.00
	50/20	18.10	19.20	17.20	18.17	0.97	1.03
	50/30	5.60	3.60	5.80	5.00	1.40	0.80
40 cm	clay/water	r1	r2	r3	average	(-)	(+)
	50/10	26.70	25.20	25.90	25.93	0.73	0.77
	50/20	23.80	21.10	22.70	22.53	1.43	1.27
	50/30	10.60	6.40	11.60	9.53	3.13	2.07

A. 9 Data used for the figure 4-11 to figure 4-13

25.02.2015

Frequency MHz	Signal strength	r1	r2	r3	average	(+)	(-)
250.00	-61.42	-63.20	-61.20	-59.86	-61.42	1.56	1.78
300.00	-63.96	-65.96	-62.96	-62.95	-63.96	1.01	2.00
434.00	-77.40	-78.40	-76.40	-77.40	-77.40	1.00	1.00
500.00	-81.50	-80.60	-81.00	-82.90	-81.50	0.90	1.40
600.00	-86.96	-86.96	-85.96	-87.96	-86.96	1.00	1.00
700.00	-89.01	-90.08	-89.08	-87.87	-89.01	1.14	1.07
864.00	-90.01	-90.01	-92.01	-88.00	-90.01	2.01	2.00
900.00	-90.05	-93.07	-90.07	-87.03	-90.05	3.02	3.01
960.00	-93.51	-93.00	-92.80	-94.72	-93.51	0.71	1.21
01.05.2015	Signal strength	r1	r2	r3			
250.00	-33.40	-31.90	-33.40	-34.90	-33.40	1.50	1.50
300.00	-49.90	-51.53	-49.17	-48.99	-49.90	0.91	1.63
434.00	-42.80	-41.80	-42.80	-43.81	-42.80	1.00	1.01
500.00	-58.90	-56.30	-59.90	-60.50	-58.90	2.60	1.60
600.00	-54.30	-52.90	-54.10	-55.90	-54.30	1.40	1.60
700.00	-66.20	-65.15	-65.90	-67.55	-66.20	1.05	1.35
868.00	-72.40	-74.01	-72.01	-71.19	-72.40	1.21	1.61
900.00	-64.20	-64.25	-63.25	-65.10	-64.20	0.95	0.90
1000.00	-74.30	-73.90	-73.00	-75.70	-74.20	1.20	1.50
1100.00	-72.80	-71.62	-72.88	-73.90	-72.80	1.18	1.10
1200.00	-88.00	-89.20	-88.60	-86.50	-88.10	1.60	1.10
1300.00	-78.50	-77.29	-78.10	-80.10	-78.50	1.21	1.60
25.06.2015	Signal strength	r1	r2	r3			
250.00	-35.45	-35.71	-34.20	-36.45	-35.45	1.25	1.00

300.00	-54.20	-55.70	-53.80	-53.10	-54.20	1.10	1.50
434.00	-75.85	-73.75	-77.10	-76.70	-75.85	2.10	1.25
500.00	-65.30	-66.90	-64.20	-64.80	-65.30	1.10	1.60
600.00	-61.90	-60.90	-61.90	-62.90	-61.90	1.00	1.00
700.00	-69.80	-68.80	-71.10	-69.50	-69.80	1.00	1.30
868.00	-73.15	-73.20	-72.20	-74.40	-73.27	1.07	1.13
900.00	-73.65	-72.90	-75.50	-72.55	-73.65	1.10	1.85
1000.00	-76.15	-75.15	-76.10	-77.20	-76.15	1.00	1.05
1100.00	-74.80	-77.40	-72.90	-74.10	-74.80	1.90	2.60
1200.00	-79.85	-79.25	-79.70	-80.60	-79.85	0.60	0.75
1300.00	-83.80	-82.40	-83.80	-85.20	-83.80	1.40	1.40

Appendix B:

Appendix B is included the raw data for the figures in the chapter three.

B. 1 data used in figure 3-3

Distance cm	Filled container	Empty container
10	-26.7	-29.4
20	-32.6	-34
30	-29.7	-40.1
40	-38	-46

distance	r1	r2	r3	Filled average	(-)	(+)
10	-25.4	-26.9	-28.7	-27.00	-1.60	-1.70
20	-31.3	-32.1	-34.6	-32.67	-1.37	-1.93
30	-28.4	-29.1	-31.6	-29.70	-1.30	-1.90
40	-37.4	-38.1	-38.6	-38.03	-0.63	-0.57

distance	r1	r2	r3	Empty average	(-)	(+)
10	-28.5	-29.4	-30.4	-29.43	-0.93	-0.97
20	-33.2	-34	-34.8	-34.00	-0.80	-0.80
30	-39.1	-40.1	-41.1	-40.10	-1.00	-1.00
40	-45.1	-46	-46.9	-46.00	-0.90	-0.90

B. 2 Data used for figure 3-6

Distance	Trial 1	Trial 2	Trial 3	(-)	Soil average	(+)
8.5	-36	-36.9	-37	0.98	-36.61	1.01
15.5	-40.6	-42.2	-43	0.97	-41.82	1.03
23.5	-37	-42.5	-40.8	0.94	-39.47	1.08
30	-50	-56	-49	0.97	-50.77	1.10

distance	r1	r2	r3	Air average	(-)	(+)
10	-28.5	-29.4	-30.4	-29.43	-0.93	-0.97
20	-33.2	-34	-34.8	-34.00	-0.80	-0.80
30	-39.1	-40.1	-41.1	-40.10	-1.00	-1.00
40	-45.1	-46	-46.9	-46.00	-0.90	-0.90

B. 3 Data used for figure 3-8

Distance (cm)							
	Trial 1	Trial 2	Trial 3	Trial 4	ER+	434 MHz averages	ER-
10	-42.2	-42.2	-42.2	-42.2	0.14	-42.34	0.56
20	-49	-49.6	-50.14	-49.6	0.628	-49.628	0.512
30	-45.8	-45.6	-46.3	-46.2	0.44	-46.04	0.26
40	-54.4	-54.6	-55.1	-54.4	0.22	-54.62	0.48
50	-53.5	-53.4	-53.4	-53.6	0.18	-53.58	0.42

B. 4 Data used for the figure 3-10

						error	**error**
	434 air				Average	(+)	(-)
Distance	10	-8.3	-8.7	-10	-9.00	0.70	1.00
	20	-9.2	-9.4	-13.3	-10.63	1.43	2.67
	30	-11.5	-11.9	-12.4	-11.93	0.43	0.47
	40	-13	-12.5	-16.7	-14.07	1.57	2.63
	50	-16.2	-13.7	-16.9	-15.60	1.90	1.30
	868 air						
Distance	10	-56.1	-55.6	-55.6	-55.77	0.17	0.33
	20	-60	-63.7	-59.1	-60.93	1.83	2.77
	30	-63.8	-59.3	-64.2	-62.43	3.13	1.77
	40	-65.1	-64.2	-65.4	-64.90	0.70	0.50
	50	-66.7	-65.8	-64.4	-65.63	1.23	1.07
	868 EC						
Distance	10	-52.65	-53.04	-52.66	-52.79	0.13	0.26
	20	-59.11	-59.77	-60.86	-59.91	0.80	0.95
	30	-61.77	-61.80	-60.47	-61.35	0.88	0.46
	40	-64.55	-63.85	-62.54	-63.65	1.10	0.90
	50	-66.06	-65.80	-63.84	-65.23	1.39	0.83
	434 EC						

Distance	10	-8.96	-8.13	-9.37	-8.82	0.69	0.55
	20	-10.92	-10.78	-11.69	-11.13	0.35	0.56
	30	-12.37	-11.03	-12.75	-12.05	1.02	0.70
	40	-13.34	-15.13	-15.95	-14.81	1.46	1.14
	50	-15.37	-16.12	-15.21	-15.57	0.36	0.55
	868FC						
Distance	10	-68.23	-69.50	-68.31	-68.68	0.45	0.82
	20	-74.70	-74.79	-73.95	-74.48	0.53	0.31
	30	-79.08	-77.30	-76.06	-77.48	1.42	1.60
	40	-81.38	-81.16	-82.86	-81.80	0.64	1.06
	50	-86.57	-85.52	-86.15	-86.08	0.56	0.49
	434FC						
Distance	10	-43.57	-42.65	-43.44	-43.22	0.57	0.35
	20	-48.36	-47.92	-47.08	-47.79	0.71	0.58
	30	-57.74	-55.32	-56.95	-56.67	1.35	1.07
	40	-60.71	-59.87	-58.30	-59.63	1.32	1.08
	50	-66.69	-65.15	-64.30	-65.38	1.08	1.31

B. 5 Particle size distribution for used sand

Location	**CIVIL LAB**	**41723.00**	**particle size distribution**		
Soil Description	SAND LB 100% natural				
Initial Dry Mass m1 (g)	151.11				
Sieve Size	**Weight of the Sieve (g)**	**Sieve and Retained Material (g)**	**Net Weight of Material m (g)**	**Percentages Retained (m/m1)x100**	**Cumulative Percentages Passing**
Tray	243.72	243.72	0.00	0.00	0.00
0.06	258.21	258.21	0.00	0.00	0.00
0.15	266.23	266.23	0.00	0.00	0.00
0.21	271.08	271.08	0.00	0.00	0.00
0.30	279.14	279.16	0.02	0.01	0.01
0.43	293.97	296.51	2.54	1.68	1.69
0.60	315.25	461.01	145.76	96.46	98.15

1.18	341.99	344.80	2.81	1.86	100.01
2.00	387.43	387.43	0.00	0.00	100.01
3.35	405.54	405.54	0.00	0.00	100.01
5.00	418.11	418.11	0.00	0.00	100.01
Tray	243.72	243.72			
Total	3480.53				

B. 6 The GWC calculation for the PSD

Samples	Tray	Tray + soil	Tray + Dry soil	GWC %
s1	9.88	51.71	51.66	0.0012
s2	9.38	52.50	52.46	0.0009
s3	9.76	52.27	52.23	0.0009
s4	9.76	49.42	49.38	0.0010

Appendix C:

Appendix C includes Matlab program was developed in order to determine the apparent permittivity, and estimating the signal attenuation based on the Crim-Fresnel and Modified-Friis.

%% Find the soil dielcteric properties of soil

```
% This Matlab code is using the information from the measured data by
% TDR in order to calcualte apparent permitivity, real and imaginary

% constant of dielcteric perrmitivity based on Topp, peplinski and mironov models and volumetric water
content of soil
% based on Topp model,

%using all information to estimate the attenuation of signal basedd on
%Friis and CRIM model.
% Thses functions must be run in the same time (TDR.m , Lmin.m , conductivity.m , Peplinski.m ,
Friis_modified.m , CRIM.m, Attenuation.m) )
clc
clear all
close all
%hold all
% uiopen()
% pdata= val;
% uiopen()
% cdata=val;
[pdata,cdata]= ImportSignal();

startwave=4;                % Start of the plot in m (Aparent)
win=2.5;                    %lenght of the window in m (aparent)
n=2048;                     %number of data points
lop=win/n;                  %length of each point (aparent)
L0c=[0.03465,0.03765,0,0,0,0.03249,0,0];        % List of calibration values          0,0.03249
Lcalc=[0.07522,0,0,0,0.13101,0.12853,0,0];      % List of calibration values          0.12853
kpc=[6.1425,0,0,0,1.5911,1.6054,0,0,0];         % List of calibration kp values
po=[0.973125795,0,0,0,0.97197723,0.97183103,0,0,0,0,0,0,] ;     % List of calibration Resistance load values

%probe=input('enter probe number')
probe=1;


L0=L0c(probe);
Lcal=Lcalc(probe);
Kp=kpc(probe);
Po=po(probe);
Rc=0.03;                    %Cable Resistance array loaded by variables
R0=0.05;                    %series resistance
Zout=50;                    %Zout value
```

```
c=2.9979*10^8;                  % speed of light (m/s)
e0=8.8542/10^12;                %Free space dielectric permittivity
u0=1.2566/10^6;                 %Free space magnetic permittivity
uabs=u0;                        %material magnetic permittivity
u=uabs/u0;                      %relative magnetic permittivity
ttotal=(2*win)/c;               %Total sampling time
df=1/ttotal;                    %frequency interval
fs=df*n;                        %sampling frequency
dt=ttotal/n;                    %time interval
wd1=diff(pdata);                % first Derivative of data points
wd2=diff(wd1);                  % second Derivative of data points
wcd11=diff(cdata);
% trsh=0.001;

[min1,min1v,min2,min2v,cp1,cp2,max_value,tl2,min3,min3v]=Lmin(pdata,wd2,wd1);    % importing Lmin
function
x=1:2048;                       % drow a line for mins
xa=x*lop;
min1y=0*xa+min1v;
min2y=0*xa+min2v;
min3y=0*xa+min3v;
hold all
[ec,mcdata]=conductivity(cdata,wcd11, Kp, Lcal, Rc, R0,Po, Zout);     % importing conductivity function
ec

lt=(cp2-cp1);
lapp=lt-L0;
Ea=(lapp/Lcal)^2                % find apparent permitivity


vwc=(-5.3*10^-2)+(2.92*10^-2*Ea)-((5.5*10^-4)*(Ea^2))+((4.3*10^-6)*(Ea^3))  % Topp Volumetric water
content _


%title('Time Domain Reflectometry TDR','FontSize', 12)
ylabel('Reflection Coefficient','FontSize', 16)
xlabel('Apparent Length','FontSize', 16)
plot (xa,pdata,'LineWidth',2);          %plot all the data
plot(xa,min1y,'g')
plot(xa,min2y,'r')
plot(xa,mcdata,'k')
plot(xa,min3y,'b')
%plot(xa,mcdata,'b','LineWidth',2)
%plot(wd1)
%plot(wd2)
%swd1=smooth(wd1,5);
%swd2=smooth(wd2,5);
%plot(swd1)
%plot(swd2)
plot (cp1,min1v,'.','MarkerSize',10)
plot (cp2,min2v,'.','MarkerSize',10)
axis([0 win (min(pdata)-0.2) (max(pdata)+0.2)])
sEa = num2str(Ea);
text(1.2,((max(pdata))/2),'Aparent permitivity = ')
text(1.9,((max(pdata))/2),[sEa])
svwc = num2str(vwc);
smcdata = num2str(ec);
text(1.2,((max(pdata))/2)-0.1,'VWC% = ')
text(1.55,((max(pdata))/2)-0.1,[svwc])
text(1.2,((max(pdata))/2)-0.2,'Ec = ')
```

```
text(1.55,((max(pdata))/2)-0.2,[smcdata])

%%
                        % finding the cross of conductivity with tangent 2
method=0; %0=pctdr,1=matlab
% Construct a questdlg with three options
choice = questdlg('Which method to use for permitivity calculation?', ...
   'File Type Selection', ...
   'Topp','AMS','Topp');
% Handle response
switch choice
   case 'Topp'
      mcdata=min3v;
   case 'AMS'

end


cp3=(mcdata-tl2(2))/tl2(1);
plot (cp3,mcdata,'.','MarkerSize',10)
rise=(cp3-cp2)/lop*dt;
eff=((log(0.9/0.1))/(0.8*rise*2*pi))/10^6
seff = num2str(eff);
text(1.2,((max(pdata))/2)-0.3,'EF = ')
text(1.55,((max(pdata))/2)-0.3,[seff])

……

%%
function [ATCRIMTDR,ATCRIMPeplinski,d,ATCRIMMironove,ATCRIMvN/A]=
CRIM(Ereal2,Eim2,PeplinskiREAL2 ,PeplinskiIM2,ec2,e0,erMironove,frequency,vN/Are,vN/Aim);

f=frequency

%%%%%%%%%%%%%%%%%%%%%%%% attenuation based on TDR real and imaginary valuse
e1=Ereal2;
e2=Eim2;
d=0:.001:.6;                        %distance in meter
R=((1-sqrt(e1))/(1+sqrt(e1)))^2;        %Reflection Coefficient to be used for CRIM-FRESNEL  model
Rc1=10*log10(2*R/(1+R));                %Atenuation due to signal reflection

x=60*pi*((2*pi*f*e0*e2)+ec2);
y=(1+((e2+(ec2/2*pi*f*e0)))/e1)^2;
ac=8.68*x/(sqrt((e1/2)*(1+sqrt(y))))

ATCRIMTDR=(ac*d)+Rc1;   % total atenuation

% Attenuation based on Peplinski real and imaginary values

e1=PeplinskiREAL2;
e2=PeplinskiIM2;

R=((1-sqrt(e1))/(1+sqrt(e1)))^2;        %Reflection Coefficient to be used for CRIM-FRESNEL  model
Rc=10*log10(2*R/(1+R));                 %Atenuation due to signal reflection

x=60*pi*((2*pi*f*e0*e2)+ec2);
y=(1+((e2+(ec2/2*pi*f*e0)))/e1)^2;
ac=8.68*x/(sqrt((e1/2)*(1+sqrt(y))));

ATCRIMPeplinski=(ac*d)+Rc;   % total atenuation
```

```
% Attenuation based on MIRONOV real and imaginary values
e1=erMironove;
e2=PeplinskiIM2;

R=((1-sqrt(e1))/(1+sqrt(e1)))^2;        %Reflection Coefficient to be used for CRIM-FRESNEL  model
Rc=10*log10(2*R/(1+R));                 %Atenuation due to signal reflection

x=60*pi*((2*pi*f*e0*e2)+ec2);
y=(1+((e2+(ec2/2*pi*f*e0)))/e1)^2;
ac=8.68*x/(sqrt((e1/2)*(1+sqrt(y))));

ATCRIMMironove=(ac*d)+Rc;   % total atenuation

e1=vN/Are;
e2=vN/Aim;
d=0:.001:.6;                        %distance in meter
R=((1-sqrt(e1))/(1+sqrt(e1)))^2;        %Reflection Coefficient to be used for CRIM-FRESNEL  model
Rc=10*log10(2*R/(1+R));                 %Atenuation due to signal reflection

x=60*pi*((2*pi*f*e0*e2)+ec2);
y=(1+((e2+(ec2/2*pi*f*e0)))/e1)^2;
ac=8.68*x/(sqrt((e1/2)*(1+sqrt(y))));

ATCRIMvN/A=(ac*d)+Rc;   % total atenuation

……..
%%
function [LpTDR,LpPeplinski,d,LpMironove,LpvN/A]=
Friis_modified(Ereal,Eim,PeplinskiREAL3,PeplinskiIM3,ec3,e03,erMironove,frequency,vN/Are,vN/Aim);
% ,nchTDR,nchpep,nchmir
f=frequency;
% e1=18;                  %real part of the permitivity of random soil
% e2=8;                   %imaginary part of the permitivity of random soil

% path loss calculated based on TDR real and imaginary values and
e1=Ereal;
e2=Eim;
d=0:.001:.6;
m=1;

b=(2*pi*f/1000000000)*sqrt((m*e1/2)*(sqrt(1+(e2/e1)^2)+1));   %the frequency is used in GB hertz
a=(2*pi*f/1000000000)*sqrt((m*e1/2)*(sqrt(1+(e2/e1)^2)-1));

LpTDR=6.45+20*log10(d)+20*log10(b)+(8.69*a*d);%path loss


% e0=1.8542;
% k=sqrt(e1*cos(45)/e0*cos(45));
% R=((1-sqrt(e1))/(1+sqrt(e1)))^2;
% nchTDR=6.45+20*log10(d*b*k*sqrt(2*R/1+R))+(8.69*a*d);


% path loss calculated based on the peplinski real and imaginary values
e1=PeplinskiREAL3;
e2=PeplinskiIM3;
b=(2*pi*f/1000000000)*sqrt((m*e1/2)*(sqrt(1+(e2/e1)^2)+1));   %the frequency is used in GB hertz
a=(2*pi*f/1000000000)*sqrt((m*e1/2)*(sqrt(1+(e2/e1)^2)-1));

LpPeplinski=6.45+20*log10(d)+20*log10(b)+(8.69*a*d); %path loss
```

```
% k=sqrt(e1*cos(45)/e0*cos(45));
% R=((1-sqrt(e1))/(1+sqrt(e1)))^2;
% nchpep=6.45+20*log10(d*b*k*sqrt(2*R/1+R))+(8.69*a*d);

% path loss calculated based on the mironov real and imaginary values
e1=erMironove;
e2=PeplinskiIM3;
b=(2*pi*f/1000000000)*sqrt((m*e1/2)*(sqrt(1+(e2/e1)^2)+1));   %the frequency is used in GB hertz
a=(2*pi*f/1000000000)*sqrt((m*e1/2)*(sqrt(1+(e2/e1)^2)-1));

LpMironove=6.45+20*log10(d)+20*log10(b)+(8.69*a*d);  %path loss


% k=sqrt(e1*cos(45)/e0*cos(45));
% R=((1-sqrt(e1))/(1+sqrt(e1)))^2;
% % nchmir=6.45+20*log10(d*b*k*sqrt(2*R/1+R))+(8.69*a*d);

e1=vN/Are;
e2=vN/Aim;
b=(2*pi*f/1000000000)*sqrt((m*e1/2)*(sqrt(1+(e2/e1)^2)+1));   %the frequency is used in GB hertz
a=(2*pi*f/1000000000)*sqrt((m*e1/2)*(sqrt(1+(e2/e1)^2)-1));

LpvN/A=6.45+20*log10(d)+20*log10(b)+(8.69*a*d); %path loss
```